Impact of Basin-Scale Air-Sea Interaction between the Pacific and Indian Ocean on the Seasonally Asymmetric Transition Process of ENSO

January 2010

Masamichi OHBA

Impact of Basin-Scale Air-Sea Interaction between the Pacific and Indian Ocean on the Seasonally Asymmetric Transition Process of ENSO

A Dissertation Submitted to
the Graduate School of Life and Environmental Sciences,
University of Tsukuba
In Partial Fulfillment of the Requirements
for the Degree of Doctor Philosophy in Science

Masamichi OHBA

Abstract

Physical processes that are responsible for asymmetric transition processes between El Niño and La Niña event are investigated by use of observational data, climate model dataset and physical models. The air-sea coupled system of El Niño-Southern Oscillation (ENSO) phenomenon is able to remain in a weak cold event for up to two years, while warm events relatively quickly turn into cold phase. Through observational analysis, we find that there exists a strong difference in the thermocline variation in relation to surface zonal wind anomalies in the equatorial Pacific for the mature to decay phase of ENSO. The atmospheric response for El Niño causes a rapid reduction of the equatorial Pacific westerlies for the boreal winter, that play a role in hastening the following ENSO transition through the generation of upwelling oceanic Kelvin waves. However, the anomalous equatorial Pacific easterlies of the La Niña persist to the subsequent spring, that tend to counteract the turnabout from cold to warm phase of ENSO.

A suite of idealized atmospheric general circulation model (AGCM) experiments are performed by imposing two different ENSO-related sea surface temperature (SST) anomalies, which have equal amplitude but have opposite sign from each other. The asymmetric climate response in the AGCM is found at the mature to decay phase of ENSO that closely resembles the observations, including a zonal and meridional shift in the equatorial positions of the atmospheric wind. It is also diagnosed that the asymmetric responses of the equatorial zonal wind results in differences in recovery times of the thermocline in the eastern equatorial Pacific. Thus, the differences in transition process between the warm and cold ENSO event are fundamentally due to the nonlinear atmospheric (convective) response to SST, which originates from the distribution of climatological SST and its seasonal changes. Our intermediate air-sea coupled

model, by including the asymmetric wind responses, demonstrates that the essential elements of the redevelopment of La Niña arise from the nonlinear atmospheric response to SST anomalies.

In addition to the asymmetry of the air-sea interaction over the Pacific, possible impact of SST anomalies in the Indian Ocean on the ongoing El Niño is investigated, by use of an air-sea coupled general circulation model (CGCM). CGCM experiments are conducted by imposing the Indian Ocean basin-wide warming (BW), to assess the feedback effects of the El Niño-related SST anomalies on the Pacific. The BW during boreal winter enhances the surface easterlies over the equatorial western Pacific during the mature-decay phase of El Niño. These enhanced easterlies induce an advanced transition to La Niña phase. The results imply that the BW in the Indian Ocean, in some extent, can be hastening the El Niño to La Niña transition.

Finally, the relationship of the reproducibility between the climatological state and transition processes of warm/cold event of simulated ENSO are investigated based on the Coupled Model Intercomparison Project phase 3 (CMIP3) multi-model dataset. The mechanisms, in relation to a rapid transition of strong El Niño, are mainly related to the intensity of the simulated climatological precipitation over the western-central Pacific. The transition processes of the models, which have weak western central Pacific precipitation, are relatively later compared to those of the strong western central Pacific precipitation. This relationship is not applicable for the La Niña phase. The reproducibility of La Niña persistency is mainly related to the seasonal evolution of the climatological precipitation in the western central Pacific.

Key Words: ENSO, basin-wide warming, climate model, air-sea interaction, Pacific, Indian Ocean.

Contents

List of Tables

List of Figures

Chapter 1

Introduction

1.1 El Niño-Southern Oscillation

The El Niño-Southern Oscillation phenomenon (ENSO) is associated with a quasi-periodic (3-7-yr timescale) warming (El Niño) and cooling (La Niña) of the tropical central and eastern Pacific (180°-100°W) that influences the global climate. A number of investigators have suggested several conceptual theories to explain the self-sustained oscillation of the ENSO. Especially, the "delayed oscillator" (e.g., Schopf and Suarez 1988), "recharge oscillator" (e.g., Jin 1997), and "western Pacific oscillator" (e.g., Weisberg and Wang 1997) theories are three of the most influential ones, provided a comprehensive idea regarding cyclic nature of ENSO (Wang 2001).

The phase transition from an El Niño event to a La Niña one takes place through a delayed negative feedback that originates from ocean dynamical adjustments and related atmospheric responses. In particular, the theory of the "western Pacific oscillator" has focused on the role of the western Pacific wind variability in the ENSO transition. This theory emphasized a role for anomalous easterlies (westerlies) in the equatorial western Pacific during the mature phase of El Niño (La Niña). The wind anomalies excite the equatorial oceanic Kelvin wave response, which plays an important role in the ENSO transition. Recently, several studies have also suggested that the easterly wind anomalies during ENSO are associated with the anomalous Philippine Sea anticyclone (Wang et al. 2000; Kug and Kang 2006). These studies emphasized the role of the local air-sea interaction in the western Pacific (e.g., Wang et al. 2001; Wang and Zhang

2002). In the east (west) of the anticyclone, the anomalous anticyclonic winds enhance (reduce) the surface wind speed in the boreal winter, which favors local SST cooling (warming) through the modulation of the surface heat exchange and the ocean vertical mixing. The phase shift between the anticyclone and sea surface cooling implies a local feedback that can amplify and sustain the Philippine Sea anticyclone. Thus, the anomalous equatorial easterly wind can be regarded as a part of this anticyclone (Wang et al. 2001; Wang and Zhang 2002).

In the recharge oscillator mechanism, on the other hand, the negative feedback is achieved by the slow adjustment of the total heat content/mass due to the meridional mass exchange between the equator and off-equator (Jin 1997) and the zonal mass flux at the eastern and western boundaries (An and Kang 2000). Meinen and McPhaden (2000) found that the observations roughly follow the cyclic paths in the SST and the thermocline, confirming the phase relationship of the recharge oscillator picture. This mechanism adequately reproduces the linear oscillation of the ENSO; in other words, it demonstrates that the termination of El Niño is consistent with a cyclic nature. However, some studies have pointed out that a kind of break in the ENSO cycle has been observed when La Niña goes to El Niño. The air-sea coupled system over the Pacific somehow remains in a weak La Niña state for a while (Kessler 2002).

1.2 Asymmetry of the ENSO

Several observational studies have pointed out that El Niño is typically stronger than La Niña due to nonlinear dynamical processes (e.g., Burgers and Stephenson 1999; An and Jin 2004; An et al. 2005), a phenomenon which is particularly significant over the eastern Pacific. While the asymmetry of the ENSO is likely connected to its amplitude in relation to the nonlinear dynamics of the ocean surface processes, there are only few studies about the transition

process. Recent studies have reported that the asymmetric atmospheric response to the Pacific SST forcing causes the zonal shift of the SST pattern, which can enhance the difference in the location of the tropical heat source for El Niño and La Niña events (Kang and Kug 2002) as well as northward tele-connections thereafter (Hoerling et al. 1997; Hoerling et al. 2001). However, how these asymmetric atmospheric responses to the ENSO give feedback to these asymmetric features of their transition processes as argued in Kessler (2002) and Nagura et al. (2008) is not adequately clear.

The duration of a cold episode can cause severe droughts, such as those that took place in central Asia from 1999 to 2001 and are thought to be associated with the continuance of cold ENSO events (e.g., Hoerling and Kumar 2003; Ueda and Kawamura 2004). Given that the skill of seasonal climate forecasts hinges on predicting the ENSO signal accurately, the practical benefits of understanding the asymmetry in the duration of El Niño and La Niña may be important. Improvements in seasonal forecast skill can be expected by incorporating the effects of warm and cold ENSO events separately and will ultimately depend on clarifying the asymmetric impact of the atmosphere on the ocean subsurface.

1.3 Impact of the ENSO on the Indian Ocean

In comparison with the large fluctuations in SST in the tropical Pacific during ENSO, inter annual SST variations in the Indian Ocean are rather modest. Statistical analyses of historical SST records have indicated that the anomalous surface conditions of the Indian Ocean are highly correlated with ENSO events (e.g., Tourre and White 1995; Klein et al. 1999; Yu and Rienecker 1999; Alexander et al. 2002; Lau and Nath 2003). Some of these studies reported that the most dominant SST variation in the Indian Ocean is basin-wide warming (BW), typi-

cally appear several months after the mature phase of El Niño. Influence of the second dominant SST variations has also expanded considerably, recently, in part due to the debate about the Indian Ocean "Dipole/Zonal Mode" (IODZM). The mode of climate variability is associated with cooling in the equatorial eastern Indian Ocean and warming in the western basin during fall (Saji et al. 1999; Webster et al. 1999; Murtugudde and Busalacchi 1999). IODZM has two aspect of theory that the events are a coupled ocean–atmosphere mode internal to the Indian Ocean itself (e.g., Yamagata et al. 2003) or forced by ENSO (e.g., Xie et al. 2002; Hastenrath 2002; Annamalai et al. 2003: Tokinaga and Tanimoto 2004; Ohba and Ueda 2005) because of the high simultaneous correlation between IODZM and Niño-3.4 SST anomalies during fall (Allan et al. 2001; Baquero-Bernal et al. 2002).

The IODZM and the BW in the Indian Ocean appears to be primarily forced by SST anomalies in the equatorial eastern Pacific via atmospheric teleconnection (Lau and Nath 2003, 2004; Shinoda et al. 2004). Using the reduced gravity ocean mode and climate model, Ohba and Ueda (2005; 2009a) suggested that the IODZM and BW can be triggered by attenuated Walker circulation over the equatorial Indian Ocean associated with the El Niño event. These recent studies have emphasized the impact of El Niño on the Indian Ocean SST bears considerable season-dependent feature. The question is how these El Niño-related SST anomalies conversely affect the ENSO variability. However, the SST anomalies over the tropical Indian Ocean often co-occur with those in the tropical Pacific and therefore it is difficult to quantify their effects separately from observations alone. To study their individual effects, it is important to conduct a set of experiments by use of a stand-alone CGCM and caught the influence of the two Indian Ocean SST anomalies on the ENSO variability as a physical feedback to the ENSO.

Very recently, Annamalai et al. (2005) and Ohba and Ueda (2006) using the atmospheric

models, indicate that the Indian Ocean SST anomalies can influence zonal wind variation in the western Pacific. By analyzing the observational data and long-term CGCM simulation, Kug and Kang (2006) and Kug et al. (2006) suggest the presumable dynamics. As a forcing from the Indian Ocean to Pacific, above studies reveal the impacts of the Indian Ocean BW on the ENSO, paying attention to the atmospheric circulation. However, how the enhanced equatorial easterly gives feedback to the eastern Pacific subsurface and air-sea interaction over the western Pacific is not adequately clear.

1.4 ENSO in climate models

Recent assessments for the future climate projections are summarized in the Fourth Assessment Report of the Intergovernmental Panel on Climate Change (IPCC AR4). In this report, the future projections are based on 24 state-of-the-art CGCMs from many climate research centers and institutes of the world which participate in the World Climate Research Programme's (WCRP's) Coupled Model Intercomparison Project phase 3 (CMIP3: Meehl et al. 2007). However, by using the IPCC AR4 scenarios, future climate changes do not show any clear evolution of ENSO properties (Meehl et al. 2007, Guilyardi et al. 2009). Part of the uncertainty is due to model systematic errors. Indeed, CGCMs still have errors in reproducing the observed characteristics of ENSO events (AchutaRao and Sperber 2002; An et al. 2005; van Oldenborgh et al. 2005; AchutaRao and Sperber 2006; Joseph and Nigam 2006; Guilyardi 2006; Capotondi et al. 2006; Yamagucih and Noda 2006; Park 2008; Guilyardi et al. 2009; Lengaigne and Vecchi 2009). The simulated transition process of ENSO is directly linked with their frequency. However, many CGCMs tend to have occurred consistently with a strong cyclic nature, namely La Niña tends to turn into El Niño, suggesting the weak nonlinearity of ENSO (Hannachi et al.

2003). Monahan and Dai (2004) also analyzed several CGCMs and found that the nonlinear structure in ENSO simulated in CGCMs is highly model dependent. Many CGCMs fail to represent the spatial and temporal structure of the El Niño-La Niña asymmetry. They argued that the divergence between the nonlinearity of ENSO as simulated in different CGCMs is mainly from difficulties in representing the mean state of the tropical Pacific.

Recently, several studies have pointed out the dominant role of the atmospheric component in setting ENSO characteristics in state-of-the-art models (Guilyardi et al. 2004; Kim et al. 2008; Neale et al. 2008) with the change in the mean state of spatial SST and precipitation distribution. The change in the simulated climatological mean state can influence the ENSO-related feedback processes and have the potential to modify ENSO properties. However, it is unclear how these mean states are a key to correct ENSO biases. In order to further improve the simulated ENSO in the CGCMs, it is important to compare the detailed physical processes between the CGCMs and observations, and then assess the role of simulated mean state over the tropical Pacific. Therefore, the investigation of the cause of the discrepancy between the observation and simulation of ENSO in the CMIP3 CGCMs could also contribute to the understanding of the nature climate, namely on the decadal variation of the tropical Pacific state (e.g., Zhang et al. 1997) in relation to the asymmetry of ENSO (e.g., Dewitte et al. 2009; Choi et al. 2009).

1.5 Objectives

This study aims to investigate the mechanism of the seasonally asymmetric transition process of ENSO. The following three goals are the objectives of this study.

i) Our analysis of observational data and model experiments focuses on both the atmos-

pheric and oceanic components and tries to find more convincing evidence to support previous studies for the role that ENSO-related SST anomalies in the tropical region play in its transition.

ii) Our CGCM experiments, which cast a spotlight on the ocean components, seek more convinced evidences for the role of the Indian Ocean on ENSO transition so that will support the previous studies and confirms its impact on the El Niño itself.

iii) We identify the signature of the asymmetric transition process of ENSO in each of the CMIP3 climate model and investigate its relationships to their atmospheric climatological Pacific conditions in the models.

The paper is organized as follows. Section 2 presents the datasets used and a brief description of models. Section 3 examines the asymmetric feature of the transition process between the warm and cold ENSO. Section 4 examines dynamical response of the El Niño in the CGCM to SST anomalies in the Indian Ocean. Section 5 examines the feature of the transition process of the warm and cold ENSO in CMIP3 CGCMs. Finally, we summarize our conclusions in Section 6.

Chapter 2

Data and Model

2.1 Observational data

This study mainly focuses on the tropical Pacific and Indian Ocean, defined as 40°S-40°N, 40°E-60°W. We use the Niño-3.4 index, which is area averaged SST over the equatorial central eastern Pacific (5°S-5°N, 170°-120°W) in each CGCM. As is well known, the Niño-3.4 index adequately captures both the warm and cold ENSO events. We define months in the ENSO onset year as (0) and those in the succeeding year as (1).

We utilized the European Center for Medium-Range Weather Forecasts (ECMWF) Re-Analysis (ERA-40; Simmons and Gibson 2000) as atmospheric data. These data cover the period from mid-1957 to mid-2002. SSTs are from the Extended Reconstructed Sea Surface Temperature, version 2 (ERSST.v2; Smith and Reynolds 2004). For the calculation of the interannual fluctuation of the SST and the reanalysis data, we also apply a high-pass filter to temporarily remove periodicities longer than ten years. In order to analyze the simulated anomalous precipitation for long period, we also use the monthly averaged vertically integrated apparent heat sources (Q_1, Yanai et al. 1973) in place of precipitation. Q_1 reflects the contributions from individual physical processes, such as radiative heating, cumulus convection, and turbulent processes. It is well known that convective heating contributes the most to the total Q_1 exceeding the radiative cooling and turbulent processes at the low level. The Q_1 anomalies are obtained from the ERA40 by use of classic Q_1 and Q_2 approach (Yanai et al. 1973; Ishizaki and Ueda 2006). We also use the CPC Merged Analysis of Precipitation (CMAP; Xie and Arkin

1997) for climatological precipitation. Oceanic three-dimensional temperatures are obtained from the Simple Ocean Data Assimilation (SODA) reanalysis (Carton et al. 2000) and are available for the 47-year period from January 1958 to December 2004.

2.2 Climate model

The model we use is MRI-CGCM2.3, the latest version of the air-sea coupled model developed at Meteorological Research Institute in Japan (Yukimoto et al. 2001; Yukimoto et al. 2006). The model consists of an atmospheric general circulation model (AGCM) coupled with an oceanic general circulation model (OGCM). The AGCM is a global spectral model, which we ran at T42 resolution with 30 sigma-pressure coordinate levels in the vertical. The nonlinear terms and the parameterized physical processes are calculated on a 128 × 64 Gaussian grid with a horizontal resolution of about 2.8° × 2.8°. Readers are referred to Shibata et al. (1999). The oceanic component of the model is a Bryan-Cox type OGCM with a global domain. The horizontal grid spacing is 2.5° in longitude and 2.0° in latitude. The meridional grid spacing is non-uniform with the finest resolution of 0.5° near the equator (between 4°S and 4°N) gradually increasing to 2.0° pole ward of 12°S and 12°N. This finer resolution enables the OGCM to give a better representation of the equatorial oceanic waves. This model includes both of a land process and a sea ice model. The simulated SST pattern in relation to the ENSO activity in the tropical Pacific is similar to what is typically observed (Yukimoto and Kitamura 2003), with a somewhat higher frequency. The CGCM control run also well reproduces the Indian Ocean SST anomalies both of IODZM in the fall and BW in winter to spring. We define months in the El Niño onset year as (0) and those in the succeeding year as (1).

Figure 2.1 shows a time series of simulated SST anomalies averaged in the Niño-3.4 region (5°S-5°N, 170°-120°W) and central Indian Ocean (20ºS-20ºN, 50º-100ºE) in the 75-yr CGCM control run. The correlation coefficient between the Indian Ocean and Niño-3.4 SST anomalies in the CGCM is 0.74 by a 3-month lag, which implies that the relationship between the Indian Ocean and Pacific is clearly simulated with a slightly stronger link, compared with the observation (Klein et al. 1999; Ohba and Ueda 2005). Thus, the CGCM broadly simulates the interaction between the Indian Ocean and Pacific, which enables us to conduct idealized experiments in view of air-sea coupled system.

2.3 1.5-layer linear ocean model

To estimate the variation of the equatorial central eastern Pacific thermocline due to the remote surface wind forcing, a 1.5-layer reduced-gravity ocean model (Zebiak and Cane 1987) is used. The model grid has a horizontal resolution of 1° latitude by 0.5° longitude. The SST is determined by a balance between the surface heat fluxes, horizontal advection due to imposed winds, horizontal diffusion, and entrainment from below the mixed layer. The length of the spin-up period is 3 years. To compute the surface-sensible and latent heat fluxes, we use a standard bulk formula. Short- and long-wave radiation data are obtained from the atmospheric reanalysis data. In this model, the sea water temperature anomaly below the mixed layer, hereafter referred to as the subsurface temperature, is estimated on the basis of the thermocline depth anomaly.

2.4 CMIP3 multi model database

The simulations analyzed in this paper are largely from models available via the

IPCC-AR4/CMIP3 database (Meehl et al. 2007). Analyzed data are basically obtained from the twentieth century (20C3M) simulation of the CMIP3 data for 100-year (1900–1999). The comparison about the El Niño amplitude is not the purpose of the paper. Our target is mainly asymmetric transition process of relatively strong ENSO events. Hoerling et al. (2001) reported that the nonlinearity in atmospheric responses requires that central eastern Pacific SST anomalies exceed one standard deviation of their interannual variability. Therefore, the asymmetry of ENSO is strong in the strong ENSO events (Ohba and Ueda 2009b). To capture the more systematic biases that do not depend on the amplitude of the simulated ENSO, the following seven models with the Niño-3.4 indices standard deviations less than a half or more than twice of the observed ones are not applied for this study; CGCM3.1-T47, CGCM3.1-T63, GISS-AOM, GISS-ER, IAP-FGOALS1, MIROC3.2-hires and MIROC3.2-medres. The model list is given in Table 2.1, including their short names used in this paper. In this study, we focus on the interannual fluctuation of the CGCM systems, without introducing added complexity of changes in radiative forcing. Therefore we apply a high-pass filter to temporarily remove periodicities longer than twenty years. The datasets are interpolated (2-D linear interpolation) onto a common 2.5° longitude by 2.5° latitude grid. Monthly anomalies are calculated by removing a mean climatological cycle.

2.5 One-sided linear regression

We conducted one-sided linear regression (and correlation) analysis separately for positive and negative Niño-3.4 indices, as Hoerling et al. (2001) did. The procedure involves calculating the linear relation between all occurrences of one sign of the index and the observational data. Anomalies used in this analysis are calculated with respect to means based on samples asso-

ciated with a single sign of the SST index. The one-sided regressions are estimated from half of the record of the observational data. The regressions thus indicate the change of a particular atmospheric and oceanic variable for a unit change of the warm or cold index. In the method of one-sided regression as implemented herein, the regression lines cut through the point corresponding to the average of the prediction for all warm (cold) SST states, as determined by the positive (negative) values of the Niño-3.4 index. Our argument is available for mainly strong El Niño or strong La Niña case rather than a moderate El Niño or La Niña case.

ID	Model	Short name	Country
A	BCCR-BCM2.0	BCCR2	Norway
B	CNRM-CM3	CNRM	France
C	CSIRO-MK3.0	CSIRO	Australia
D	CSIRO-MK3.5	CSIRO35	Australia
E	GFDL-CM2.0	GFDL0	USA
F	GFDL-CM2.1	GFDL1	USA
G	GISS-EH	GISSh	USA
H	UKMO-HadCM3	HadC3	UK
I	UKMO-HadGEM1	HadGem	UK
J	INGV-ECHAM4	INM	Italy
K	INM-CM3.0	INGV	Russia
L	IPSL-CM4	IPSL	France
M	MIUB-ECHO-G	MIUB	Germany, Korea
N	ECHAM5/MPI-OM	MPI	Germany
O	MRI-CGCM2.3.2	MRI	Japan
P	NCAR-CCSM3	NCARc	USA
Q	NCAR-PCM	NCARp	USA

Table 2.1: List of the CGCMs used in the present study.

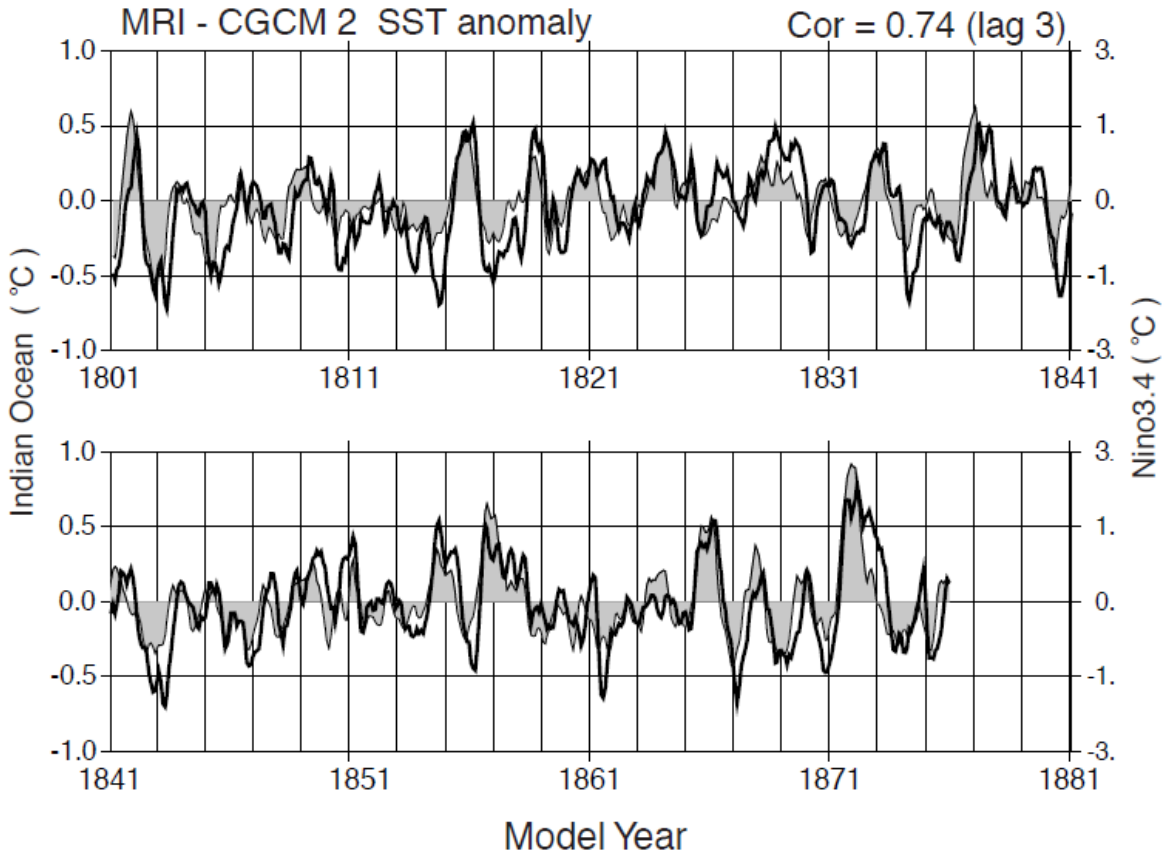

FIG. 2.1: The 3-month running mean of simulated SST anomalies (solid line) over the Indian Ocean (20ºS-20ºN, 50º-100ºE), and Niño-3.4 SST anomalies (light shading: 5ºS-5ºN, 170º-120ºW).

Chapter 3

Asymmetric transition process of ENSO

3.1 Asymmetric feature of the transition process between El Niño and La Niña

In this section, an analysis of the temporal evolution of the atmospheric and oceanic component for the area-average over the Niño-3.4 region is discussed using the ERSST.v2, ERA40, and SODA. The datasets are analyzed for the 47-year period from January 1958 to December 2004. Displayed in Figs. 3.1a and 3.1b are the evolutions of the equatorial monthly mean SST anomalies obtained through one-sided regressions to positive DJF (0/1) Niño-3.4 SST (El Niño: Fig. 3.1a) and negative (La Niña: Fig. 3.1b) phase. Concurrent with the mature phase of the warm and cold events, substantial anomalies are manifested over the central eastern Pacific. A closer look at Fig. 3.1 will demonstrate that some conspicuous features are apparent. One of the most remarkable features is the difference in spatial structure. The location of the maximum SST anomaly during La Niña is shifted to the west by about 30° in the central eastern Pacific relative to that of El Niño. This asymmetric structure of the SST anomalies is consistent with the composite analysis conducted by Hoerling et al. (1997). It is particularly noted that the following SST anomalies on the positive phases turn into a negative phase in the following year (Fig. 3.1a). In contrast, the negative event is not resulted in the significant opposite SST anomalies (Fig. 3.1b), suggesting that the cold events tend to remains cold SST anomalies. This is

consistent with recent studies (Kessler 2002) indicating the less cyclic nature of La Niña termination. Thus, to some extent, the separate regression for the positive/negative index could capture the nature of ENSO asymmetries.

Presented in Figs. 3.1c and 3.1d is the 20°C isotherm depth (Z20, a widely used proxy for thermocline depth). In a simple theoretical analysis based on a Zebiak and Cane (1987) modeling framework, Z20 is determined to be of critical importance for the ENSO cycle and is often referred to as the indicator of the so-called thermocline feedback in the tropical coupled ocean-atmosphere interaction. The modulation of the Z20 describes the most important dynamical feature in both wave transition-type oscillators (delayed-oscillator/western Pacific-oscillator) and recharge oscillator paradigms. In agreement with the theories, the Z20 shown in Fig. 3.1c not only serves as the key positive feedback that overcomes a damping effect but is also one of the primary factors responsible for the phase turnaround from warm to cold. Eight months prior to the peak warm phase of the ENSO, the thermocline feedback already contributes to the initiation of warming, whereas, after the peak of the warm phase, the Z20 gives rise to a cooling of the SST (Fig. 3.1c).

A closer look at Figs. 3.1c and 3.1d shows that the Z20 is considerably different during the mature to the decay phase of the ENSO between the warm-to-cold and cold-to-warm phases. In the warm phase, as presented above, the turnabout of the thermocline anomalies is recognized in the DJF (0/1) (Fig. 3.1c), namely, in its mature phase. The ENSO transition from the El Niño to the La Niña phase is well established in the calendar end of the following year in Fig. 3.1a. However, that of the negative phase is not. Its turnabout in the negative phase (cooling to warming) is delayed by about one season (Fig. 3.1d) relative to that in the positive phase. Thus, the cooling via thermocline feedback continues until March (1). The following positive over the

central Pacific is also considerably weak. It is conceivable that the difference in Z20 could be one of the most important points for the asymmetric behavior of the ENSO.

The thermocline feedback is regulated by the modulated ocean dynamical feature in both the equatorial wave transition and the meridional mass exchanges through the Sverdrup transport. The Sverdrup transport reflects a variation of the meridional mass transport under the ocean Ekman layer. As in previous studies (e.g., Jin 1997; Meinen and McPhaden 2000), the meridional heat flux under the Ekman layer interferes with the evolution of the ENSO event in both the warm and cold phases (not shown). However, in terms of their total contribution to the ENSO, the processes are nearly symmetric during the mature to the decay phase of El Niño and La Niña events. The zonally integrated meridional heat flux over the off-equatorial region reveals a relatively symmetric behavior (not shown).

To describe the time evolution of the ENSO transition in relation to variability in wind forcing, we also plot a longitude-time section of the regression on the zonal wind anomalies and time rate of the change in Z20 near the equator (Fig. 3.2). A precursor to the ENSO phase transition is the buildup of heat content in the western Pacific (Weisberg and Wang 1997; Guilyardi et al. 2003), which is attributed to western Pacific wind changes (Wang et al. 1999). Displayed in Figs. 3.2a and 3.2b, respectively, are the evolutions of monthly mean surface zonal wind anomalies obtained through the regression to DJF Niño-3.4 SST anomalies in the positive and negative phases. In the developing stage of El Niño (from June through October), the Pacific wind anomalies in the western Pacific are relatively close to the opposite of that of La Niña (Figs. 3.2a and 3.2b). A strong anomalous westerly (easterly) at the surface is recognized during the developing stage of El Niño (La Niña), corresponding to the atmospheric response to the associated heating (cooling) over the central eastern Pacific. In contrast, the anomalous westerly

in the central eastern Pacific is rapidly reduced in the mature phase of El Niño (Fig. 3.2a), which may be related to the southward shift of the peak of the anomalous zonal wind during the boreal winter (Harrison and Vecchi 1999; Vecchi and Harrison 2003). The wind changes over the equatorial central Pacific can generate eastward-propagating thermocline shallowing, leading to the turnaround of the SST tendency in the central eastern Pacific.

In correspondence to the rapid reduction of the equatorial westerly anomalies, easterly wind anomalies intrude on the equatorial western Pacific over the 120°E-160°E. The wind anomalies are mainly forced by the anomalous SST cooling in the western-north Pacific (e.g., Wang et al. 2000) and basin warming in the Indian Ocean (e.g., Annamalai et al. 2005). In contrast, the anomalies in the equatorial western Pacific at the mature phase of La Niña still remain easterlies over the central Pacific (Fig. 3.2b). The significant anomalous easterlies continue into the next season. Although the zonal wind over the western Pacific during the decay phase of the warm ENSO shows a strong easterly, this is not clear in the cold phase.

The zonal wind stress associated with the surface wind anomalies directly displaces the thermocline vertically via Ekman pumping. The anomalies rapidly propagate eastward and then change the oceanic vertical structure in the equatorial Pacific. Thus, we will show the observed equatorial thermocline behavior, especially at the end of the warm and cold ENSO. In Fig. 3.2, we additionally present the time rate of the change in the equatorial Z20 (Figs. 3.2c and 3.2d) lag-regressed onto the DJF Niño-3.4 SST anomalies. In tandem with the slow eastward movement of the equatorial zonal wind anomalies, both phases show a slow eastward propagation of Z20 anomalies in their developing stage (e.g., Chao and Philander 1993). The opposite Z20 anomalies in the equatorial western Pacific appear in the mature phase of the El Niño event. This negative anomaly then propagates eastward along the equator and forces the El Niño event

to terminate (Fig. 3.1a). Although the evolution of the Z20 in the cold phase is similar to that in the warm phase, the temporal progress of the thermocline in the decay phase is obviously different, as demonstrated in Fig. 3.1d.

In the mature to the decay phase of the warm (cold) ENSO event, seasonally fixed shallowing (deepening) anomalies of Z20 take place along the equatorial band (Figs. 3.2c and 3.2d). In the warm phase, the signal of Z20 shallowing propagates eastward from western Pacific at a speed of about 40-50 longitudes per month, roughly the propagation speed of the first and second baroclinic Kelvin modes (e.g., Boulanger et al. 2003). The amplitude increases eastward. As a consequence, the warmed condition in the eastern Pacific starts to recover its slope and returns to the cooled condition (not shown). This is the linear response of the ocean to a wind forcing, which could be recognized as a combination of a weakening of the central eastern Pacific westerly and an intrusion of the western Pacific easterly anomalies at the equator. In comparison with the Z20 tendency in the warm phase of the ENSO, the anomalies in the cold phase decrease gradually and retain the negative anomalies in the boreal spring (Fig. 3.2d). From winter to spring, the tendency at the east of 160°E takes negative values. The adjustment of the thermocline depth is relatively slow and, therefore, could be recognized as a result of the horizontal heat transport via the anomalous geotropic current rather than the propagation of the Kelvin wave.

Near the end of the calendar year, the responses of the atmosphere to the mature phase of the ENSO have asymmetric features, especially over the equatorial western Pacific. To seek more conclusive evidence to confirm the difference in the atmospheric responses between the warm and cold phases of the ENSO, we show the one-sided regression of the vertical integrated monthly average apparent heat sources (Q_1, Yanai et al. 1973) with the surface wind vector in

SON (0), DJF (0/1), and MAM (1) (Fig. 3.3) onto the DJF Niño-3.4 index. Q_1 reflects the contributions from individual physical processes, such as radiative heating, cumulus convection, and turbulent processes. It is well known that convective heating contributes the most to the total Q_1 exceeding the radiative cooling and turbulent processes at the low level. The Q_1 anomalies are obtained from the ERA40 by use of classic Q_1 and Q_2 approach (Yanai et al. 1973).

The anomalous spatial patterns of Q_1 associated with El Niño and La Niña, respectively shown in Figs. 3.3a and 3.3b, have some differences from each other; the first is that the location of the maximum Q_1 anomaly during La Niña is shifted to the west in the central Pacific relative to that of El Niño. Associated with the westward shift of Q_1, the spatial pattern of surface wind anomalies during La Niña shown in Fig. 3.3b is also shifted to the west relative to the positive phase. The second is the evolution of the anomalous wind and Q_1 after their mature phase. The reduction of the diabatic heating over the central Pacific during La Niña event remains mature at the equatorial region in the decay phase. However, the spatial pattern of El Niño is shifted southward across the equator, and the anomalous equatorial westerlies over the central eastern Pacific then turn into a cross equatorial northwesterly in the DJF (0/1). This process is closely linked to the seasonal warming of the southern part of the off-equatorial Pacific from the boreal winter to spring (Vecchi 2006), which could be associated with the generation of the double ITCZ (Intertropical Convergence Zone) in the eastern part of the basin. The third is the generation of the anomalous equatorial wind over the western Pacific opposite to the wind direction over the central eastern Pacific, which is attributed to the additional hastening process to the ENSO transition (Wang et al. 1999). In the MAM (1), the anomalous surface wind over the western-north Pacific in the warm phase is relatively similar to that in the cold phase. Thus, the asymmetry of the atmospheric response is particularly strong from the boreal

winter to spring.

3.2 Model study

In this section, the nature of the asymmetric transition process of ENSO is studied with idealized experiments by use of AGCM and 1.5-layer reduced gravity ocean model. Presented figures in this section are base on the model simulation.

3.2.1 Experimental design of the symmetric SST experiment

The westward shift of the anomalous atmospheric responses during the negative phase of ENSO is mainly due to the zonal asymmetry of the climatological SST, as pointed out by Hoerling et al. (1997). In the western Pacific, the diabatic heating/cooling associated with the anomalous convection appears to be proportional to the SST anomaly. On the other hand, a strongly nonlinear relationship exists in the central eastern Pacific; in other words, the convective activities for the cold phases of the SST anomaly have no further effect on the relatively cold eastern Pacific (Hoerling et al. 2001). Equatorial wind anomalies over the Pacific are important to excite oceanic Kelvin waves, which rapidly propagate eastward and then change the oceanic vertical structure in the equatorial Pacific. Thus, the question we will address is whether the asymmetric surface wind variation recognized as an atmospheric response to El Niño and La Niña can affect the decaying phase of the ENSO itself.

By use of symmetric SST anomaly forcing, recent studies with an atmospheric general circulation model (AGCM) demonstrated that the difference between the spatial structure of El Niño and La Niña is caused by the nonlinearity in the tropical convection (Kang and Kug 2002). Our simple experiment is relatively similar to those in Kang and Kug (2002) but focuses on the

self-transition process. In their experiments, the AGCM runs are fixed in the boreal winter condition. Our experiments extend their experiments for temporal direction and evaluate the importance of the seasonality on the ENSO transition. It is useful and illuminating to simply show the atmospheric response to the SST anomalies over the tropical Pacific, which could be important to understand the observed response of the transition process of the ENSO. The following experiments using the AGCM may provide sufficient support for the present study.

To isolate the effect of the SST on the Pacific, two AGCM experiments are carried out. In the first experiment, SST anomalies in relation to the positive phase of the ENSO are imposed for two years from January (0) through the following December (1) in the Indian Ocean-Pacific; ENSO-related SST forcing is specified for the Indian Ocean-Pacific sector, and the monthly varying climatological values are prescribed in the other regions. We use the SST anomalies derived from El Niño minus La Niña composite. This experiment can fairly estimate the asymmetric response of the surface wind to the SST forcing. In the following, this experiment is referred to as the forced symmetric positive phase (SP) run. The second experiment is similar to the SP run except that the cold phase SST anomalies are imposed for the region. This experiment is referred to as the forced symmetric negative phase (SN) run. The symmetric negative (SN) run uses the same SST forcing but opposite (multiplied -1) anomalies. In both the SP and SN runs, the ENSO-related SST anomalies over the central eastern Pacific peak in December (0) and turn into the opposite phases in July (1) of the following year. Displayed in Fig. 3.4 is the imposed SST anomaly during the DJF (0/1) and the time series of the Niño-3.4 index. As the boundary forcing, the SST anomalies are derived from the ERSST.v2. We extracted the five strongest El Niño years (1965, 1972, 1982, 1987, and 1997) and La Niña years (1955, 1973, 1988, 1998, and 1999) measured by the DJF Niño-3.4 SST in the period from 1950 to 2004.

The time-series is also derived from the difference between the positive and negative phase of ENSO composites from the onset year to decaying year. Therefore, their time-series are approximately intermediate between the positive and negative phase of ENSO. Because of the strong and stable transitional mechanism of El Niño events, the SST forcing used in this experiment turns into opposite phase at the boreal summer in the following year.

Outside of the basin, we use the climatological SST, derived from the 50-yr mean of the ERSST.v2. For each forcing scenario, the model is run for the 2 yr from January through the following year without a sufficiently long spin-up period. To account for the atmospheric sensitivity to the initial conditions, a 15-member ensemble approach is conducted for each forcing scenario. The initial conditions, January 1, are taken from the AGCM control run, in which the climatological SST was used as the boundary forcing. We only change the initial conditions selected from 15 snapshots of the AGCM control run in preserving the same SST forcing. Our experimental setup only uses the composited SST anomalies as an alternative of the individual ENSO events. This experimental setup allows us to catch the qualitative feature involved in the air-sea coupled system in the Pacific.

3.2.2 Impact of the SST anomalies and asymmetry of the resultant equatorial wind

Figure 3.5 shows the composited anomalies of precipitation and wind stress over the Pacific for each forcing scenario during the DJF (0/1). The results presented here are based on ensemble averages over 15 individual integrations. The anomalies are obtained by the difference from the climatology of the 50-year AGCM control run, in which the climatological SST derived from the observational data is prescribed. In both experiments, the simulated precipitation ano-

malies during the DJF (0/1) have a large-scale structure, recognized as the east-west contrast between the western Pacific and the central Pacific. As is evident in Fig. 3.5, the SP and SN runs can reproduce many of the features of the zonal wind stress evolution seen in the observation (Fig. 3.3); the character of the evolution of the near-equatorial precipitation variability agrees with the available observations as well. The SP run reveals an anomalous anticyclonic circulation centered over the Philippine Sea during DJF (0/1) and strong positive precipitation anomalies to the east of the date line. The most plausible explanation for the generation of equatorial western Pacific easterlies is related to the SST cooling of the western-north Pacific and the warming in the Indian Ocean, which possibly cause the enhancement of the Philippine Sea anticyclone (e.g., Wang et al. 2000; Watanabe and Jin 2002). The equatorial easterly anomalies over the western Pacific can be regarded as a part of this anticyclone. Although the cyclonic circulation is clearly seen over the Philippines, as suggested by Wang and Zhang (2002) and Wang et al. (2001) in the SN run, the center of the circulation is shifted north-westward compared to the opposite experiment. Therefore, the westerly wind anomalies are distant from the equatorial western Pacific, and, rather, easterly anomalies are dominant over the region.

A comparison of the wind stress anomalies between the SP and SN runs clearly exhibits the asymmetric role of the atmosphere in response to the symmetric SST forcing (Figs. 3.5a and 3.5b). Although the SP run reveals strong easterly anomalies in the equatorial western Pacific centered around 140°E, the SN run does not, suggesting that the nonlinearity in tropical convection causes not only the difference in its amplitude (Hoerling et al. 2003) but also the spatial distribution. The maps also show that the southward shift of the zonal wind anomalies over the central eastern Pacific is only seen in the positive phase. These differences might be accounted for by a zonal shift of the convection anomalies. Compared to the active convection in the SP

run, the center of the suppressed anomalies in the SN run slightly shifted westward by about 20-30 degrees. In particular, it can be also seen that the spatial pattern over the simulated precipitation anomalies at around 150-170°E, 0-15°N are the same sign. These features are quite similar to the observation (Fig. 3.3). Thus, the asymmetric circulation patterns during the mature to the decay phase of the ENSO are recognized as a result of the nonlinear atmospheric response to the ENSO-related symmetric SST anomalies. The seasonally-fixed rapid change of the air-sea coupled system could be a trigger for the ENSO termination. The spatially asymmetric response to the opposite SST anomalies might be important to understand the asymmetric transition process of the ENSO.

To seek more convincing evidence for the impact of the asymmetric atmospheric response on the asymmetric ENSO transition, we plotted a time series of the simulated wind stress anomalies along a narrow equatorial band 2°S-2°N (Fig. 3.6). Near the end of the calendar year, there is a southward shift of the equatorial zonal wind anomalies. Using complex models, Vecchi and Harrison (2006) and Vecchi (2006) showed that this feature is related to the seasonal movement of the warmest SST to south of the equator, which changes the convective anomalies from centered on the equator to centered south of the equator. The shift of the wind could be a main mechanism for the thermocline shallowing (Harrison and Vecchi 1999). Following the anomalous zonal wind shift, the thermocline at the eastern Pacific returns to its normal condition. Recent studies (e.g., Kug and Kang 2006) additionally pointed out the importance of the equatorial trade wind in the western Pacific and the subsequent ENSO turnabout. Therefore, it will be useful to look at the timing of the reduction of equatorial zonal wind anomalies.

In Fig. 3.6, we show the time evolution of the composited anomalies of the zonal wind

stress for each experiment, zonally averaged on the equatorial Pacific region. Following the onset of positive (negative) ENSO SST anomalies, the westerly (easterly) wind stress anomalies gradually increase in these experiments. In the positive phase experiments (thin and bold solid lines), maximum westerly wind anomalies appear in the boreal fall. The SP run reveals a rapid decrease in the anomalies at the mature phase and gets closer to zero in the subsequent season. The rapid reduction of the zonal wind stress can be accounted for by the southward shift of the anomalous westerly and the expansion of the easterly over the western Pacific, which acts as a counterbalance to the westerly. In comparison with the westerly anomalies in the positive phase experiments, opposite anomalies in the negative experiments decrease gradually from the boreal winter to the spring of the subsequent year. Therefore, the equatorial easterlies remain for the boreal winter and subsequent season.

3.2.3 Impact of the symmetric SST forcing on equatorial thermocline variation

The differences in the wind stress anomalies in response to the symmetric SST forcing are expected to contribute to the asymmetry of the ENSO variability because the central eastern Pacific SST is closely related to the equatorial zonal wind through the generation of oceanic upwelling Kelvin waves. The resultant eastward propagation of the Kelvin wave induces thermocline displacement, which can potentially contribute to the demise of warming or cooling of the central eastern Pacific. To explore the relative importance of the difference in directly forced motions between the warm and cold phase, we carried out a series of idealized ocean experiments in an initially quiescent ocean (by using the climatological condition) of the 1.5-layer ocean model. The 1.5-layer ocean model is suitable for our purpose because it has been used in many studies of the ENSO (e.g., Zebiak and Cane 1987; Yan and Wu 2007). The

control simulation forced by the ERA-40 surface conditions and momentum flux adequately capture the asymmetric feature of the thermocline and SST variation (not shown), as seen in the observation (Fig. 3.1). Two experiments are additionally conducted by use of the ocean model. We imposed the anomalous wind stress derived from the SP and SN runs, maintained from the "ENSO" onset (April of the onset year) to its decay (July of the following year). The wind stress forcing is limited to the tropical Pacific region (130°E-90°W, 30°S-30°N). These experiments are named OSP and OSN runs; the letter O is added to refer to each AGCM experiment. This allowed us to evaluate the quantitative difference in the wind-induced response generated from the ENSO asymmetry.

In Fig. 3.7, we show the time evolution of the simulated thermocline depth anomaly on the Eastern Pacific 150°W-110°W, 5°S-5°N. Following the onset of surface westerly (easterly) wind anomalies in relation to the boundary "ENSO" forcing, the thermocline deepens (shallows) progressively in OSP (OSN), as expected from linear theories. In the OSP run, the maximum thermocline depth occurs in November (0) and is followed by rapid shoaling through the subsequent boreal winter. The rapid shoaling continues until May (1) and reaches values of about -15 m. In contrast, the recoveries on the OSN run are significantly weaker than those in the OSP. The negative anomalies of the thermocline depth continue until the end of the boreal spring (Fig. 3.7b). Thus, the OSN run does not cause significant thermocline deepening until the wind anomalies are removed. It is evident that the asymmetry of the directly wind-forced motions over the equatorial Pacific results in the difference in the thermocline variation in the idealized experiments.

These results imply that the gradual decrease of the thermocline depth anomalies over the eastern part of the Pacific in the decay phase of La Niña is mainly due to the equatorial wind

forcing. As suggested in a previous study, the seasonal changes in the state of the ocean may impact the coupling strength (e.g., Xie 1995) and are especially strong during the boreal summer-fall (e.g., Zebiak and Cane 1987; Galanti et al. 2002). If the thermocline anomalies over the Pacific maintain the negative phase with the cold SST in the boreal spring to summer, the air-sea coupled system could strengthen the anomalies. Therefore, the slow thermocline displacement could be a trigger for the redevelopment of La Niña.

3.3 Cyclic and noncyclic nature of the ENSO

Now, we intend to demonstrate, using an intermediate coupled model, that the duration mechanism of the ENSO could be involved in the air-sea coupled system in the Pacific, as suggested in the section above. The coupled model covers the entire tropical Pacific. The oceanic component is a 1.5-layer linear ocean model. The empirical model used for the atmosphere describes seasonally different anomalous wind responses to the underlying SSTA over the central eastern Pacific (Fig. 3.8). A certain type of surface response is switched on when SST anomalies appear in the Niño-3.4 region. Three types of anomalous wind patterns are derived based on regressions of the observed wind with the SST anomalies over the Niño-3.4 region. The amplitude of the wind response is defined to be a unit value, which corresponds to the box-averaged SST anomalies in the region.

There are two different models. The first uses a type 1 wind response (Fig. 3.8a), which is derived from a standard linear regression on the simultaneous Niño-3.4 index. This model uses the same spatiotemporal pattern of wind stress for the positive and negative phases of Niño-3.4 SST. Thus, this wind type assumes that the atmospheric response to the warm and cold ENSO is symmetric. The second model considers the effect of asymmetric wind patterns. For this

purpose, we employed the same model used above except that the wind responses were derived from the one-sided regression on the observed surface wind patterns. The wind responses in the warm and cold phases are presented in Figs. 3.8b (type 2) and 3.8c (type 3), respectively. Type 2 (type 3) of the atmospheric response is switched on when the Niño-3.4 SST anomalies present positive (negative) values. In order to use the observed wind anomalies in the Pacific domain, the spatial function of the wind stress is multiplied by a weighting function, which is unity between 30°S and 30°N and decays poleward with a zero value at 40°S and 40°N.

The coupled model is integrated for 60 yrs. Figure 3.9 shows the time evolution of the SST anomalies averaged in the Niño-3.4 region after a 15-year spin-up period. As seen in the figure, the coupled models produce an ENSO-like oscillation with slightly strong amplitudes for both El Niño and La Niña. In the first intermediate coupled model, an oscillator solution with a period of about 2 yrs emerges in a reasonable parameter regime (Fig. 3.9a). The SST anomalies in the region show a pronounced linear oscillation with relatively reasonable amplitude. Corresponding to the earlier oscillation mechanisms, the ENSO transition system is apparently symmetric. The termination of both El Niño and La Niña is consistent with a cyclic nature.

On the other hand, when we use the asymmetric wind responses, the oscillation is significantly modulated (Fig. 3.9b). The present model produces an asymmetric behavior of the ENSO and then, to some extent, simulates the observed characteristics of the ENSO more closely. Although the model could not capture the rapid development of the warm event associated with stochastic atmospheric forcing of the tropical weather system, their rapid transition to the cold phase is well reproduced. It is especially noteworthy that the coupled model with the asymmetric atmosphere reasonably reproduces the observational redevelopment of La Niña. The coupled experiment above suggests that the duration of La Niña can be attributed to the asym-

metric atmospheric responses to the Niño-3.4 index, which causes a modulation of the oscillator dynamics.

We also conduct additional model experiments by use of larger atmospheric surface wind anomalies in response to a given value of the Niño 3.4 SST anomalies. Presented in Fig. 3.9c is the result of the experiment of which the atmospheric sensitivity to the SST is multiplied by 1.2. The higher atmospheric sensitivity results in the enhanced asymmetry on the evolution of the warm and cold events. Duration of the cold phase of ENSO in the model is more salient and becomes longer, although the ENSO transition from the warm to cold phase is differ little from Fig. 3.9b.

3.4 Concluding remarks

Recently, some observational studies have indicated that, while the termination of El Niño is consistent with a cyclic nature, its initiation is less obvious (Kessler 2002). Using the method of one-sided regressions applied to reanalysis data and simple experiments by use of AGCM, we have confirmed the existence of asymmetric responses of the atmosphere associated with the opposite phases of the ENSO, especially at the calendar year end. Regarding the nonlinear response of the tropical convection, the air-sea coupled system over the tropical region tends to facilitate the warm-to-cold ENSO transition more rather than the cold-to-warm phase. This asymmetric behavior witnessed in observations is reproduced in simple experiments to some extent, implying that our suggestions capture a part of the air-sea coupled system, which causes the redevelopment of the La Niña event.

The asymmetric transition process of the ENSO is illustrated schematically in Fig. 3.10. The atmospheric response for the warm phase of the ENSO causes a rapid reduction of the zonal

wind stress at the equator via a southward shift of the anomalous westerly and an enhancement of the western Pacific easterly in relation to the Philippines anticyclone, as shown in the upper-middle panel in Fig. 3.10. This process plays a significant role in accelerating the following ENSO transition through a displacement of the thermocline depth anomalies (Fig. 3.10: top-right panel). However, the anomalous equatorial easterlies on the cold event persist until the subsequent spring, which tends to counteract the turnabout from a cold to a warm event of the ENSO, as illustrated in the bottom-middle and -right panels. Enhanced equatorial rainfall during stronger warm events expands eastward across the climatological cold tongue, whereas suppressed rainfall during cold events is displaced toward the climatological warm pool. Namely, it is conceivable that the main reason for the asymmetric response is connected to the both western Pacific wind anomalies (i.e., western Pacific oscillator) and wind anomalies over the central eastern Pacific. These asymmetries of the atmospheric responses to the SST are strong especially in the boreal winter to spring.

The difference in a seasonally fixed spatial shift of the tropical anomalous convective activity, which is apparent in observations, is replicated in the AGCM experiments by use of symmetric “ENSO” SST forcing. A qualitatively similar or relatively weak phase shift of the local convection occurs over the tropical Pacific region. The larger phase shift of the atmospheric response is particularly noted at the western Pacific in both the observations and experiments. A simple experimental approach by use of the composited SST anomalies succeeds in producing asymmetry of the thermocline variation associated with the nonlinear response of the atmosphere to underlying SST anomalies. The matter of how the gradual decrease of the thermocline depth anomalies on La Niña phases reproduces the cold event still remains unresolved from these datasets and experiment alone. Additional analysis with the use of simpler dynamical

models is needed with consideration given to the nonlinearity that predicts the asymmetry of the ENSO transition process.

As reported above, we attribute the duration of La Niña to the nonlinearity of the tropical Pacific rainfall response. In a direct link with the wind responses, the weak thermocline displacement in the eastern Pacific could be responsible for the redevelopment of La Niña. Observational evidence shows that convective activity increases sharply above a threshold SST of 27°C (e.g., Graham and Barnett 1987), while the SST above that temperature has little effect on the enhancement of convection. Because of the nonlinear relationship between the SST and convection, changes in the climatological SST fundamentally alter the response of equatorial atmospheric conditions to the symmetric SST anomalies, leading to an asymmetric equatorial wind stress responses. It is conceivable that the nonlinear atmospheric response to the SST in the mature to the decay phase of the ENSO is principally due to how the ENSO-related SST anomalies modulate the line of 27°C. The distribution of the climatological SST and its seasonal changes could be one of the most important factors for a realistic simulation of the ENSO oscillation in air-sea coupled models.

Regarding the spatial expressions of the atmospheric response to the ENSO, our current study suggests that at least two different thermocline variations exist during the ENSO decay phase that arise due to different sensitivities to opposite ENSO phases. These asymmetric features of the ENSO turnabout might be enhanced in a strong event. Hoerling et al. (2001) reported that the nonlinearity in atmospheric responses requires that central eastern Pacific SST anomalies exceed one standard deviation of their interannual variability. For the forcing of larger-amplitude SST anomalies, a spatial phase shift of the atmosphere between the signals must emerge. Thus, our analysis implicitly implies that a strong positive ENSO event tends to

turn into a negative phase, as is evident in the observational results (e.g., Horii and Hanawa 2004; Hasegawa et al. 2006), which report the relationships between the amplitude of a warm El Niño episode and its following transition.

By analyzing the observational data, Tomita and Yasunari (1993) suggests that there exist two types of warm phase event where its termination is quick and slow. Previous studies (Tomita and Yasunari 1993; Hasegawa et al. 2006) point out the importance of difference in strength of anomalous clockwise eddy wind at the off equatorial western Pacific between the quick and slow termination of ENSO. This point is relatively similar to those of cold ENSO. However, we consider that the duration mechanism of the warm phase is different from the cold phase. Our following studies should clarify the processes and could contribute to improve the precision of forecasting for ENSO activity and drought.

Very recently, several studies pointed out the importance of the Indian Ocean on the ENSO transition (e.g., Kug and Kang 2006; Ohba and Ueda 2007). They have shown that the Indian Ocean basin-wide warming during El Niño can influence on the tropical Pacific wind variability through the enhancement of the western Pacific Oscillator. According to them, the basin-wide warming during boreal winter enhances the surface easterlies over the equatorial western Pacific which induces an advanced transition to the La Niña phase. How the Indian Ocean SST anomalies during the boreal winter contribute to the asymmetric response of the western Pacific is not well understood. Additional analysis from a quantitative viewpoint is needed for further clarification of the role of the Indian Ocean SST forcing on the asymmetric transition process of ENSO.

The results presented in this study are dynamically consistent with other studies investigating the transition features of the ENSO. In the decaying phase of El Niño, the remote and

local impacts of El Niño-related SST anomalies contribute to the turnabout of the central eastern Pacific via modulation of wind stress. Their effect of a rapid reduction accelerates the seasonally fixed transition system, which is dependent on the Pacific climatological conditions, as argued in many studies (e.g., Zebiak and Cane 1987; Yan and Wu 2007). In contrast, in the decay phase of La Niña, the equatorial westerly wind anomalies generally appear over the maritime continent, and the decreasing speed of the equatorial wind over the Pacific is not worth even one-half of that in the El Niño phase. The thermocline variation is considerably slow and drags La Niña down to an El Niño transition that could be linked to the redevelopment of La Niña. This point is also consistent with the previous studies (Jin et al. 2003; Wu and Kirtman 2005), that noted the role of the anomalous zonal advection on the transition process of ENSO. The previous studies argued that the near mobile mode, which is closely associated with an anomalous zonal advection, is active during a cold event, resulting in a prolonged period of cold event compared to a warm event. It is conceivable that the atmospheric part on the cold-to-warm phase could enhance the anomalous zonal advection through the wind stress forcing at the ocean surface. However, this point is not explored in detail in this study. The relationship between the atmospheric forcing and the zonal advection of the ocean surface should be deeply analyzed by use of some atmospheric and oceanic reanalysis with tropical Pacific buoy data.

The results of this study implicitly suggest that the nonlinear climate response to the ENSO is an important factor to understand the nonlinear ENSO cycle, particularly in its decay phase. In a recent study, it was revealed that a number of the CGCM failed to reproduce the skewness of the SST anomalies over the central eastern Pacific (Monahan and Dai 2004; An et al. 2005). The speculation here is that the inaccurate reproductions of these features could also

be due to the linear behavior of the model ENSO cycle. It remains uncertain, however, whether the asymmetric response of the atmosphere in the tropical Pacific is a key to understanding the features of the subsequent behavior on the warm and cold events after its mature phase. Capturing the features could contribute to not only more advanced ENSO predictions but also a deeper understanding of the generation of decadal variation (e.g., Luo and Yamagata 2001; Minobe and Jin 2004). Therefore, identification of the asymmetric impact of the ENSO calls for a more accurate and stable measurement of surface wind over the tropical/subtropical Pacific. More research by use of the coupled models will provide further understanding of the duration mechanism of La Niña.

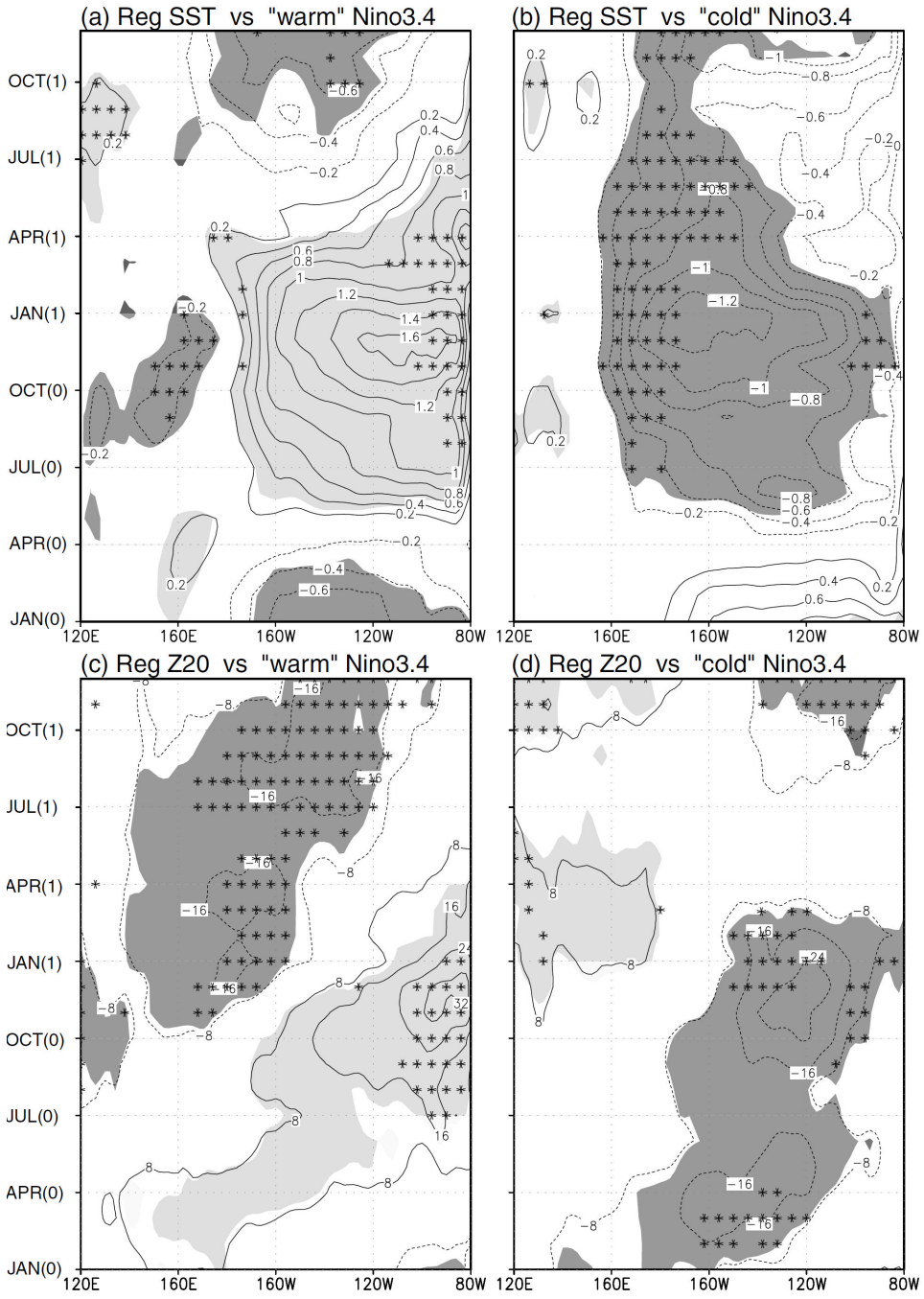

FIG. 3.1: Evolution of SST anomalies averaged over 2°S-2°N obtained through one-sided regression on the (a) positive and (b) negative Niño-3.4 index during DJF (0/1). (c) and (d) are the same as (a) and (b) except for the evolution of Z20 depth anomalies. The shaded areas indicate where the regression is above the 95% significant level. The asterisks indicate the statistical significance of the difference between the warm and minus the cold at the 95% level. The mark is plotted only over the shaded region.

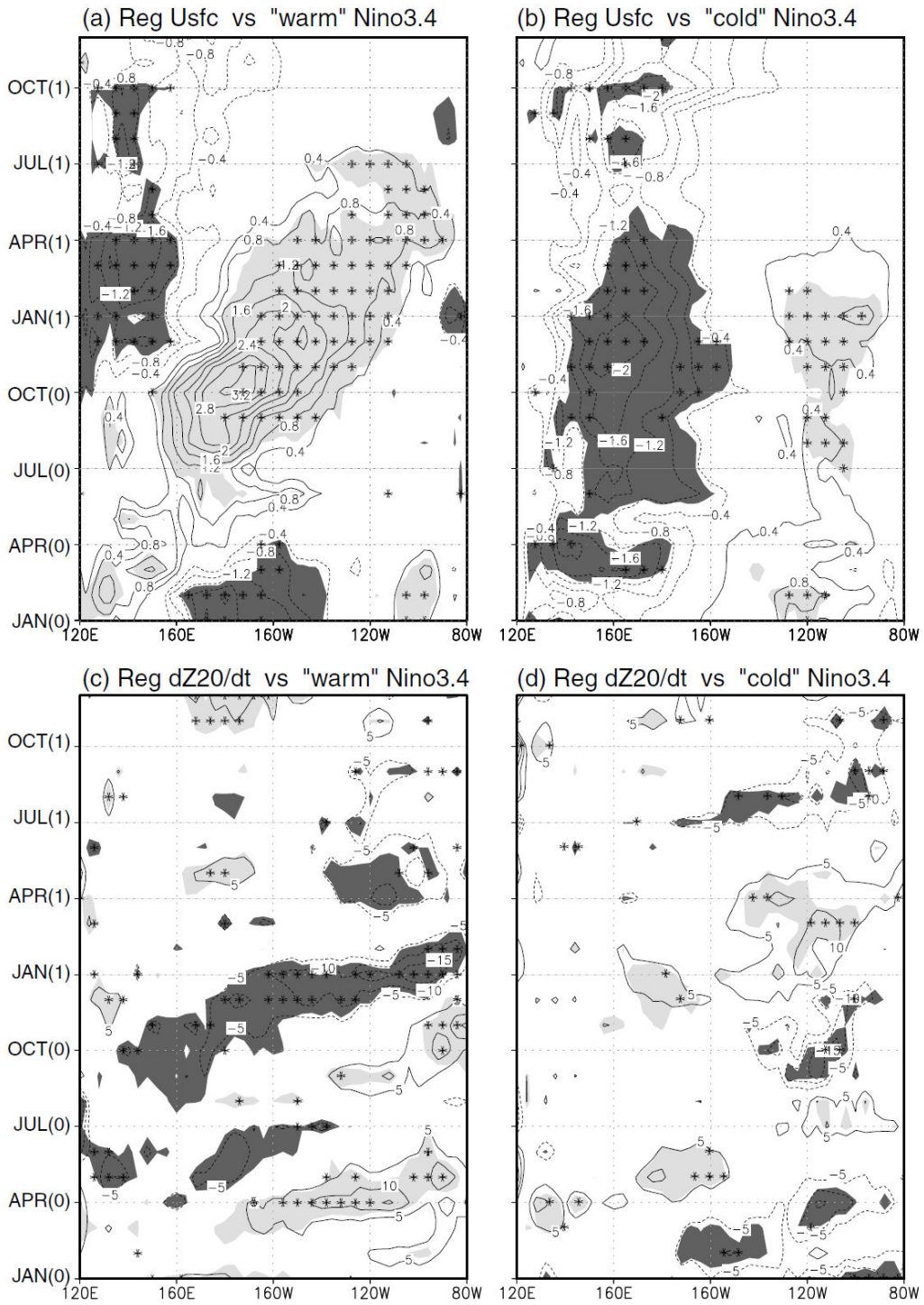

FIG. 3.2: Same as Fig. 3.1 except for a one-sided regression for the (a and b) surface zonal wind and (c and d) Z20 tendency anomalies.

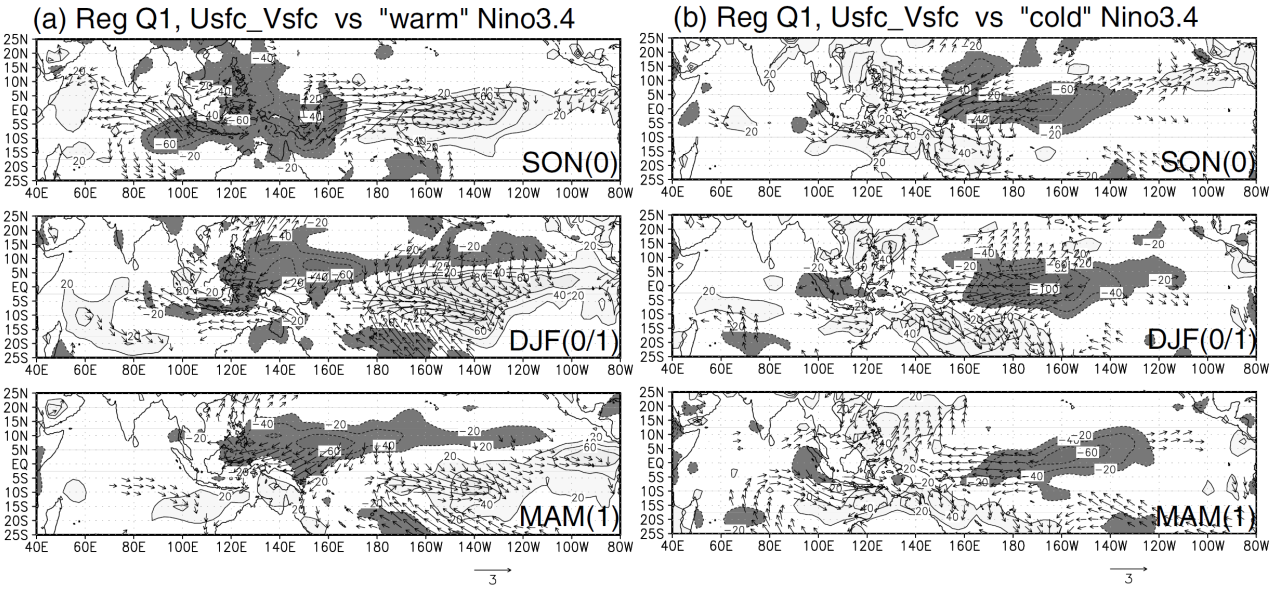

FIG. 3.3: One-sided regressions of the observed SON (0), DJF (0/1), and MAM (1) surface wind and diabatic heating for (a) warm and (b) cold phases of the Niño-3.4 index. The light- (dark-) shaded areas indicate where the positive (negative) regression coefficient is greater (smaller) than 20 (-20) W/m^2.

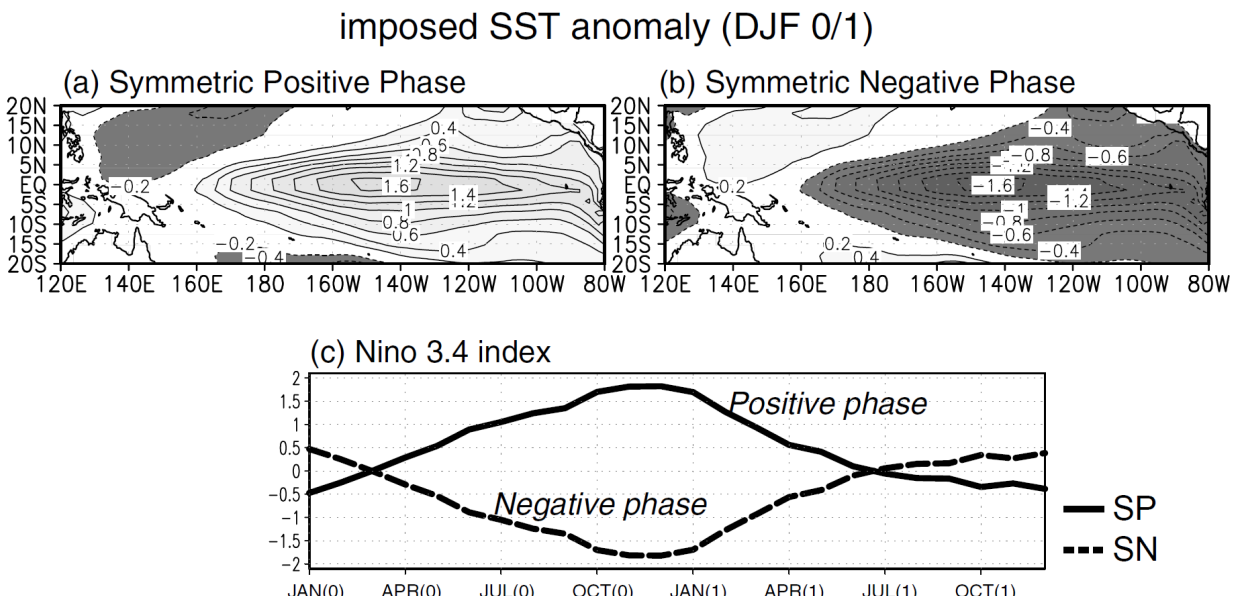

FIG. 3.4: Imposed composited SST anomalies (°C) in the symmetric (a) positive and (b) negative runs for DJF (0/1). The light- (dark-) shaded areas indicate where the positive (negative) regression coefficient is greater (smaller) than 0.2 (-0.2) °C. (c) Evolution of the imposed SST anomalies over the Niño-3.4 region (170°W-120°W, 5°S-5°N) for the SP (bold solid) and SN (bold dash) runs.

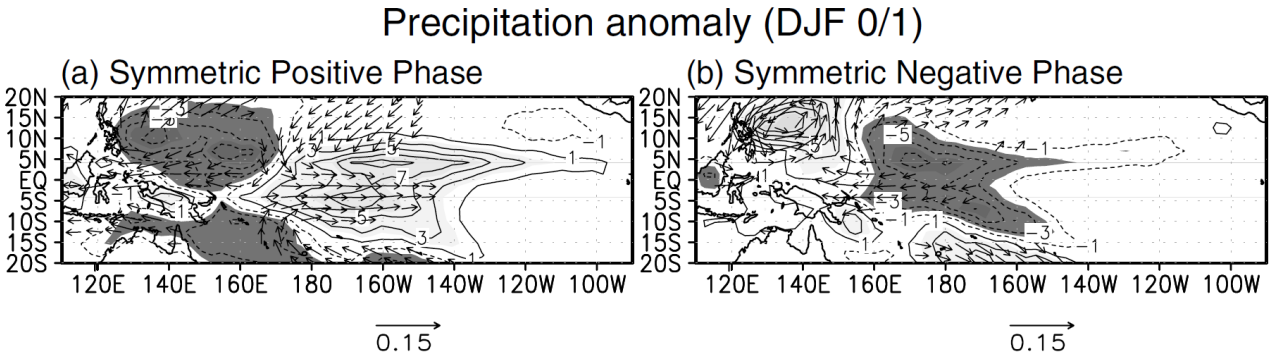

FIG. 3.5: Composite anomalies of the AGCM-simulated DJF precipitation (contour: mm/day) and wind stress (vector: N/m^2) in response to the symmetric (a) positive and (b) negative phase of tropical Pacific SST anomalies during DJF (0/1). The contour interval is 1 (mm/day). The positive (negative) precipitation anomalies greater (smaller) than 2 (-2) mm/day are light- (dark-) shaded.

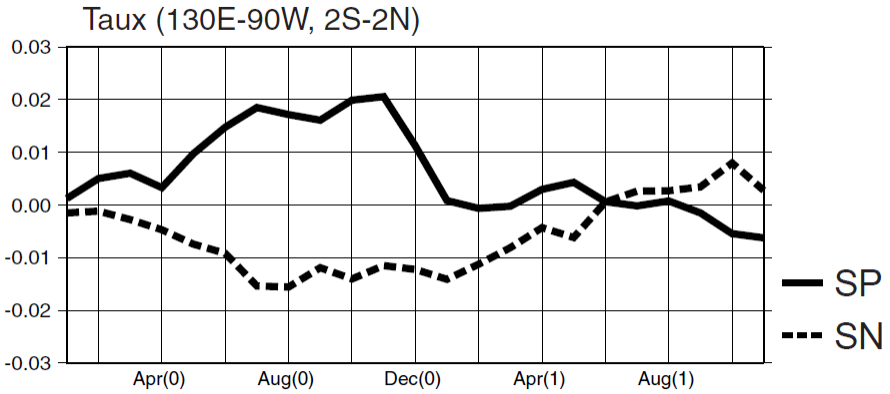

FIG. 3.6: Composite anomalies of the simulated wind stress (N/m^2) for the SP (bold solid) and SN (bold dash) run averaged over the equatorial band (130°E-90°W, 2°S-2°N).

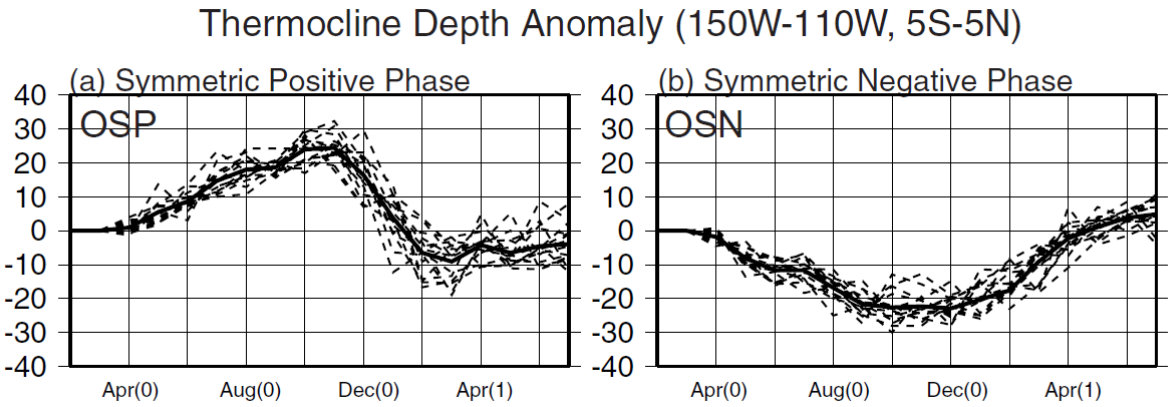

FIG. 3.7: Composite anomalies of the simulated thermocline depth over the central eastern Pacific (150°W-110°W, 5°S-5°N) for the (a) OSP and (b) OSN run for the February through the July after the next year for the individual ensemble member (dash line). The solid line shows the composite anomalies of the individual ensemble member.

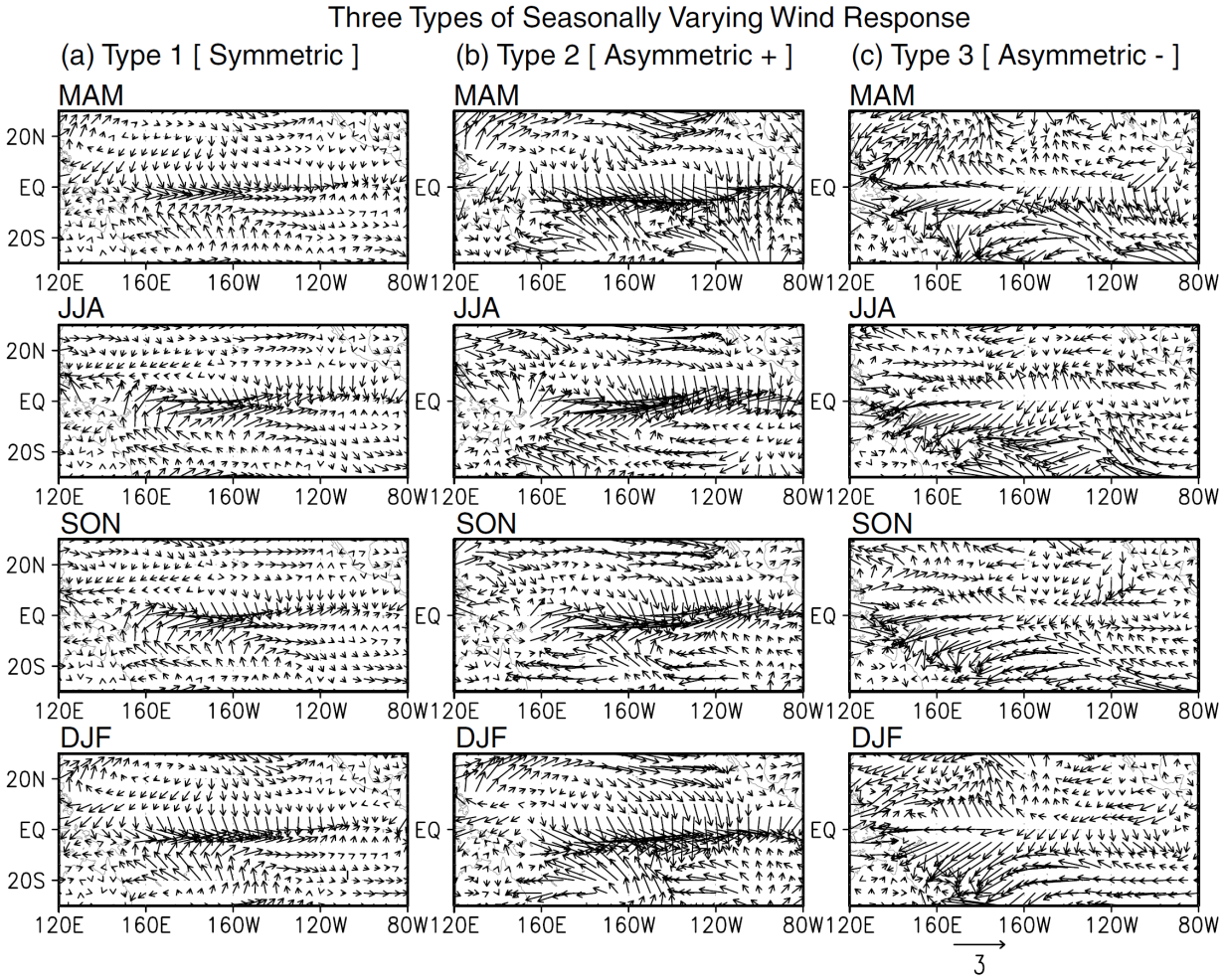

FIG. 3.8: Patterns of an anomalous surface wind in response to the SST anomalies in the Niño-3.4 region (5°S-5°N, 170°-120°W). The patterns are derived from (a) a simultaneous linear regression on the Niño-3.4 index (type 1). (b) and (c) are the same as (a) except for a simultaneous one-sided regression on the positive and negative Niño-3.4 indices, respectively.

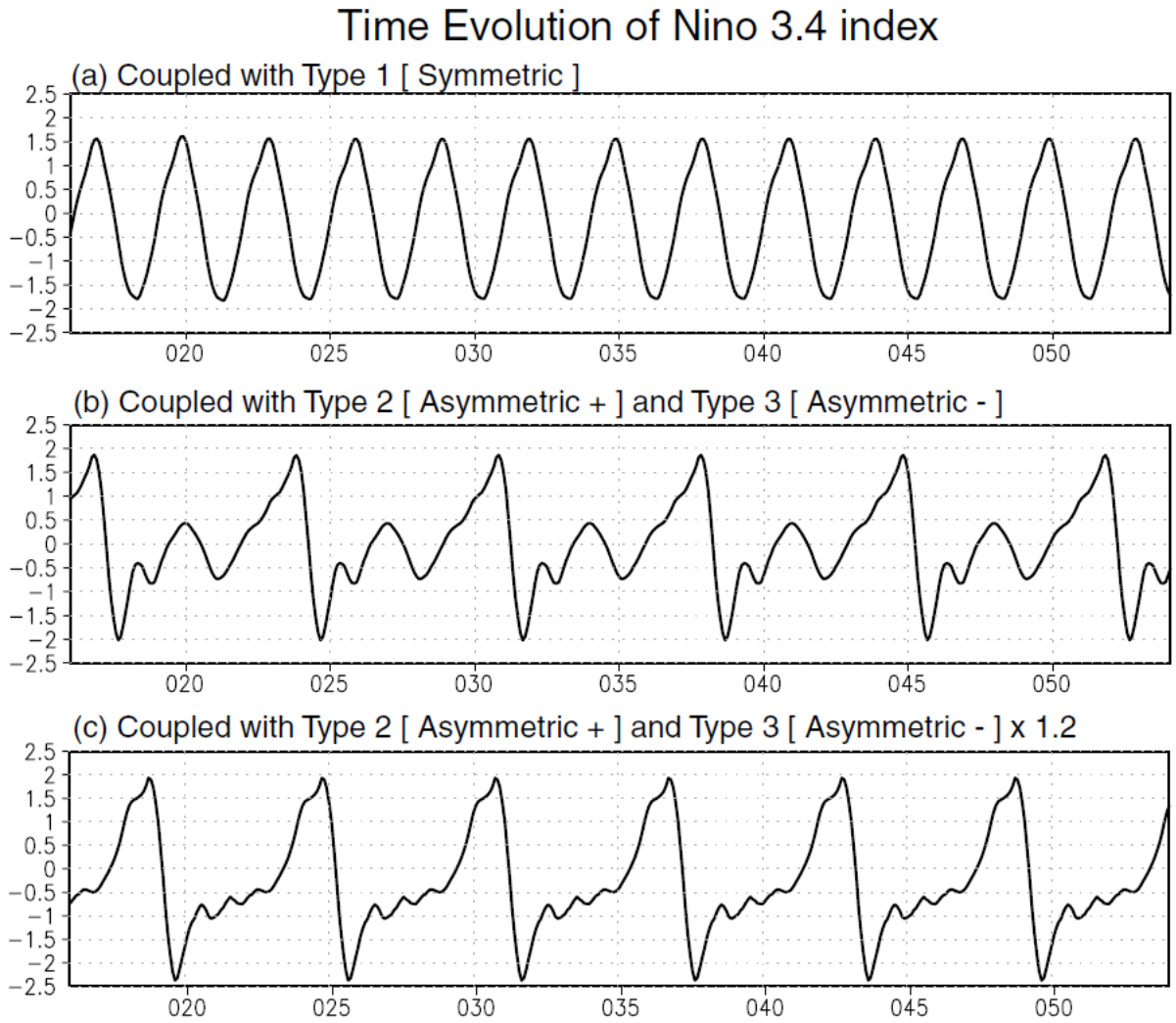

FIG. 3.9: Time evolution of the SST anomalies in the Niño-3.4 region (5°S-5°N, 170°-120°W) simulated by an intermediate air-sea coupled model with (a) a type 1 wind response and (b) type 2 and type 3 wind responses.

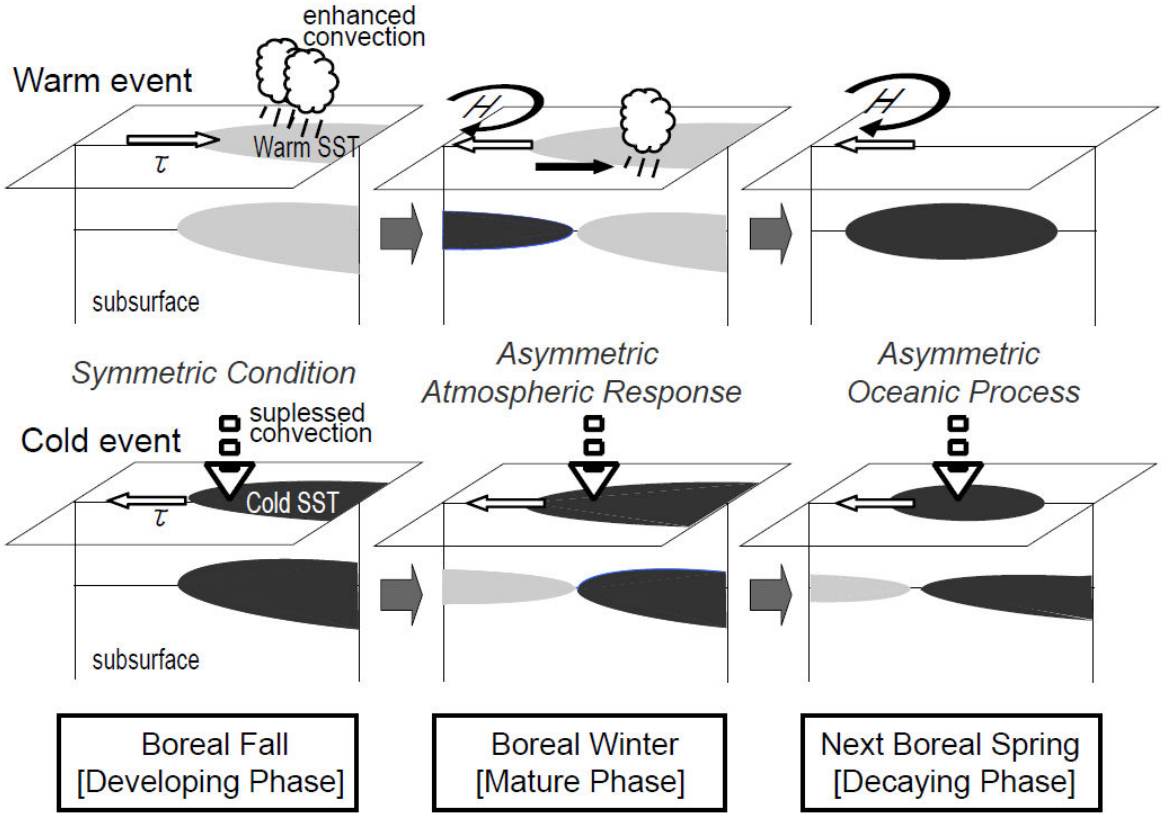

FIG. 3.10: Schematic diagram illustrating the asymmetric transition processes of the ENSO. The top figures represent the El Niño conditions, and the bottom ones, the La Niña conditions. Light (black) shading indicates the positive (negative) SST and subsurface temperature anomalies. The white outlined arrows represent the anomalous equatorial wind stress. The black arrows represent the anomalous off-equatorial wind stress. The clouds and downward arrows indicate the enhanced and suppressed atmospheric convective activity, respectively.

Chapter 4

Physical Feedback from the Indian Ocean to ENSO

4.1 Experimental design of forced BW and IODZM Experiment

The anomalous easterlies in the western Pacific during the El Niño in the above section are recognized as a result of anomalous anticynlone. Recent investigators also pointed out the importance of the Indian Ocean SST for the variation of zonal wind over the western Pacific. Kug et al. (2005) revealed that the Indian Ocean SST anomaly is partly correlated to the zonal wind anomalies over the western Pacific during the preceding year of an ENSO event. Using moist baroclinic model, Watanabe and Jin (2002) also showed that Indian Ocean SST warming is critical for developing the Philippines anticyclone in addition to the local SST forcing. Recent studies with CGCM (Yu et al. 2002; Wu and Kirtman 2004) demonstrated that the Indian Ocean affects the ENSO variability through modulating convective heating over the Indian Ocean and the Walker circulation over the tropical Indian Ocean and Pacific. They found that, when the Indian Ocean is decoupled from the atmosphere, the ENSO variability in the coupled model is significantly reduced. Recent studies (e.g., Annamalai et al. 2005; Terao and Kubota 2005; Kug et al. 2005, 2006) also pointed out the possible linkage between the Indian Ocean SST anomalies and development of the anomalous easterlies in the western Pacific, and so finally ENSO transition. The western Pacific wind anomalies are important to excite oceanic Kelvin waves, which rapidly propagate eastward, then change the oceanic vertical structure in the equatorial Pacific. The question we will address is whether the BW in the Indian Ocean and IODZM, recognized as a seasonal response to the El Niño, actually affect the development or decay phase

of El Niño. The following experimental modeling may help understand the present study.

To isolate the effect of the Indian Ocean SST on the Pacific, four CGCM experiments are carried out. In the first experiment, the BW in the Indian Ocean imposed for December-January-February (DJF) in the Indian Ocean; the SST forcing is specified in the Indian Ocean sector for the three months and the coupling is maintained in the other regions. In the following, this experiment is referred to as the forced Indian Ocean-BW (FIO-BW) run. The second experiment is similar to the FIO-BW run, except that the zonally asymmetric SST anomalies included in the IODZM are imposed for September-October-November (SON). This experiment is referred to as the forced Indian Ocean dipole/zonal SST anomalies (FIO-DZ) run. As the boundary forcing, the BW and zonally asymmetric SST anomalies are derived from the EOF-1 (Empirical orthogonal functions analysis) on the extended reconstructed SST version 2 (ERSSTv2: Smith and Reynolds 2004) in DJF and SON, respectively. For the calculation of the interannual fluctuation of the Indian Ocean SST, we apply high-pass filter to temporarily remove periodicities longer than ten years. Figures 4.1a and 4.1b show the imposed SST anomalies in the Indian Ocean. In order to compare the results from above SST anomalies forced run, we also conducted an experiment similar to above two, except that the monthly varying climatological SST is imposed in the Indian Ocean (FIO-CL run) for DJF and SON, respectively. As the initial conditions of ocean component in these runs, composited ocean temperature anomalies associated with El Niño (Fig. 4.2a) are inserted in the tropical Pacific region from 20°S to 20°N for December 1 (in the FIO-BW run) and September 1 (in the FIO-DZ run) respectively, while climatological ocean temperature are inserted elsewhere. It should be noted here that we use the different months for the initial conditions to accord the seasonal dependence of the IODZM and BW. We reveal the response of precipitation (Figs. 4.1c and 4.1d) to the BW and

IODZM, respectively. The amplitude and spatial structure of the precipitation responses correspond to the composited observational analysis of the BW (Lau and Nath 2003, Fig. 4.3). Though the anomalies are relatively strong over the western Indian Ocean, those of the IODZM (Fig. 4.1d) is also reproduced in the SON (Annamalai et al. 2005).

Figure 4.2b provides some details of the experimental design. For each forcing scenarios, the model is run for 2 yr from January through the next year, without sufficiently long spin up period. To account for the atmospheric sensitivity to the initial conditions, a 10-member ensemble approach is conducted for each forcing scenario. We change only the initial conditions in preserving the same ocean temperature anomalies in the Pacific and SST forcing in the Indian Ocean, respectively. Initial conditions, September 1 and December 1, are taken from the AGCM control run in which the climatological SST was used as the boundary forcing. To avoid a generation of the unrealistic Pacific condition in response to the sudden input of the anomaly, the initial conditions are spun up for one month with prescribing the anomalous Pacific SST, extracted from the composited ocean temperature.

4.2 Impact of the Indian Ocean basin-wide warming on ENSO variability

As first, we report the differences in SST and low-level atmospheric circulation patterns between the FIO-BW and FIO-CL run to assess the influence of BW in the Indian Ocean on a decaying phase of the El Niño. Figure 4.3 shows the composite anomalies of the simulated SST

with 850-hPa wind during the DJF (0/1) and DJF (1/2) for each run. The results presented here are based on ensemble averages over ten individual integrations. The anomalies are obtained by difference from the climatology of 75-year CGCM control run. In both experiments, simulated low-level wind anomalies during the DJF (0/1) have a large-scale structure, as shown in Fig. 4.3a. In comparison between FIO-BW and FIO-CL run, the anomalous wind and SST patterns during the DJF (0/1) is very similar to each other by a narrow margin, especially central-eastern Pacific. Although both experiments also reveal an anomalous anticyclonic circulation centered over the Philippine Sea during DJF (0/1), their magnitude differs significantly. The 850-hPa wind anomalies over the western-north Pacific, concurrent with the low-level Philippine anti-cyclone, in the FIO-CL run is much weaker than that in the FIO-BW run. A comparison of SST anomalies between the FIO-BW and FIO-CL during the following DJF (1/2) clearly exhibit the role of the Indian Ocean-BW in hastening the ENSO transition (Fig. 4.3b). Despite the FIO-BW run reveals strong negative SST anomalies in the equatorial central Pacific, those of the FIO-CL run is still weak positive, suggesting that the ENSO transition is still not established at this time.

To describe the time evolution of the ENSO transition, we also plot a longitude-time section of the SST with 850-hPa wind anomalies near the equator for the FIO-BW and FIO-CL run. In comparison with the eastern-Pacific SST anomalies in the FIO-CL run, those of the FIO-BW run decrease rapidly and reveal negative anomalies in the boreal summer (Fig 4.4a). From the summer to succeeding winter, the SST anomalies in the FIO-BW run show negative values over the tropical Pacific with easterly wind anomalies, indicating that the transition process to La Niña phase is well established. Conversely, in the case of the FIO-CL run, the warm SST anomalies in the central-eastern Pacific still remain in this year (Fig. 4.4b). The low-level western Pacific easterlies included in the anticyclone in the DJF (0/1) are also much weaker than those

of the FIO-BW run, and therefore they have little impact on the central-eastern Pacific SST. The El Niño slowly decays with the seasonal perturbation and the development of La Niña is delayed about a half year in comparison with the BW-imposed run (Fig. 4.4b).

If we take a closer look at Figure 4.4, some conspicuous features of the SST and wind anomalies are apparent in the western Pacific. Concurrent with the enhanced anticyclonic circulation over the Philippine Sea, substantial easterly wind anomalies are manifested over the western Pacific especially DJF (0/1) (Fig. 4.4a). Lagged behind the easterly wind anomalies by a few months, the SST anomalies in the eastern Pacific reveal remarkable negative values after the MAM (1), and expand to the westward gradually. This feature of the simulated turnabout from El Niño to La Niña is well corresponding to the observation. In response to the SST cooling in the central-eastern Pacific during the subsequent MAM (1), the easterly anomalies in the western Pacific is reproduced along the equator in 140-160°E. Most plausible explanation for the generation of the easterly anomalies over the western Pacific during the winter is linking to the BW in the Indian Ocean, which possibly causes the atmospheric Kelvin wave response over the western Pacific (Annamalai et al. 2005; Terao and Kubota 2005) and enhancement of the Philippine Sea anticyclone (Watanabe and Jin 2002). The easterly anomalies in the DJF (0/1) reinforce the climatological trade wind over the western Pacific, which intrudes on the Indian Ocean. This causes the local SST cooling through the enhancement of heat exchange at the ocean surface and vertical mixing at the subsurface in addition to the anomalous equatorial upwelling (Fig. 4.4a). These enhanced wind anomalies are expected to contribute to ENSO variability because the eastern Pacific SST is closely related to the equatorial zonal wind through the generation of oceanic upwelling Kelvin waves. The resultant eastward propagation of the Kelvin wave induces thermocline displacement that can potentially contribute to the demise of the

eastern-central Pacific warming.

To seek more conclusive evidence which confirm the difference in ocean dynamical response between the FIO-BW and FIO-CL, we show the composited anomalies of the ocean heat content from the surface to 400 m depth (Fig. 4.5). Also shown are longitude-depth sections of the ocean temperature along the equatorial band (5°S-5°N) in the Pacific (Fig. 4.6). Ocean heat content reflects a variation of thermocline depth. It is well recognized that the negative ocean heat content anomalies in the equatorial western Pacific appear at the mature phase of El Niño event. This negative anomaly then propagates eastward along the equator, and forces to terminate El Niño event. This scenario is in line with equatorial wave dynamics ("delayed oscillator theory"), and consistent with the works that pointed out the importance of direct atmospheric forcing in the equatorial western Pacific (e.g., Weisberg and Wang 1997). Both FIO-BW and FIO-CL run show strong negative anomalies of the ocean heat content in the equatorial western Pacific and the positive anomalies in the eastern Pacific during the DJF (0/1) (Fig. 4.5a). The zonal wind stress associated with the zonal wind anomalies directly displaces the thermocline vertically via Ekman pumping.

Difference between FIO-BW minus FIO-CL (Fig. 4.5) sheds light on the remote impact of the Indian Ocean SST anomalies that can be directly compared with the difference of the results. Consistent with the BW-enhanced easterly during the mature phase of El Niño, the difference between FIO-BW minus FIO-CL reveal the enhanced generation of oceanic Kelvin wave along the equatorial central Pacific (Fig. 4.5a). The enhancement of the equatorial easterly anomalies concurrently force off-equatorial downwelling Rossby waves around 150°E of the both hemisphere. These characteristics are recognized as zonal contrast of the OHC anomalies, which indicates the presence of off-equatorial downwelling in the western Pacific and equatorial upwel-

ling in the central-eastern Pacific. During the MAM (1), the downwelling Rossby and upwelling Kelvin response are propagated to the westward and eastward, respectively (Fig. 4.5b). In response to the anomalous curl of the wind stress over the off-equatorial central Pacific in both runs (Fig. 4.3a), the meridional heat transport from the equator to the high latitude is clear over the central-eastern Pacific. However, the meridional heat transport in the FIO-BW run at this period is not considerably different from the FIO-CL run, anticipating that the acceleration mechanism of the ENSO transition in the early stage is predominantly due to the zonal wave propagation. The consecutive generation and passage of upwelling Kelvin waves into the eastern Pacific can effectively erode equatorial surface cooling as they journey to the east. Therefore, the BW-enhanced generation of the Kelvin wave also significantly contributes to the central-eastern Pacific SST cooling, in addition to the local heat exchange.

The reinforced anomalous easterlies over the equatorial western Pacific during the boreal winter induce oceanic upwelling, which causing temperature decreases at its mean depth (Fig. 4.6). The signal of upwelling Kelvin waves then migrated eastward at a speed of about 40-50° longitudes per month. The consecutive eastward passage of upwelling Kelvin waves contributed to the recovery of the thermocline slope in the eastern Pacific and thereby the decay of the warm condition. These characters are manifested as a slow eastward propagation of negative upper ocean heat content anomalies (e.g., Chao and Philander 1993), which is in tandem with the slow eastward movement of the central Pacific easterly anomalies. The cold SST anomalies in the central-eastern Pacific in Fig. 4.3b originate from subsurface cold anomalies in the equatorial western Pacific (Figs. 4.6a–d), which propagate upward and eastward to meet the surface along the thermocline (Fig. 4.6e). This feature of the simulated ENSO transition is consistent with an analysis of observational ocean perturbations during El Niño/La Niña. The

BW-enhanced easterly anomalies in the western Pacific during DJF (0/1) are signified by a decrease of thermocline temperature and its eastward propagation (Fig. 4.6a). As a consequence, the warmed condition in the eastern Pacific starts to recover its slope (Fig. 4.6b). Although the evolution of the ocean heat content in the FIO-BW run is similar to the FIO-CL run, the temporal progress of the thermocline is obviously hastening the ENSO transition. The ENSO transition from the El Niño to La Niña phase is well established with positive ocean temperature anomalies around the 140°E during the DJF (1/2) in the FIO-BW run (Fig. 4.6e). In contrast, the FIO-CL run still have strong negative ocean temperature anomalies in the western Pacific. Therefore, the difference between imposed BW run minus non-BW run reveal the La Niña like ocean temperature anomalies from MAM (1) to DJF (1/2). This result confirms that the ENSO transition speed certainly delay about a few seasons per year in the case of FIO-CL run.

In order to estimate the relative contribution of the BW for the Pacific SST anomalies, we show the evolution of the Niño-3.4 index, which is defined as the SST anomalies area averaged in 170º-120ºW, 5ºS-5ºN. The model simulates a gradual decrease of the SST anomaly in the boreal spring of the El Niño decaying year as shown in Fig. 4.7. Note that the difference between the FIO-BW run and FIO-CL run gradually began to spread from MAM (1). It is conceivable that this feature is related to the amplification of the oceanic Kelvin waves and its eastward propagation period. As for the FIO-BW run, despite changes in initial conditions, the simulated SST anomalies display the same sign in the all ensemble member with low variability (Fig. 4.7a). This implies that the effect of the BW in the Indian Ocean stabilize the ENSO transition in some extent. By contrast, particularly after the March of El Niño decaying year, the FIO-CL run has a wide spread of variability among each ensemble member and the several runs reproduce the Pacific SST warming (Fig. 4.7b). To compare the relative importance of the BW

in the Indian Ocean, we calculated the composited Niño-3.4 index from December (0) of the decaying year to following February (1). In a case of BW imposed run, the index is -0.57 °C. By contrast, the FIO-CL run simulate 0.27 °C. The value of the difference is 0.84 °C. Although the difference is relatively small, this result supports our argument that the BW, basing on the seasonal phase-locking response of the Indian Ocean to the El Niño impact, is one of possible contributers to the ENSO transition through the zonal wind modulation in the equatorial western Pacific.

4.3 Impact of the IODZM on ENSO variability

Observational study (Behera and Yamagata 2003) have suggested that the IODZM influences the Darwin pressure variability, that is, one pole of the Southern Oscillation. In this subsection, we note the result of FIO-DZ and FIO-CL run. In comparison with the result of BW-prescribed run, the difference of SST between the two experiments is relatively small and their distributions are scattered over the tropical Pacific (not shown). The wind anomalies in the western Pacific are very similar to each other, and therefore their effect to the subsurface ocean dynamics does not differ significantly. The evolutions of the Niño-3.4 index in the FIO-DZ and FIO-CL run are also similar to each other by a narrow margin. This result indicates that the impact of the zonally asymmetric SST anomalies on the low-level circulation over the tropical Pacific is rather weaker than those of BW in the Indian Ocean. Therefore the transition of the Indian Ocean SST pattern from the IODZM to the BW provides abrupt negative feedback to El Niño.

For the sake of comparison between the impacts of the BW and IODZM SST anomalies on the Walker circulation, we also present the longitude-height section of the composite zonal-vertical wind anomalies for FIO-BW minus FIO-CL run and FIO-DZ minus FIO-CL during DJF (0/1) and SON (0), respectively (Fig. 4.8). The vertical circulation in the BW imposed run

shows anomalous rising motion over the Indian Ocean in response to the local SST warming. Of particular interest of the equatorial western Pacific, in relation to the convergence over the eastern Indian Ocean, is that the anomalous atmospheric cell over the eastern Indian Ocean and western Pacific are manifested with divergent easterly anomalies in the lower troposphere (Fig. 4.8a). This result implies that the BW in the Indian Ocean causes the eastward extension of the anomalous Walker circulation, as pointed out in Watanabe and Jin (2002) by use of the linear AGCM. When the zonally asymmetric SST anomalies are imposed in the Indian Ocean, the local ascending and downward motion is manifested in the western Indian Ocean and eastern Indian Ocean, respectively (Fig. 4.8b). Despite strong low-level divergent easterly anomalies over the Indian Ocean, the zonal and vertical wind anomaly over the western Pacific could not be excited. Recently, Annamalai et al. (2005) showed from linear baroclinic model and AGCM experiments that the east-west contrast of the Indian Ocean SST anomalies does not generate a significant atmospheric Kelvin wave response, although the basin-wide positive anomaly can influence on the tropical Pacific wind variability. This is due to the existence of the positive and negative anomalies placed too close in the zonal direction, resulting in the cancellation of the Kelvin wave response over the western Pacific.

4.4 Discussion

What we would like to emphasize here is the importance of the Indian Ocean to the seasonality of the ENSO itself. During the coincidence years when the IODZM is followed by the major El Niño event during boreal fall, dipole structure in the tropical Indian Ocean tends to turn into the BW in the November–December period (Tokinaga and Tanimoto 2004). From boreal summer to fall, the impacts of El Niño on the Indian Ocean induce the IODZM through the modula-

tion of the atmospheric bridge, which bring the anomalous easterly over the equatorial Indian Ocean (e.g., Shinoda et al. 2004; Lau and Nath 2004). However, when we consider the reversed feedback of the Indian Ocean SST to the Pacific, the IODZM in the fall have a poor impact on the El Niño itself. In view of this, the Indian Ocean in the fall could be passive to the remote El Niño forcing. In contrast with this, due to the seasonal migration, the IODZM edgingly turn into the BW as a response to the El Niño from the fall to winter. This change of the Indian Ocean condition then operates to induce a negative feedback to the ENSO event. From this perspective, the seasonal change of the role of Indian Ocean on the ENSO can contribute to the seasonality of ENSO. The results obtained in this study are consistent with the previous study (Ohba and Ueda 2005), which describe the seasonal response of the Indian Ocean to the impact of the remote El Niño forcing before the mature phase.

Wang and An (2005) succeed to separate the continuous and transition pattern for the Indian-Pacific SST through their seasonal-reliant EOF (S-EOF) analysis. Figure 4.9 presents the spatial pattern of the S-EOF 1 & 2 modes for the Pacific SST on the ERSSTv2 and its time series of the principal component. We additionally plot the principal component of the EOF-1 mode on DJF SST anomaly over the Indian Ocean, which represents the basin-wide patterns of the SST fluctuation (Tokinaga and Tanimoto 2004). The leading S-EOF for (DJF to SON) SST anomalies reveal continuous ENSO pattern, which accounts for 35% of total variance on interannual timescale. The transition pattern of ENSO is obtained in second S-EOF mode, which accounts for 22% of total variance. It is clearly seen that the fluctuation of the principal component of the transition pattern (S-EOF 2) is well corresponding to those of the Indian Ocean basin-wide pattern. Although the correlation coefficient between the continuous pattern (S-EOF 1) and the Indian Ocean EOF-1 is 0.15, that of transition pattern and BW pattern shows signifi-

cant correlation (0.81). The result of statistical analysis by the observational data can be recognized that the Indian Ocean basin-wide pattern is mainly associated with the turnabouts of El Niño/La Niña. This result is consistent with the previous ENSO-monsoon investigators (e.g, Kawamura et al. 2003), which have suggested a combination of tropical ocean-atmosphere interactions over both the Indian Ocean and Pacific sectors is crucial for the regular phase change of ENSO.

The result presented above does not imply that the continuous pattern could not induce the Indian Ocean BW. Our experimental design and results of the above statistical analysis confine the argument about the subsequent ENSO transition processes in the delaying phase. However, the relevant question at this point, obviously, is why the Indian Ocean SST in the DJF is rather weak to the Pacific warming in the continuous pattern of ENSO (S-EOF1). We have considered that this different Indian Ocean-ENSO relationship between the patterns is responsible for the onset period of the ENSO events. Horii and Hanawa (2004), classifying the early- and late-onset type, reveal that the late onset-types tend to have a continuous El Niño conditions at the following year. The principle speculated upon here is that the onset period would be also important to understand the Indian Ocean-ENSO coupling and forecast the subsequent activity after the onset of the ENSO event, because the Indian Ocean conditions can be closely related to the amplitude of the ENSO. It still remains uncertain, however, the Indian Ocean basin-wide pattern is a one of the key to understand the subsequent behavior of ENSO after its mature phase.

4.5 Summary

Several studies have indicated that the ENSO can induce SST variations in the Indian Ocean,

through the modulation of the surface heat flux (e.g., Venzke et al. 2000; Lau and Nath 2003; Wang et al 2003) and ocean dynamics (e.g., Murtugudde et al. 2000; Xie et al. 2002). In this study, we conducted a set of experiments by use of a stand-alone CGCM to catch the influence of the El Niño-related SST anomalies in the Indian Ocean on the ENSO transition as its positive or negative feedback. During the mature-decay phase of El Niño, the Indian Ocean-BW during the winter enhances the diabatic heating over the tropical Indian Ocean, which is recognized as enhancement of the ITCZ over the region. The anomalous diabatic heating is linking to the enhancement of the low-level easterly in the equatorial western Pacific through the modification of the Walker circulation. As a consequence, the anomalous surface easterlies in the western Pacific during the mature-decay phase of the El Niño induce an advanced transition to La Niña phase by more generating the negative oceanic Kelvin wave. These results imply that the BW in the Indian Ocean, in some extent, operates as a trigger for a transition from the warm to cold phase.

The remote impacts of El Niño on the Indian Ocean SST largely depend on the Asian monsoon, which is responsible for IODZM and BW over the Indian Ocean (e. g., Shinoda et al. 2005). Especially, the impacts of the El Niño on the Indian Ocean during the boreal fall to winter are relatively stable as BW, through the modulation of the surface heat loss. The results of this study implicitly suggest that the monsoon is important to understand the seasonality of the ENSO cycle and its subsequent behavior in the decay phase. Therefore, identification of the Indian Ocean effect on El Niño calls for more accurate measurement of SST and surface wind over the tropical Indian Ocean. Much research is needed to further understand the cross basin interaction of the air-sea coupled system between the Indian Ocean and Pacific.

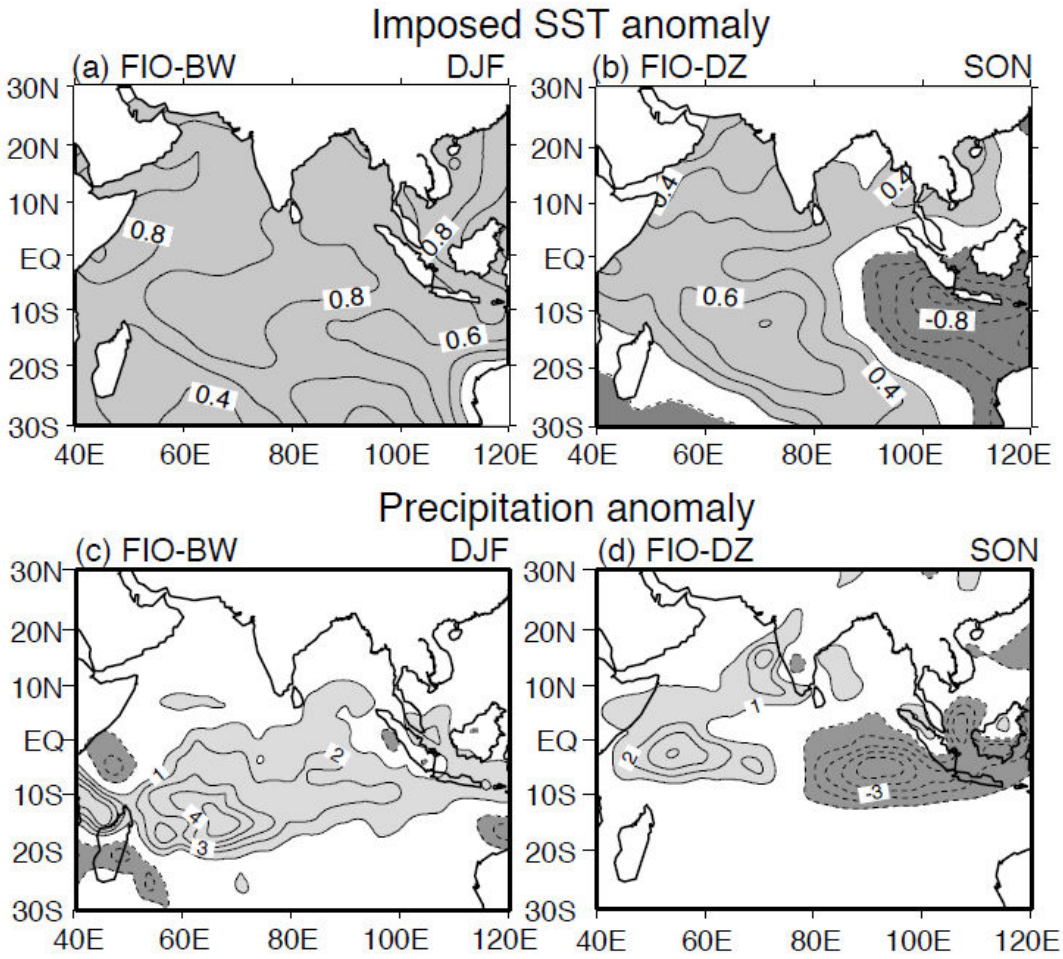

FIG. 4.1: Imposed composited SST anomalies (°C) in the experiments, which is extracted form the EOF1 on the ERSSTv2 for DJF and SON, respectively. (a) FIO-BW run (b) FIO-DZ run. The composited anomalies of the precipitation in response to imposed SST anomalies for the (c) FIO-BW run during DJF (0/1) and (d) FIO-DZ run during SON (0).

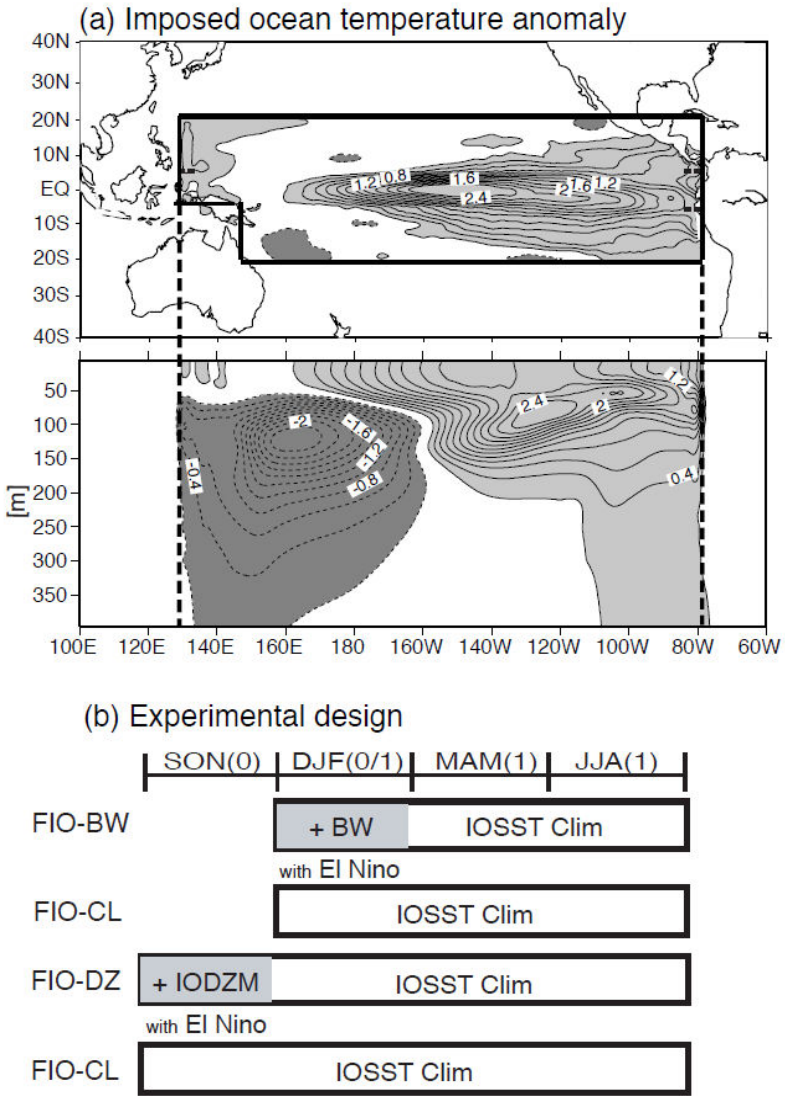

FIG. 4.2: (a) Imposed composited ocean temperature anomalies (°C) in the experiments. Top figure shows the surface anomalies and bottom figure shows longitude-depth section of the anomalies averaged over a latitudinal band of 5°S-5°N. (b) Schematic diagram of the experimental design imposed composited SST anomalies in the CGCM experiments. Light shading shows imposed anomalous Indian Ocean SST. The composited SST is imposed for DJF (SON) in the FIO-BW (DZ) run with El Niño related Ocean temperature.

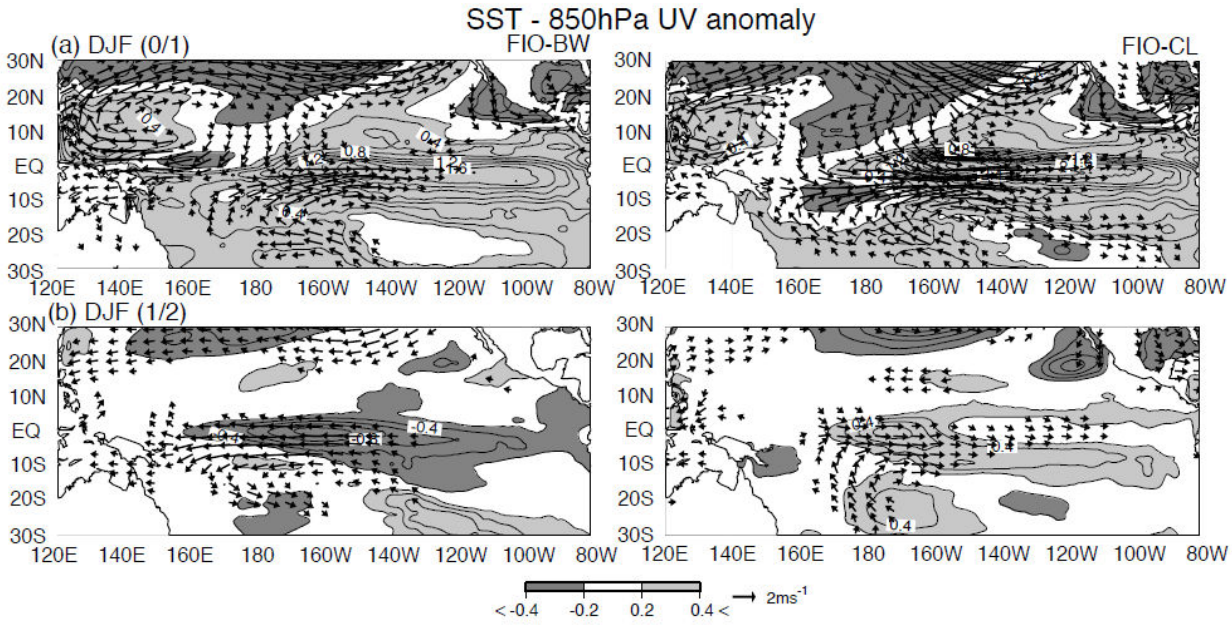

FIG. 4.3: Composite anomalies of the CGCM-simulated SST (°C) with 850-hPa wind (m s^{-1}) for FIO-BW and FIO-CL run during (a) DJF (0/1) and (b) DJF (1/2). Contour interval is 0.2 (°C). Light (dark) shading denotes SST anomalies greater (less) than 0.2 (-0.2) °C.

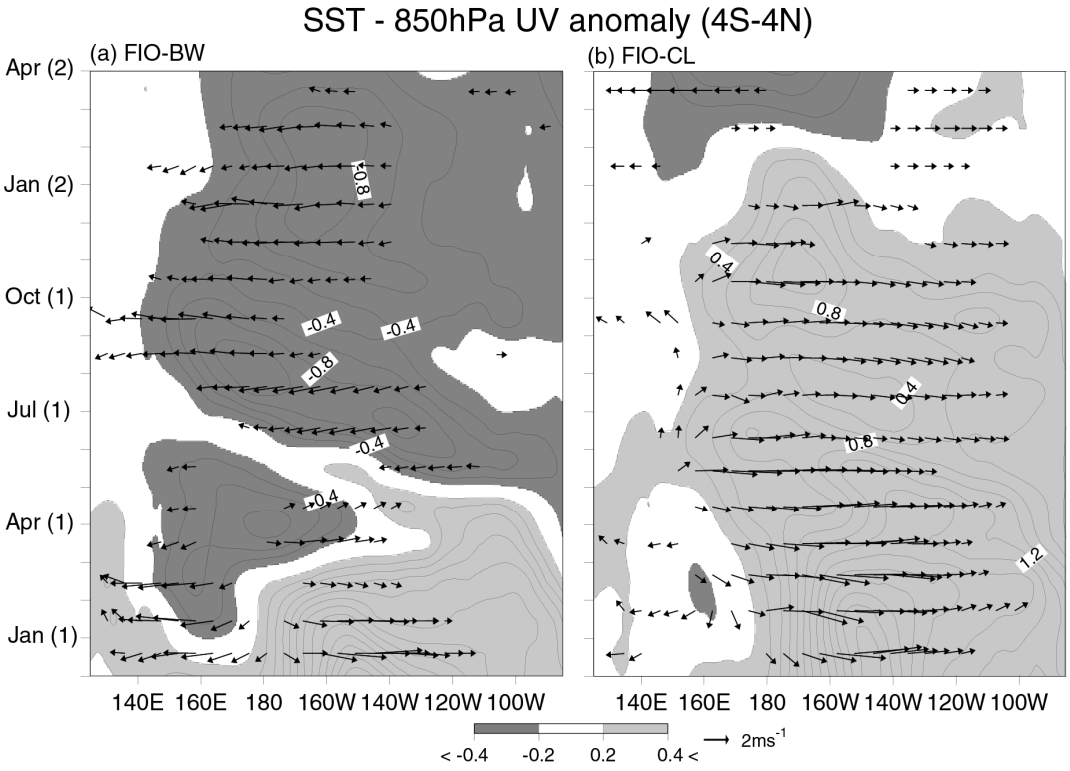

FIG. 4.4: Longitude-time section of the composite anomalies of the CGCM-simulated SST (°C) with 850 hPa wind vector averaged over 4°S-4°N from December to March of the following year for the (a) FIO-BW and (b) FIO-CL run. Light (dark) shading denotes SST anomalies greater (less) than 0.2 (-0.2) °C. Contour interval is 0.2 (°C).

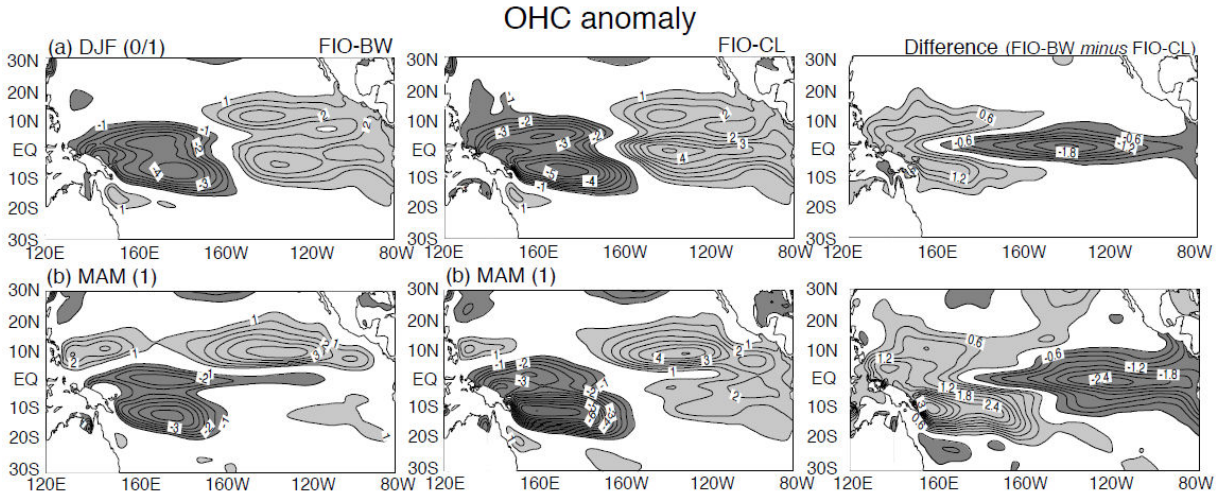

FIG. 4.5: CGCM-simulated anomalies of ocean heat content (10^8 J/m^2) from the surface to 400 m depth for the FIO-BW, FIO-CL run and difference between FIO-BW *minus* FIO-CL in (a) DJF (0/1), and (b) MAM (1).

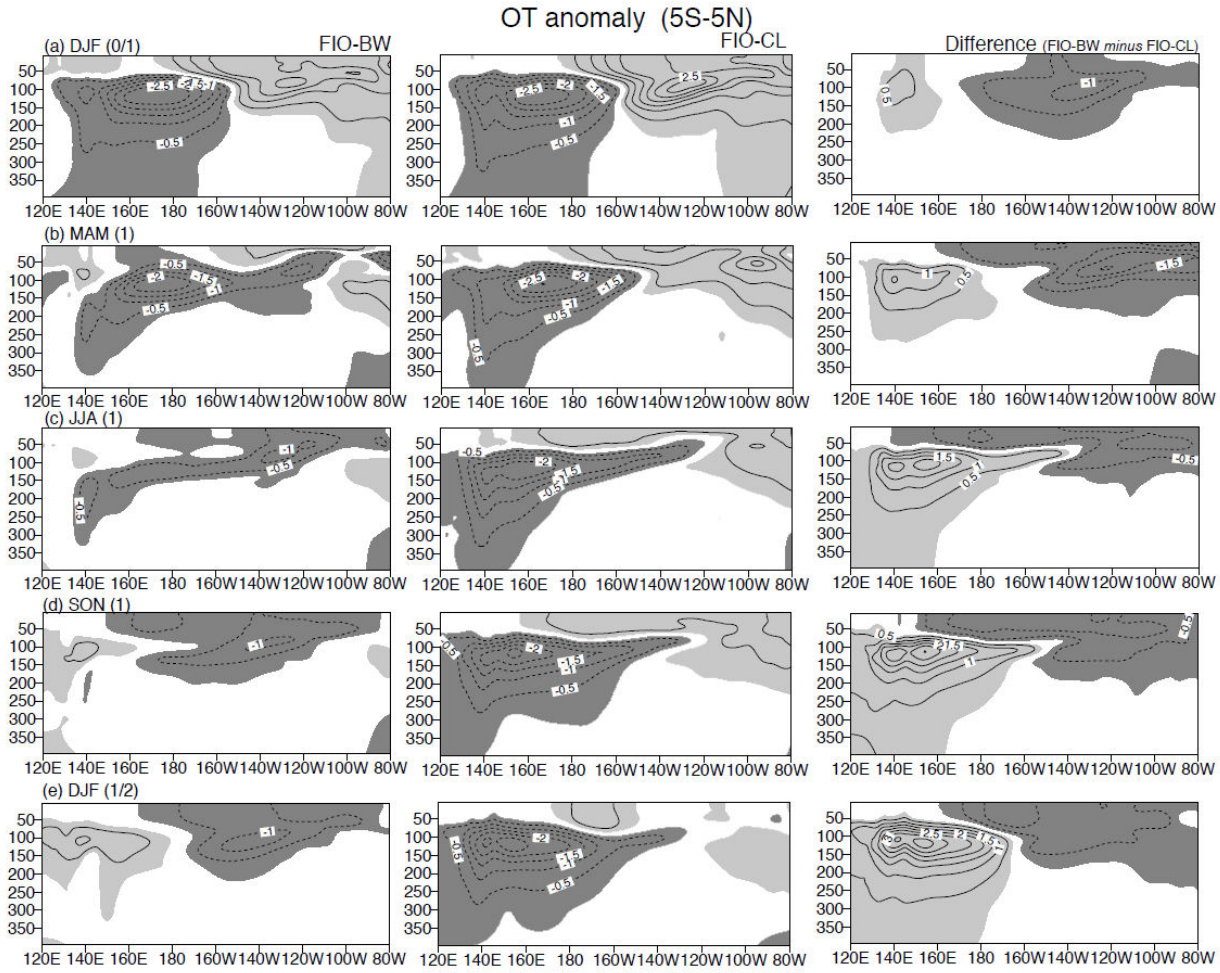

FIG. 4.6: Longitude-depth section of CGCM-simulated ocean temperature (°C) anomalies averaged over 5°S-5°N in (a) DJF (0/1), (b) MAM (1), (c) JJA (1), (d) SON (1), and (e) DJF (1/2) for the FIO-BW, FIO-CL and the difference between FIO-BW *minus* FIO-CL run. Light (dark) shading denotes ocean temperature anomalies greater (less) than 0.2 (-0.2) °C.

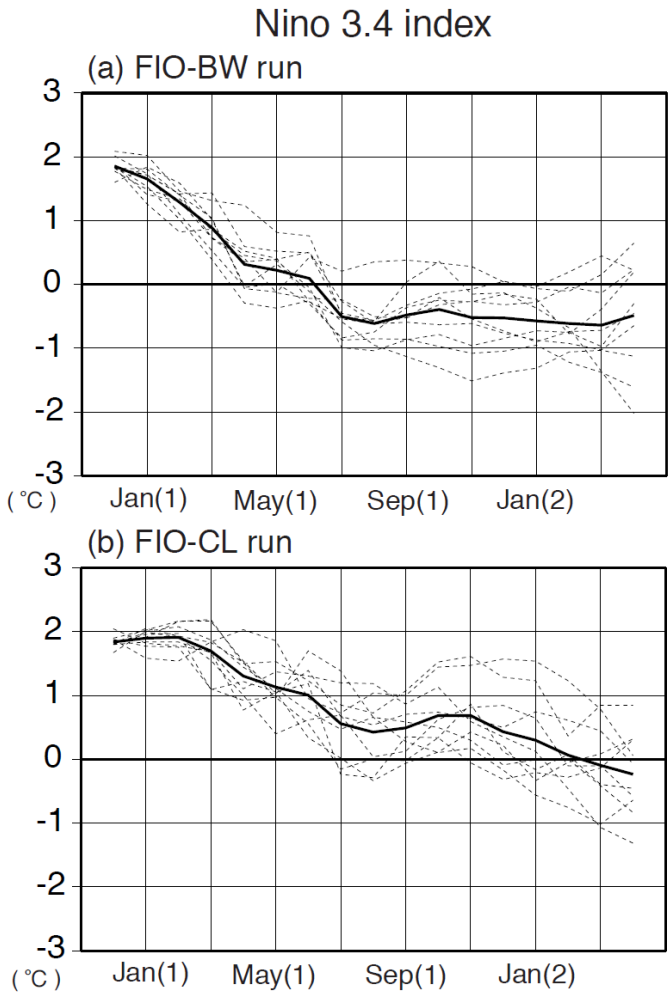

FIG. 4.7: Evolution of the monthly mean Niño-3.4 SST anomalies (5ºS-5ºN, 150º-90ºW) for the (a) FIO-BW run and (b) FIO-CL run for the December through the March after the next year for the individual ensemble member of the solutions.

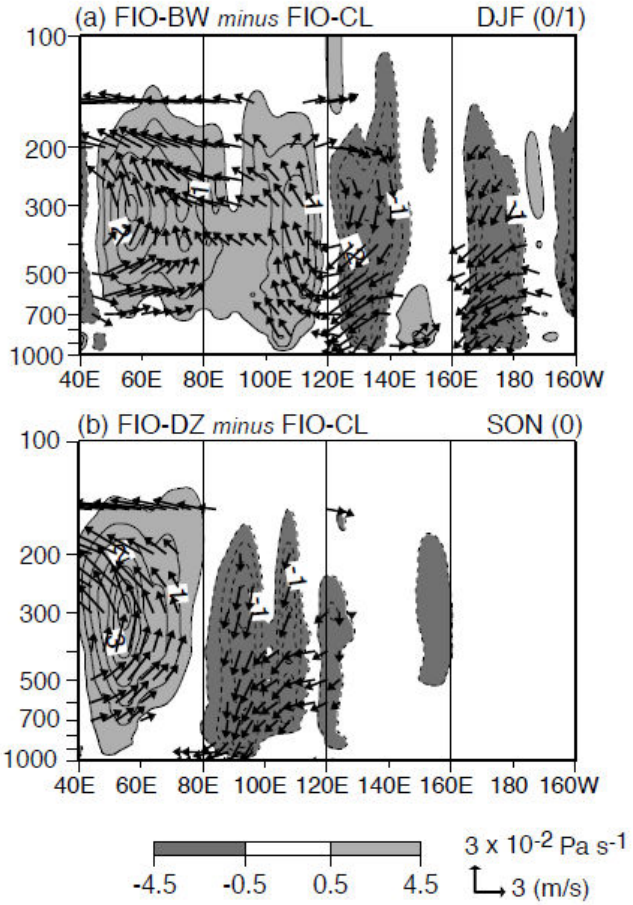

FIG. 4.8: Longitude-height section of composited anomalies of zonal and vertical winds averaged over a latitudinal band of 5°S-5°N for the difference between (a) FIO-BW and FIO-CL run during DJF (0/1) and (b) FIO-DZ and FIO-CL run during SON (0). Light (dark) shading denotes vertical wind velocity anomalies greater (less) than -1.0 (1.0) $\times 10^{-2}$ Pa s^{-1}.

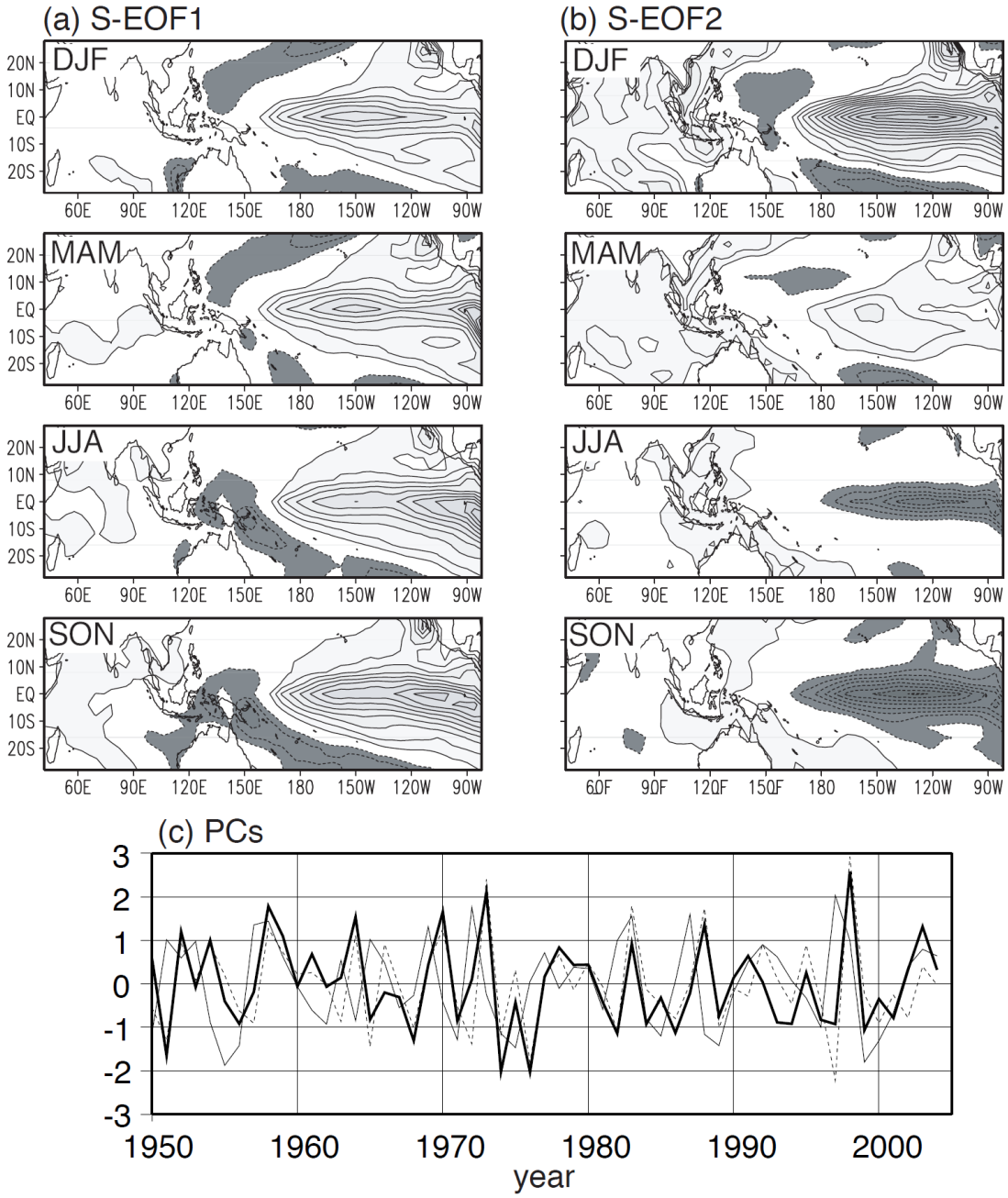

FIG. 4.9: Spatial patterns of the (a) first and (b) second S-EOF mode of SST anomalies from DJF to SON. Contour lines show the regressed SST anomaly onto the each principal component of the S-EOF at 0.1 °C intervals. Light (dark) shading denotes the value greater (less) than 0.1 (-0.1) °C. (c) Principal component of the first (thin solid line) and second (dashed line) S-EOF modes of tropical Pacific SST anomalies.

Chapter 5

Role of climatological state on the ENSO transition in the CMIP3 multi-model experiments

5.1 El Niño and La Niña transition process in CMIP3 CGCMs

The mechanism presented in previous oscillator theory adequately reproduces the linear oscillation of the ENSO; in other words, it demonstrates that the termination of El Niño is consistent with a cyclic nature. However, some studies have pointed out that a kind of break in the ENSO cycle has been observed when La Niña goes to El Niño. The air-sea coupled system over the Pacific somehow remains in a weak La Niña state for a while (Kessler 2002; Nagura et al. 2008). Recent study (Ohba and Ueda 2009) has also reported the asymmetry of the transition process of ENSO, through the nonlinear response to the central eastern Pacific SST forcing (Hoerling et al. 1997; Hoerling et al. 2001; Kang and Kug 2002). Duration of the La Niña can cause severe droughts, such as those that took place in central Asia from 1999 to 2001 (e.g., Hoerling and Kumar 2003; Ueda and Kawamura 2004), via the air-sea-land coupled systems of the Asian monsoon (Ueda et al. 2009; Futami et al. 2009). Therefore the skill of seasonal climate forecasts predicting the duration of La Niña by air-sea coupled general circulation model (CGCM) is important to predict the severe droughts.

In this section, an analysis of the temporal evolution of the anomalous atmospheric and oceanic component associated with the El Niño and La Niña is discussed using the data of CGCMs. Displayed in Fig. 5.1 are the evolutions of the equatorial monthly mean SST anomalies from January (0) to February (2), obtained through one-sided lag regressions to positive-

(El Niño phase) and negative- (La Niña phase) DJF (0/1) Niño-3.4 SST for each CGCM and observation. Observed El Niño and La Niña events tend to peak in boreal winter (Horii and Hanawa 2004). Therefore, we mainly focus on the seasonally phase-locked transition system of the ENSO from boreal winter to the subsequent season in the present study. It is noteworthy that the CMIP3 CGCMs tend to peak in fall and winter, while most of the models underestimate the percentage of ENSO peaking during these seasons compared to observations (Lengaigne and Vecchi 2009). The peak of central-eastern Pacific SST anomalies is not captured in some CGCMs, each of which shows phase locking to the wrong part of the annual cycle, although some models capture the tendency of the ENSO to peak in boreal winter (Guilyardi et al. 2009).

Concurrent with the mature phase of the warm and cold events, substantial anomalies are manifested over the central-eastern Pacific. A closer look at the observed SST (denoted as OBS) of Fig. 5.1 will demonstrate that some conspicuous features are apparent. One of the most remarkable features is the difference in spatial structure. The location of the maximum SST anomaly during La Niña is shifted to the west by about 30° in the central-eastern Pacific relative to that of El Niño. This asymmetric structure of the SST anomalies is consistent with the composite analysis of observation data (e.g., Hoerling et al. 1997; Kang and Kug 2002). It is particularly noteworthy that the following SST anomalies on the positive phase turn into a negative phase in the following year (Fig. 5.1, OBS left). In contrast, the negative event does not conclude with the significant opposite SST anomalies (Fig. 5.1, OBS right), suggesting that the cold events tend to remain cold SST anomalies. A less cyclic nature of La Niña termination (Kessler 2002) is seen. Thus, to some extent, the separate regression/correlation for the positive and negative index could capture the nature of ENSO asymmetries.

Among the CGCMs, the overall features of SST anomalies around the peak of the simu-

lated ENSO are relatively similar to each other, except for their transition process. As expected, the evolutions of the SST anomalies in few models show asymmetric responses to the Niño-3.4 index. Whereas most of the models display a nearly symmetric relationship between El Niño and La Niña (CSIRO, GFDL0, HadGem, INGV, INM, MIUB, MPI, NCARc, NCARp), especially on the transition period, a few models (GFDL1, CNRM, CSIRO35, HadC3, IPSL) reproduce the asymmetry of transition as seen in the observational data (Ohba and Ueda 2009; Okumura and Deser 2009). As for the observations, strong negative anomalies occur in DJF (1/2) in both the strong warm and cold phases after the mature phase of the ENSO.

The area-averaged lag correlation coefficient between the DJF (0/1) and DJF (1/2) SST over the Niño-3.4 for the warm and cold phases of the ENSO is shown in Table 5.1 for each model. As estimated by the lag correlation, four or five models capture the strong transitivity (persistency) of strong El Niño (La Niña) events, as seen in the observation. It is noteworthy that the model having a strong El Niño transitivity is inconsistent with the model having a strong La Niña persistency. We use the coefficients as an index for the intensity of the El Niño transitivity/La Niña persistency and denote it as the ENSO persistency index (EPI). The positive (negative) values of the EPI suggest that the models tend to have strong persistency (transitivity) after the mature phase of the ENSO event. The intensity of the asymmetricity is derived from the difference of La Niña minus El Niño. Three models (GFDL1, HadC3, and CNRM) show relatively strong asymmetry, as seen in the observation.

5.2 Reproducibility of El Niño transitivity

First, we present a composite of the one-sided lag regression of SST and precipitation with wind stress over the Pacific for the four high-El Niño transitivity (B, F, H, and M) and five

low-El Niño transitivity (G, I, J, N, and Q) models (Fig. 5.2). Figures 5.2a, 5.2b, and 5.2c show the regression of the SST during the DJF (0/1) for the observation and composite of the high- and low-El Niño transitivity models, respectively. The simulated SST and wind stress anomalies during the mature phase of El Niño in the high-El Niño transitivity model composite (Fig. 5.2b) successfully simulate the spatial structure of the El Niño as seen in the observation (Fig. 5.2a). However, those of the low-El Niño transitivity models extend too far west into the Pacific (Fig. 5.2c). These features are associated with a typical systematic error in the CGCMs (e.g., Meehl et al. 2001), which results in a westward shift of the ascending branch of the Walker circulation in the western Pacific.

To confirm the difference in the atmospheric responses between the high- and low-El Niño transitivity model, we also show the observed diabatic heating (Fig. 5.2d) and composite of the precipitation (Figs. 5.2e and 5.2f) with the surface wind vector for the high and low-El Niño transitivity models during DJF (0/1), MAM (1), and JJA(1). The simulated precipitation anomalies during the DJF (0/1) have a large-scale structure, recognized as the east-west contrast between the western and central Pacific. Several differences between the high- and low-El Niño transitivity composite emerge; the first is that the location of the maximum precipitation anomaly in the low-El Niño transitivity is shifted to the west in the Equatorial Pacific (Fig. 5.2f) relative to that of the high-El Niño transitivity (Fig. 5.2e). Associated with the westward shift in the anomalous precipitation, the spatial patterns of surface wind anomalies in the low-El Niño transitivity models is also more shifted to the west than that in the high-transitivity models. The second is the evolution of the anomalous wind and precipitation after their mature phase. The western Pacific precipitation anomalies in the low-El Niño transitivity models show positive values during the decay phase. However, the spatial pattern of high-El Niño transitivity is a

northwest-southeast contrast (Fig. 5.2e), as is also evident in the observation (Fig. 5.2d), and the anomalous equatorial westerlies over the central-eastern Pacific then turn into a cross equatorial northerly in DJF (0/1) to MAM (1). This process is closely linked to the seasonal warming of the southern part of the off-equatorial Pacific from the boreal winter to spring (e.g., Vecchi 2006), which could be associated with the generation of the double ITCZ in the eastern part of the basin. The third is the generation of the anomalous equatorial western Pacific easterly, which is attributed to the additional hastening process to the ENSO transition, namely, the western Pacific oscillator (Wang et al. 1999). While the high-El Niño transitivity models show the anomalous easterly over the western Pacific after the mature to the decay phase, those in the low-El Niño transitivity do not present.

To seek more convincing evidence for the difference in the atmospheric response to the ENSO SST between the high- and low-El Niño transitivity models, we plotted a time series of the simulated equatorial wind stress anomalies derived from the positive side regression (Fig. 5.3). Near the end of the calendar year, there is a southward shift of the anomalous equatorial westerlies. Vecchi and Harrison (2006) and Vecchi (2006) showed that this feature is related to the seasonal movement of the warmest SST to south of the equator, which changes the convective anomalies from those centered on the equator to those centered south of the equator and then causes the thermocline shallowing. Recent studies (e.g., Kug and Kang 2006; Ohba and Ueda 2007) additionally pointed out the importance of the equatorial western Pacific trade wind and the subsequent ENSO turnabout. Following the rapid change in the equatorial wind stress anomalies, the thermocline at the Eastern Pacific turns into La Niña condition rapidly (Ohba and Ueda 2009). Therefore, it will be useful to look at the timing of the change in the equatorial zonal wind anomalies.

In Fig. 5.3, we show the time evolution of the zonal wind stress anomalies for high- and low-El Niño transitivity models, zonally averaged on the equatorial Pacific region (130°E-110°W). Following the onset of positive ENSO SST anomalies, the anomalous westerlies gradually increase. In the high-El Niño transitivity models (Fig. 5.3a), the maximum westerly anomalies appear in the boreal fall (0) and then rapidly decrease during the mature phase. In the subsequent seasons, the simulated wind anomalies turn into easterlies. The rapid reduction of the zonal wind can be accounted for by the southward shift of the anomalous westerly and the expansion of the anomalous easterlies over the western Pacific (Fig. 5.2e), which acts as a counterbalance to the westerly. In comparison with the zonal wind stress anomalies in the high-El Niño transitivity models, those in the low-El Niño transitivity models decrease gradually from the boreal fall and winter (0) to the spring of the subsequent year. The equatorial westerlies remain for the subsequent season or only very weak wind anomalies.

The unrealistic features in the low-El Niño transitivity models reported above could be accompanied by several deficiencies in the simulated climatology to some extent. To discuss the impact on the model climatology and the simulated ENSO, we show the composited climatological SST, precipitation, and equatorial zonal wind stress for high- and low-El Niño transitivity CGCMs (Fig. 5.4). As presented in Figs. 5.4b and 5.4d, the low-El Niño transitivity models suffer from a cold tongue problem. The simulated climatological rainfall over the equatorial western central Pacific is reduced (Fig. 5.4d) considerably more than that in the high-El Niño transitivity models (Fig. 5.4c). This is a consequence of the simulated strong cold tongue extending too far west, pushing westward the ascending branch of the Walker circulation with the enhanced equatorial surface easterlies in the western Pacific (Fig. 5.4e).

There is a possible linkage between the transitivity of El Niño and intensity of the climato-

logical precipitation over the western Pacific. Figure 5.5 shows an inter-model relationship between the annual mean precipitation rate averaged over the equatorial western central Pacific (Fig. 5.4c, solid box: 150°E-160°W, 5°S-5°N) and the EPI of the warm phase (Fig. 5.5). The correlation coefficients are -0.69. The simulated precipitation over the equatorial western central Pacific in the CGCMs is less than that in observation, as already pointed out in previous studies (e.g., Lin 2007; Ose and Arakawa 2009). Although other factors may also affect the reproducibility of the El Niño transition in the studies mentioned above, Fig. 5.5 implies that the bias over the equatorial western central Pacific affects the intensity of the transition process of El Niño; namely, weaker western central Pacific precipitation tends to result in the weaker transitivity of the simulated El Niño in the CGCMs.

The argument presented above is mainly the simulated climatological state of CGCMs, which is related to the direct atmospheric response of the western Pacific to the El Niño during the boreal winter to spring (Wang et al. 2000; 2002). The question of how the subsequent equatorial easterly anomalies in the decay phase of the ENSO (Fig. 5.3a) appear needs to be addressed. In addition to the direct response to the El Niño-related SST anomalies, external forcing could also contribute to the enhancement of easterly anomalies over the equatorial western Pacific. Recently, several studies recognized the importance of the Indian Ocean feedback on the ENSO transition (e.g., Annamalai et al. 2005; Kug and Kang 2006; Ohba and Ueda 2007) via the generation of Indian Ocean basin-wide warming (e.g., Klein et al. 1999) in response to the El Niño forcing. They have shown that the Indian Ocean basin-wide warming during El Niño mature to decay phase can influence the tropical western Pacific wind variability. According to them, the basin-wide warming during the boreal winter strengthens the surface easterlies over the equatorial western Pacific, which induces an advanced transition to the La

Niña phase. In Fig. 5.6, we show a composite of the one-sided correlation coefficient between Indian Ocean SST and DJF (0/1) Niño-3.4 SST for high- and low-El Niño transitivity models. It is clearly evident that the high-El Niño transitivity models have a strong inter-basin coupling between the Indian Ocean and Pacific, while those of the low-El Niño transitivity models do not. The inter-modal correlation coefficients between the EPI of the warm phase and the area-averaged one-sided correlation coefficients of SST over the Indian Ocean (40°E-120°E, 30°S-30°N) is -0.61. The result presented here suggests that the simulation of the Indian Ocean basin-wide warming could be an important point that contributes to the transition process of El Niño in the CGCMs in addition to the climatological condition of the western central Pacific.

5.3 Reproducibility of La Niña persistency

The section above presents the relationship between the El Niño transitivity and climatological precipitation over the western Pacific on the CGCMs. However, the linkage between the equatorial western Pacific and the persistency of the simulated ENSO is very weak. The inter-model correlation coefficients between the EPI of the cold phase and the precipitation rate averaged over the equatorial western Pacific is 0.16. These results suggest that the persistency of La Niña could be regulated by another factor.

To seek another regulation factor of La Niña persistency in relation to the climatological base state, we also conducted a composite analysis of the cold phase for the four high-La Niña persistency (B, D, F, and H) and four low-La Niña persistency models (C, M, P, and Q), as conducted for the warm phase of the ENSO (Fig. 5.2). Figure 5.7 shows the observation and composite of the high- and low-La Niña persistency models of SST in DJF (0/1) (Figs. 5.7a, 5.7b and 5.7c, respectively) and precipitation with the surface wind vector in DJF (0/1), MAM

(1), and JJA (1) (Figs. 5.7d, 5.7e, and 5.7f, respectively). While the special pattern of the SST, precipitation and wind anomalies are relatively similar to each other in DJF (0/1) (Figs 5.7b and 5.7c), they have some differences in the following season. The precipitation and wind stress anomalies over the equatorial western central Pacific Pacific in the low-La Niña persistency models (Fig. 5.7f) are reduced more than half in MAM (1), and La Niña then terminates in JJA (1). However, the high-La Niña persistency models retain the anomalies for these seasons (Fig. 5.7e).

In Fig. 5.8, we show the time evolution of the zonal wind stress anomalies for the high-La Niña persistency and low-La Niña persistency models, zonally averaged on the Equatorial Pacific region. Following the onset of negative ENSO SST anomalies, the easterly wind stress anomalies gradually increase. In the high-La Niña persistency models (Fig. 5.8a), maximum anomalous easterlies appear in the boreal late winter (0/1) to spring (1). The anomalies in the following season retain relatively negative values (easterlies), and, therefore, the following winter (1) shows a weak easterly. The remains of the easterly anomalies can counteract the transition process of ENSO. In comparison with the zonal wind stress anomalies in the high-La Niña persistency models, those in the low-La Niña persistency models decrease rapidly from the boreal fall and winter (0) to the subsequent spring (1). The equatorial easterlies get closer to zero and then turn into westerly anomalies in the subsequent seasons.

The zonal wind stress anomalies associated with the anomalous surface wind directly displace the thermocline vertically via Ekman pumping. The signal of thermocline variations rapidly propagates eastward and then changes the oceanic vertical structure in the equatorial Pacific. Thus, we will compare the observed equatorial thermocline behavior between high- and low-La Niña persistency, especially around the mature phase of the cold ENSO. Displayed in

Fig. 5.9 is the evolution of the equatorial monthly mean ocean heat content (OHC) anomalies of the composited one-sided regressions for high- and low-La Niña persistency models. In the mature to the decay phase of a cold ENSO event, seasonally fixed cold anomalies of OHC take place along the equatorial band (Figs. 5.9a and 5.9b). The modulation of the OHC describes the most important dynamical feature in both wave transition-type oscillators (delayed-oscillator/western Pacific oscillator) and recharge oscillator paradigms. In agreement with the theories, the OHC shown in Fig. 5.9 not only serves as the key positive feedback that overcomes a damping effect but is also one of the primary factors responsible for the phase turnaround from cold to warm.

A closer look at Figs. 5.9a and 5.9b shows that the OHC is considerably different during the mature to the decay phase of La Niña between the high- and low-La Niña persistency models. Although the evolution of the composited OHC anomalies in the low-La Niña persistency models is similar to that in the high-La Niña persistency models, temporal progress of the anomalies in the decay phase is obviously different. In the high-La Niña persistency models, the OHC anomalies gradually decrease in the following season and are re-enhanced for the DJF (1/2) (Fig. 5.9a). Thus, the cooling via thermocline feedback continues until the following year (1), which is similar to the observation (Ohba and Ueda 2009). However, that of the low-La Niña persistency models is not. In the low-La Niña persistency models, the turnabout of the OHC anomalies is recognized in the DJF (0/1) (Fig. 5.9b), namely, in its mature phase. The ENSO transition of subsurface condition from the La Niña to the El Niño phase is established in the following year. It is conceivable that the difference in OHC could be one of the most important points for the different persistency of the La Niña.

To describe the time evolution of the ENSO transition in relation to variability in the wind

forcing, we also plot a longitude-time section of the composite of the zonal wind stress anomalies (Fig. 5.10a) and the time rate of the change in OHC near the equator (Fig. 5.10b) for the low-La Niña persistency models. A precursor to the ENSO phase transition is the buildup of heat content in the western Pacific (Weisberg and Wang 1997; Guilyardi et al. 2003), which is attributed to equatorial wind changes (Wang et al. 1999: Harrison and Vecchi 1999; Vecchi and Harrison 2003). In the developing stage of La Niña (from June through October), a strong anomalous easterly at the surface is recognized during the developing stage of La Niña, corresponding to the atmospheric response to the associated cooling over the equatorial Pacific. In contrast, the anomalous western Pacific easterly is rapidly reduced in the mature to decay phase of La Niña (Fig. 5.10a). The wind changes over the equatorial central Pacific can generate eastward-propagating thermocline deepening, leading to the turnaround of the SST tendency in the central-eastern Pacific. In the low-La Niña persistency models, the signal of OHC cool anomalies propagates eastward from the western Pacific at a speed of about 40-50° of longitude per month, roughly the propagation speed of the first and second baroclinic Kelvin modes (e.g., Boulanger et al. 2003). As a consequence, the cold condition in the central-eastern Pacific starts to recover its slope and returns to the warmed condition (Fig. 5.10b).

As presented above, the decrease of the anomalous easterlies in the low-La Niña persistency models is not consistent with that in the high-La Niña persistency models. The model biases that generate the difference need to be examined. One of the possible causes is seasonal changes in the sensitivity of the atmospheric response to the SST anomalies. In the observation, the seasonal change of the mean state in the western central Pacific is much weaker than that in the Eastern Pacific; namely, the western central Pacific is in a relatively stable condition that could result in the duration of La Niña (Ohba and Ueda 2009). Therefore, a seasonal change in

the mean state is important to the persistency of La Niña. Reduced intensity of the climatological precipitation could result in a decrease in the atmospheric response to underlying SST anomalies. Figure 5.11a represents a seasonal evolution of climatological precipitation over the western central Pacific (Fig. 5.4c, solid box: 150°E-160°W, 5°S-5°N) for the four low-La Niña persistency models (solid) and the observation (dash). In the observation, climatological rainfall at the equatorial western central Pacific tends to peak in the boreal spring, as is well known. However, unfortunately, those of the low-La Niña persistency models tend to peak in the boreal winter. The precipitation is reduced about 30-70% from boreal winter to spring. We also show the spatial pattern of the inter-modal correlation coefficient between the difference of the climatological precipitation from DJF to MAM and the EPI of the cold phase on each CGCM (Fig. 5.11b). Relatively high correlation is found, especially over the central Pacific. The results of the analysis suggest that the persistency of La Niña could be mainly associated with biases in the seasonality of the climatological precipitation field from winter to spring.

5. 4 Discussion

Most of the CGCMs are unable to simulate the feature of both phases of the ENSO transition. Only three models (GFDL1, HadC3, and CNRM) capture both observed El Niño and La Niña transition processes. The nonlinear climate response to the ENSO is an important factor to understand the nonlinear ENSO cycle. This study underlines the importance of the asymmetric transition process of the ENSO tied to the reproducibility of the (nonlinear) cyclic nature of the ENSO in CGCMs. In addition, as reported above, our analysis reemphasizes the importance of the spatial and seasonal cycle of the climatological condition in CGCMs, especially on the equatorial western central Pacific. Realistic simulation of the climatological precipitation over

the western central Pacific (i.e., intensity of the cold tongue) is one of the most important points to reproduce the transition system of the ENSO.

Observational evidence shows that convective activity increases sharply above a threshold SST of 27°C (Graham and Barnett 1987), while the SST above that temperature has little effect on the enhancement of convection. Because of the nonlinear relationship between the SST and convection, the difference in the climatological SST fundamentally alters the response of equatorial atmospheric conditions to the same SST anomalies, leading to a different equatorial wind stress response. It is conceivable that the atmospheric response to the SST in the mature to the decay phase of the ENSO is principally due to how the ENSO-related SST anomalies modulate the line of 27°C. Therefore, the distribution of the climatological SST and its seasonal changes could be an important factor for a realistic simulation of the ENSO oscillation in air-sea coupled models.

The intensity of the cold tongue (climatological precipitation) over the equatorial western central Pacific is relatively strong (weak) in the CMIP3 climate models, especially BCCR, HadGem, INM, and NCARp. As presented in this study, these biases could contribute to the transition system of the simulated ENSO. One of the most plausible causes is the parameterization of deep convection in the CGCMs. Deep convection is the primary heat source driving the large-scale circulation through the release of latent heat, and it drives the vertical redistribution of heat, moisture, and momentum. The representation of deep convection is, therefore, central in defining both the climatological SST and precipitation via their dynamical and heat flux atmosphere feedbacks. Several recent studies have documented the impact of a modified convection scheme on the ENSO in the CGCMs. Recently, Kim et al. (2008) and Neale et al. (2008) have shown that the inclusion of "convective momentum transport" increases the climatological

precipitation at the Equatorial Pacific through redistribution of the momentum vertically towards the surface. The enhanced precipitations over the western central Pacific result in the eastward shift of the ENSO-related anomalies. Therefore, the inclusion of "convective momentum transport" on the parameterization could enhance the El Niño transition on the CGCMs.

MIUB and MRI use flux adjustments. The use of flux adjustments approximates the simulated Pacific condition to the observation. The adjustments capture the relatively strong precipitation over the western Pacific and relatively high transitivity of El Niño, while those of the persistency of La Niña do not. The simulated climatological precipitations in both models decrease from the boreal winter to spring, which could result in an inaccurate reproduction of the La Niña persistency despite the flux adjustment. In addition, the EPI of the cold phase spreads on both the positive and the negative sides. These results imply that the reproduction of the La Niña duration, as observed during the cold events of 1971-72, 1974-76, 1984-1986 and 1999-2001, is more difficult than that of the El Niño transition system in the CGCMs.

In addition to the climatological condition of the western central Pacific, the simulation of the Indian Ocean basin-wide warming could also be an important factor that contributes to the transition process of El Niño in the CGCMs. As is well known, the ENSO impacts Indian Ocean SST variability through thermodynamic atmospheric forcing as well as ocean dynamics. The thermodynamic forcing results in basin-wide SST anomalies of the same sign over the tropical Indian Ocean, a few months following the peak of the ENSO. Some CGCMs simulated the basin-wide SST anomalies following an ENSO (Saji et al. 2006). It is beyond the scope of this paper to systematically explore the reasons for these deficiencies in simulating the Indian Ocean response to an ENSO. In addition to the amplitude of the simulated ENSO, the reproducibility of the coupling between the Indian Ocean and Pacific in the CGCMs could be responsi-

ble for the realistic response of the precipitation anomalies over the maritime continents to El Niño, as investigated by Ose and Arakawa (2009). Further research is needed for the strength of the inter-basin coupling between the Indian Ocean and Pacific, which will be the focus of our next study.

5. 5 Summary

Using the method of one-sided regression/correlation analysis applied to WCRP's CMIP3 multi-model datasets, we investigated an air-sea coupled process of El Niño and La Niña from the mature to the decay phase in terms of the reproducibility of their transitivity and persistency, respectively. Regarding the nonlinear response of the tropical convection, the air-sea coupled system over the tropical region tends to facilitate the warm-to-cold ENSO transition more than the cold-to-warm phase. This observed asymmetric behavior witnessed in observations is reproduced only in a few CGCMs, implying that the simulation of the air-sea coupled system is relatively difficult.

The atmospheric response for the warm phase of the observed ENSO causes a rapid reduction of the zonal wind stress at the equator via a southward shift of the anomalous westerly and an enhancement of the western Pacific easterly in relation to the Philippines anticyclone. This process plays a significant role in accelerating the following ENSO transition through a displacement of the thermocline depth anomalies. In the El Niño phase, some CGCMs reproduce these observed features on the transitivity of the warm phase, with their atmospheric response to the SST anomalies. For these models, the spatial distribution of the simulated precipitation and wind stress anomalies is close to what is observed in the mature to decay phase of the ENSO. These high-El Niño transitivity CGCMs capture a rapid decrease of the equatorial westerly

anomalies with the intrusion of the western Pacific easterly anomalies during the transition period, while low-El Niño transitivity CGCMs fail to simulate the mechanism. The difference in the transition process between the high- and low-El Niño transitivity is largely dependent on the inter-model variability of precipitation at the equatorial western central Pacific in addition to the Indian Ocean SST forcing. Reduced climatological precipitation, associated with the strong cold tongue bias in the equator, causes the westward shift in the center of the El Niño-related precipitation anomalies and then weakens the effect of the "western Pacific oscillator" (e.g., Weisberg and Wang 1997) and "Southward shift in convection" (Vecchi 2006) mechanisms. The transition process of the low-El Niño transitivity models can only be dependent on other factors, such as the "delayed oscillator" or "recharge oscillator," which has weak seasonality.

However, the high reproducibility of the El Niño transitivity is not consistent with those of the La Niña persistency. The La Niña persistency is also reproduced by only a few CGCMs. The anomalous equatorial easterlies on the mature phase of an observed cold event persist until the subsequent spring, which tends to counteract the turnabout from a cold to a warm event of the ENSO. Most models fail to simulate the observed persistence of equatorial easterly anomalies over the western Pacific after their mature phase, resulting in the end of the events thorough the generation of oceanic warm Kelvin waves. We consider that one possible reason is related to the seasonality of climatological precipitation over the Equatorial Pacific, namely, a decrease in the simulated-climatological precipitation from the boreal winter to spring. The bias could contribute to the decrease in the sensitivity of the precipitation anomalies to the underlying SST anomalies.

Previous studies show that changes in the simulation of intraseasonal variability (e.g., Neale et al. 2008) and the vertical state mean of the thermocline (e.g., Meehl et al. 2001) can lead to

changes in the triggering and amplification of the ENSO. In addition to them, the present study shows the importance of the climatological surface-atmospheric condition over the Pacific (and also interactive feedback from the Indian Ocean). Improvement of the western central Pacific precipitation biases could contribute not only to the magnitude and length of an ENSO (e.g., Capotondi et al. 2006) but also to the transitivity of El Niño.

One caveat to our approach is that we have given attention primarily to the mean state while ignoring other factors. In fact, the system of the ENSO can be changed by a number of other mechanisms not fully considered here, such as stochastic forcing or an external influence (e.g., Indian Ocean warming). For example, the simulated ENSO in the NCARc shows a linear oscillation, as presented in oscillator theories, while the seasonal evolution of the atmospheric response of the ENSO is relatively asymmetric. Since the seasonally phase locked system of simulated ENSO is relatively weak, we speculate that a recharge or delayed oscillator-like ocean dynamics are predominant in the model. Therefore, further validations for the four components (i.e., stochastic forcing, interactive feedback, and a climatological atmospheric and thermocline state) are needed to understand the regulation of the transition system of the ENSO in the CGCMs.

Corr. coeff. DJF(1/2) (averaged over Nino3.4 region)

ID	Model	Warm phase	Cold Phase	Asymmetricity
	OBS	-0.33	0.36	0.70
A	BCCR2	-0.12	0.18	0.30
B	CNRM	**-0.32**	**0.40**	**0.73**
C	CSIRO	-0.22	-0.29	-0.07
D	CSIRO35	-0.16	**0.39**	0.55
E	GFDL0	-0.19	0.02	0.20
F	GFDL1	**-0.52**	**0.29**	**0.81**
G	GISSh	-0.10	0.10	0.20
H	HadC3	**-0.40**	**0.41**	**0.81**
I	HadGem	-0.01	0.03	0.04
J	INM	-0.05	0.09	0.14
K	INGV	-0.22	0.18	0.40
L	IPSL	-0.27	0.16	0.43
M	MIUB	**-0.48**	-0.36	0.12
N	MPI	-0.11	0.02	0.13
O	MRI	**-0.30**	0.04	0.33
P	NCARc	-0.16	-0.16	0.01
Q	NCARp	-0.07	-0.05	0.03

Table 5.1: List of ENSO persistency index (EPI) of the El Niño and La Niña phase in each CGCM. The indexes are derived from the one-sided lag correlation analysis between the SST during the DJF (0/1) and DJF (1/2). Bold values imply the high-El Niño transitivity/La Niña persistency models. Asymmetricity is derived from the difference of La Niña minus El Niño.

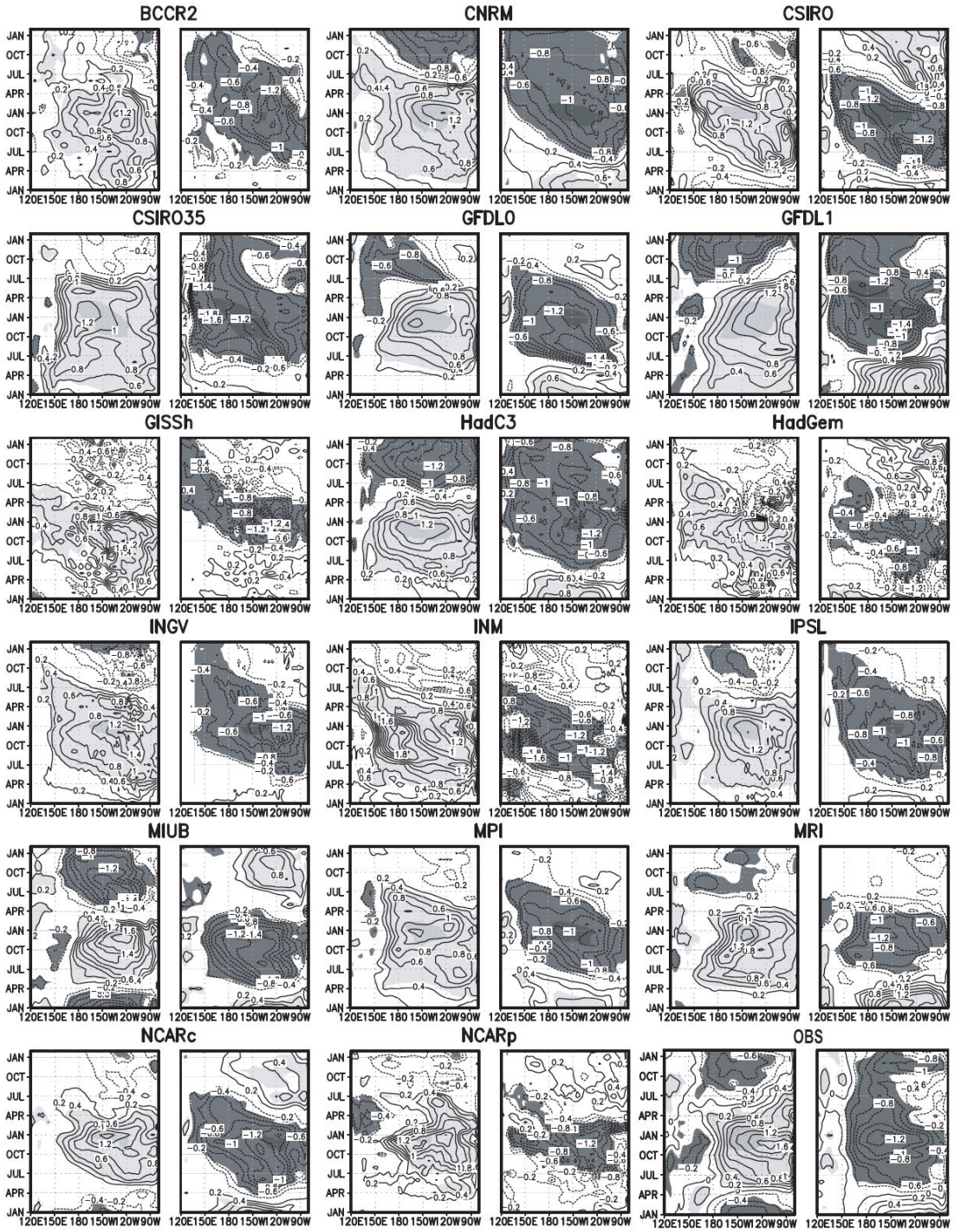

FIG. 5.1: Evolution of SST anomalies averaged over 2°S-2°N obtained through one-sided regression on the positive (left) and negative (right) Niño-3.4 index during DJF (0/1) for each CGCM and observation (denoted as OBS). The shaded areas indicate where the regression is above the 95% significant level.

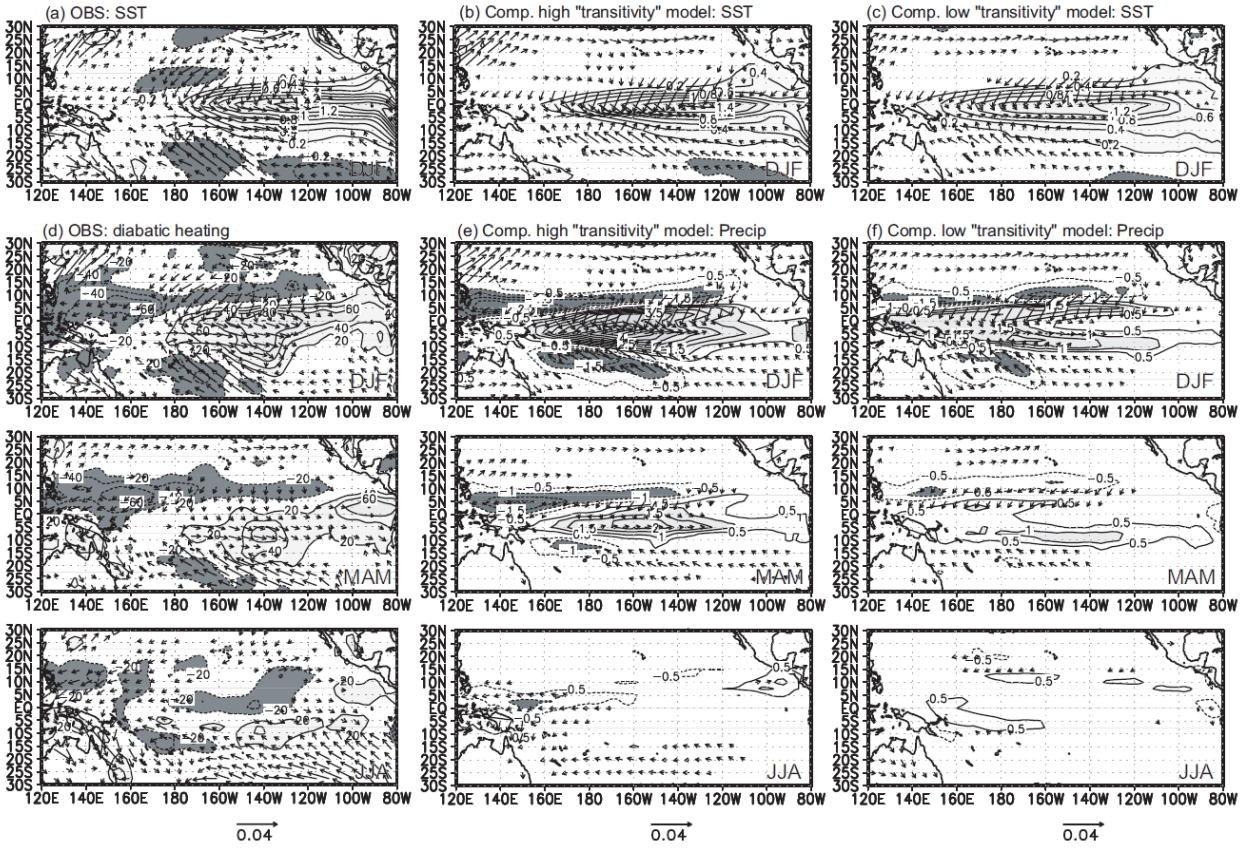

FIG. 5.2: One-sided regressions of the SST (°C) and wind stress (N/m^2) for El Niño phase of the Niño-3.4 index during DJF (0/1) for (a) observation, (b) composite derived from high transitivity models, and (c) composite derived from low transitivity models. The light- (dark-) shaded areas indicate where the positive (negative) regression coefficient is greater (smaller) than 0.2 (-0.2) °C. (d), (e) and (f) are same as (a), (b) and (c), except for diabatic heating and precipitation for DJF (0/1), MAM (1), and JJA (1). The light- (dark-) shaded areas indicate where the positive (negative) regression coefficient is greater (smaller) than 20 (-20) W/m^2 for (d), 1 (-1) mm/day for (e) and (f).

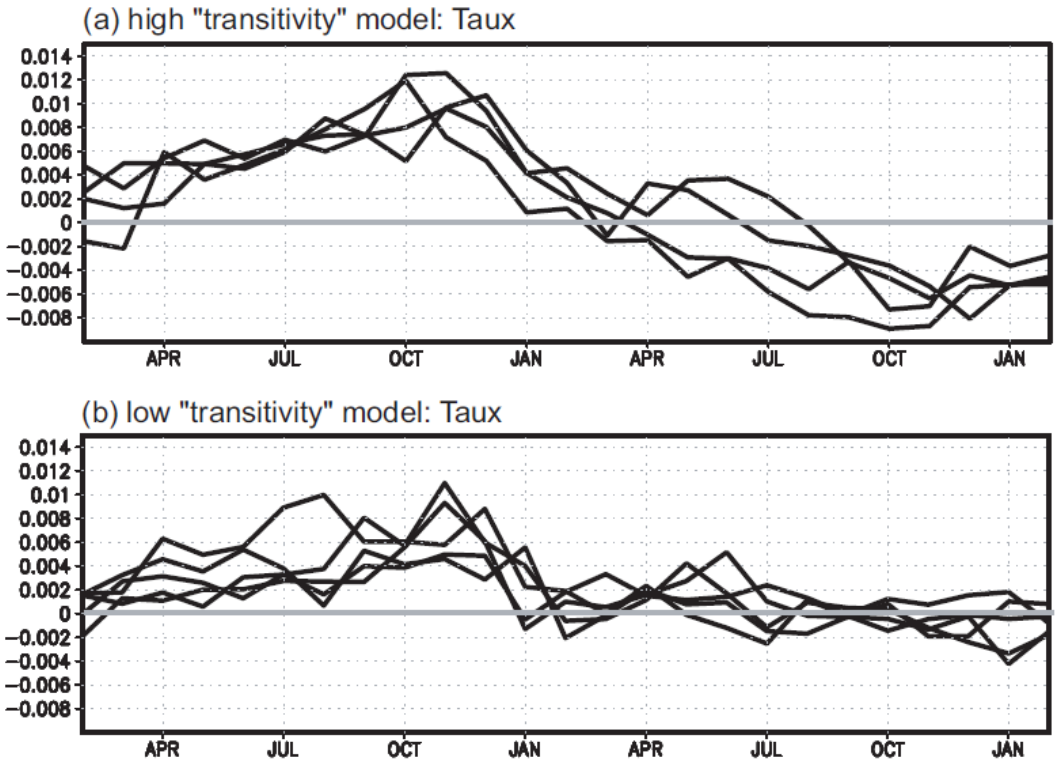

FIG. 5.3: Time evolution of the zonal wind stress anomalies (N/m^2) averaged over the equatorial band (130°E-110°W) of each CGCM for (a) four high transitivity models and (b) five low transitivity models from February (0) to February (2).

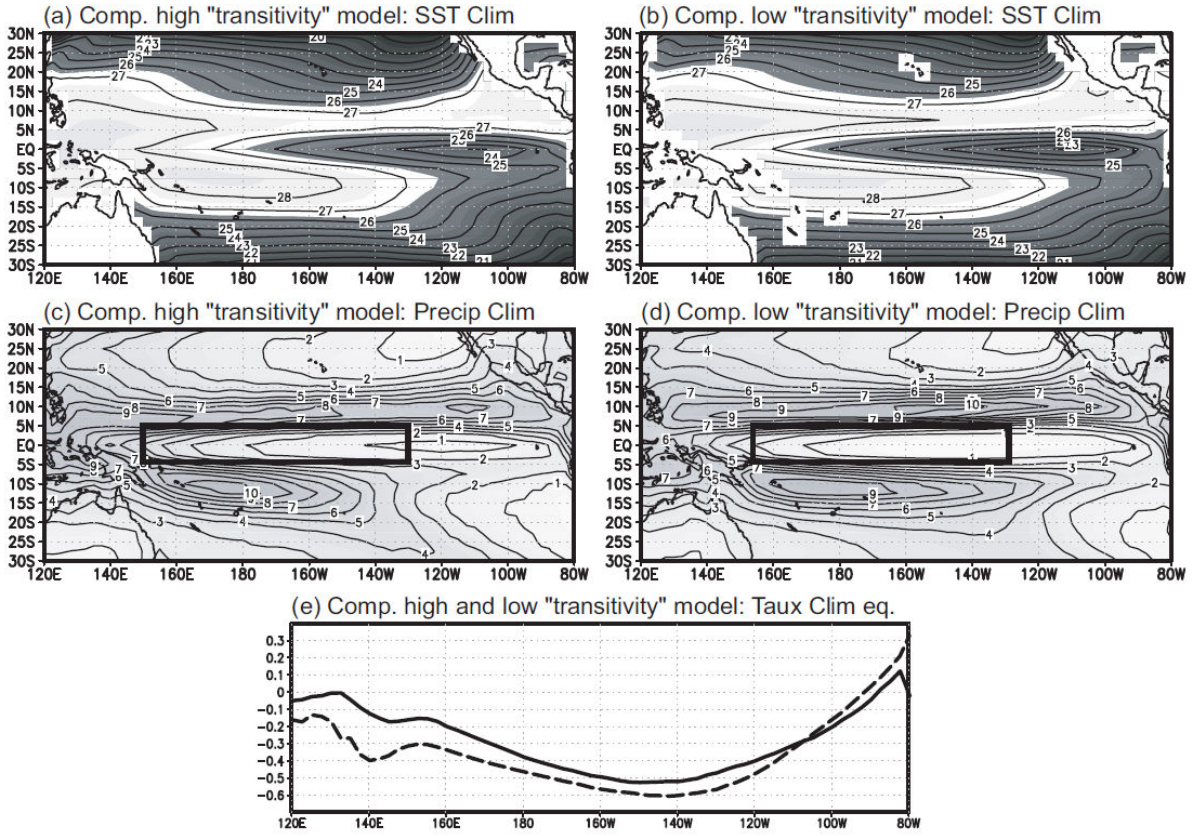

FIG. 5.4: Composited climatological annual mean simulated SST (°C) for the (a) high transitivity models and (b) low transitivity models. (c) and (d) are same as (a) and (b), except for precipitation (mm/day). (e) Composited climatological annual mean of simulated zonal wind stress (N/m^2) at the equator for the high- (solid) and low- (dash) transitivity models.

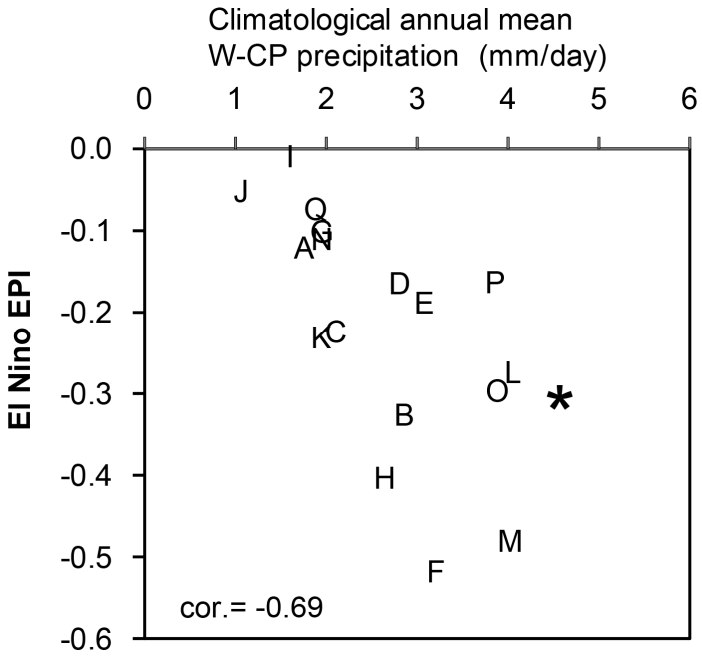

FIG. 5.5: Scatter diagrams of the climatological annual mean precipitation (mm/day) of the western-central Pacific (5°S-5°N, 150°E-130°W) and the EPI of the warm phase ENSO. Letters indicate model IDs shown in Table 2.1, and an asterisk is the observation.

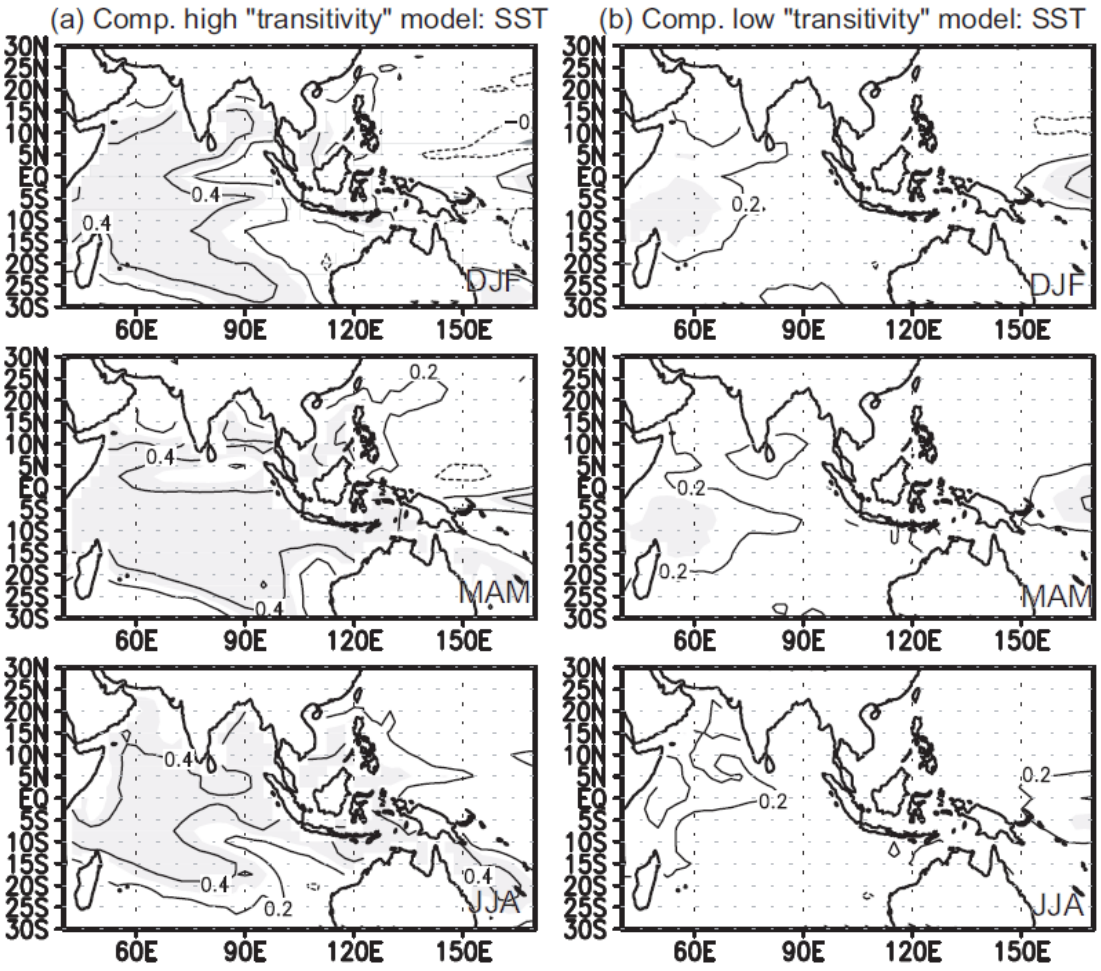

FIG. 5.6: One-sided lag correlation between the SST over the Indian Ocean for DJF (0/1), MAM (1), and JJA (1) and El Niño phase of the Niño-3.4 index during DJF (0/1), for (a) composite derived from high transitivity models, and (b) composite derived from low transitivity models. The light- (dark-) shaded areas indicate where the positive (negative) correlation coefficient is greater (smaller) than 0.3 (-0.3).

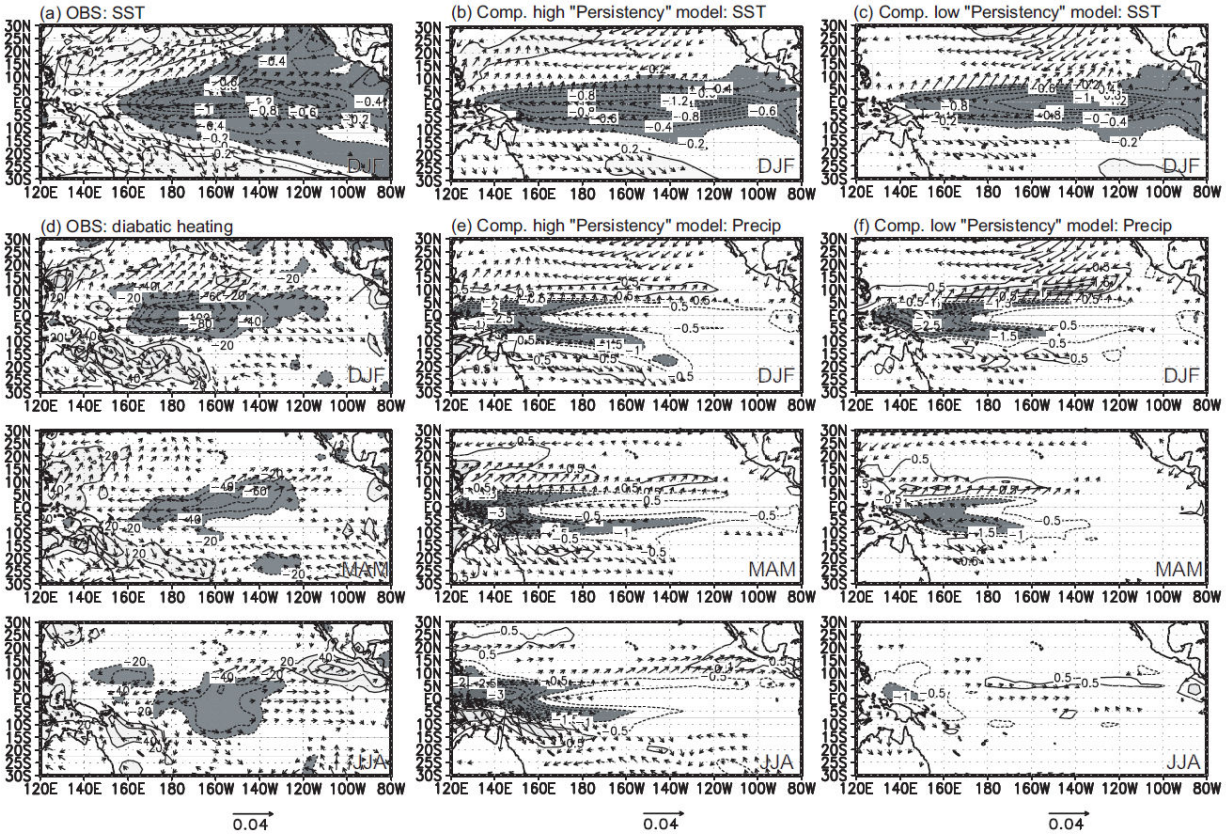

FIG. 5.7: Same as Fig. 5.2 except for (a, d) observation, (b, e) composite derived from high persistency models, and (c, f) composite derived from low-persistency models.

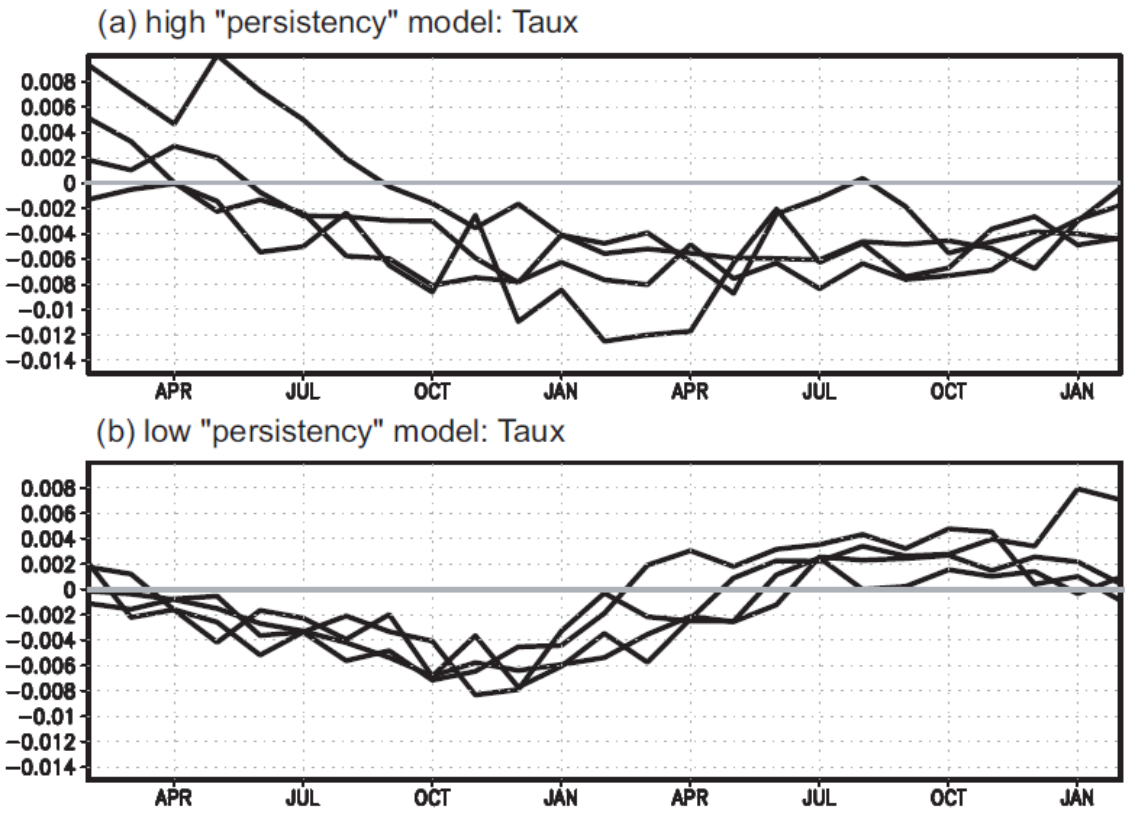

FIG. 5.8: Same as Fig. 5.3 except for (a) four high persistency models and (b) five low persistency models from February (0) to February (2).

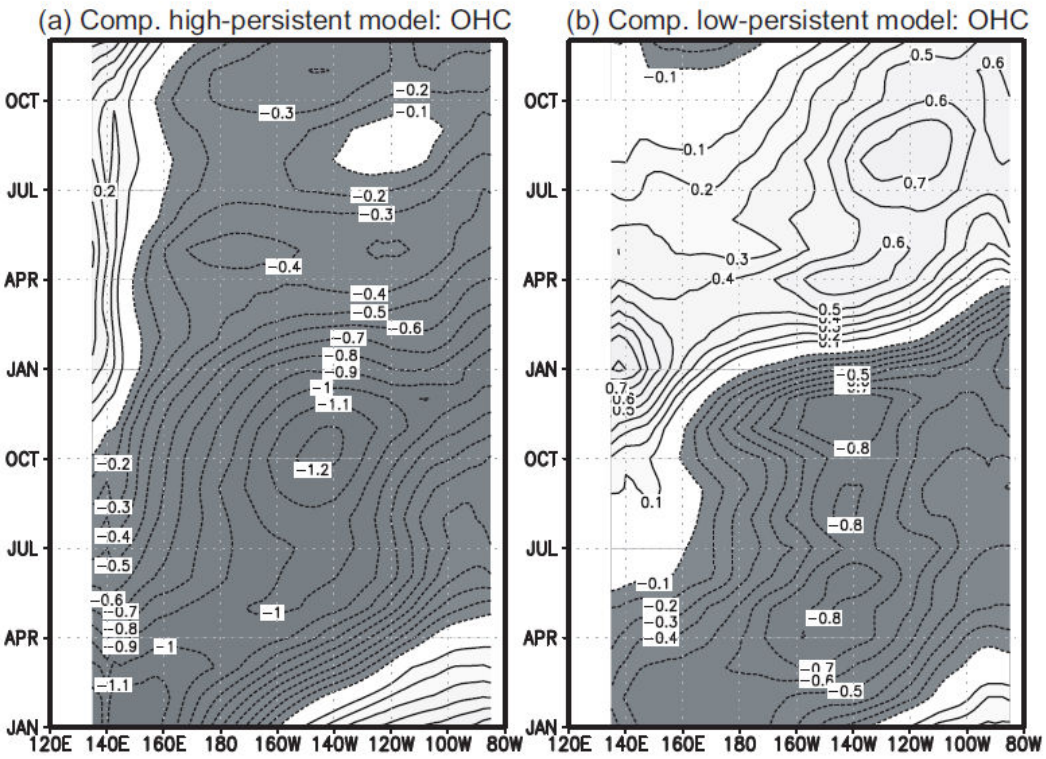

FIG. 5.9: Evolution of the composited OHC anomalies (°C) averaged over 2°S-2°N for (a) high persistency models and (b) low persistency models. The OHC anomalies of each CGCM are obtained through one-sided regression on the negative Niño-3.4 index during DJF (0/1).

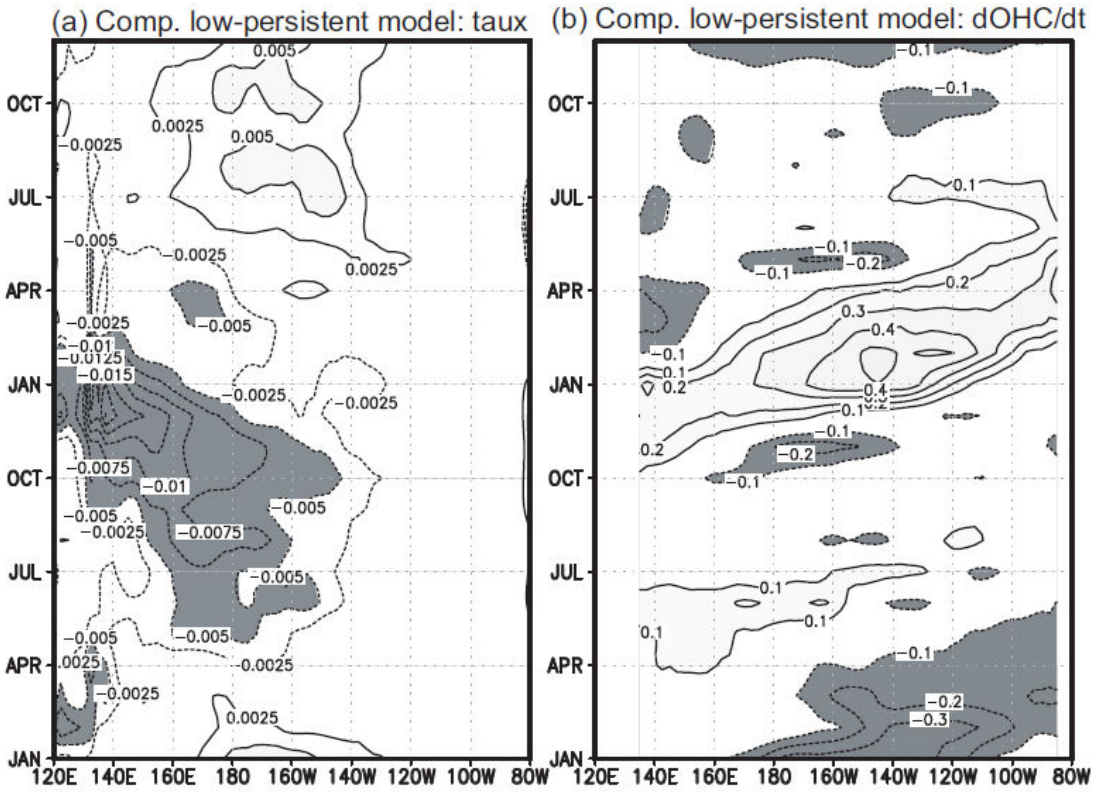

FIG. 5.10: Same as Fig. 5.9 except for composited (a) zonal wind stress anomalies (N/m^2), (b) OHC tendency anomalies (°C) derived from low persistency models.

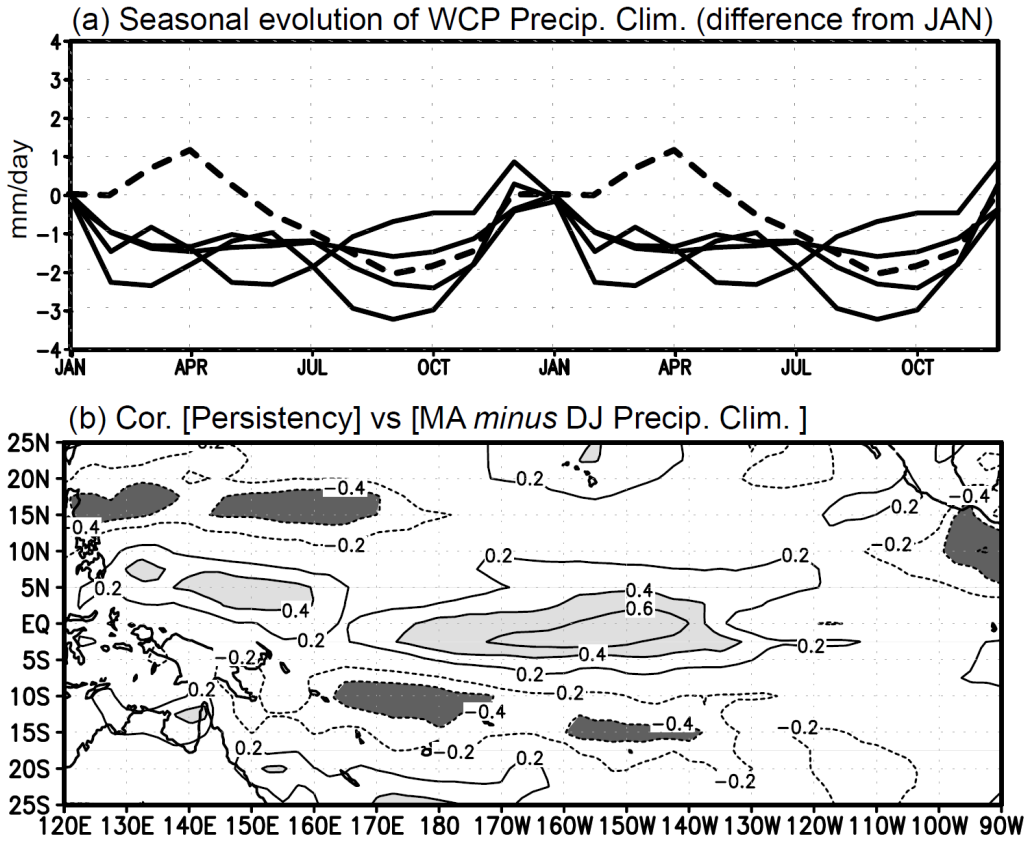

FIG. 5.11: (a) Seasonal evolutions of climatological precipitations over the western central Pacific (Fig. 5.4c, solid box: 150°E-160°W, 5°S-5°N) for the four low-La Niña persistency models (solid) and observation (dash). The precipitations are plotted as difference from the values in January. (b) Inter-modal correlation between the La Niña persistency indexes of each CGCM with the seasonal change in climatological precipitation from boreal winter to spring (March-April minus December-January).

Chapter 6

Conclusions

In Chapter 3, using the method of one-sided regressions applied to reanalysis data and simple experiments by use of AGCM, we have confirmed the existence of asymmetric responses of the atmosphere associated with the opposite phases of the ENSO, especially at the calendar year end. Regarding the nonlinear response of the tropical convection, the air-sea coupled system over the tropical region tends to facilitate the warm-to-cold ENSO transition rather than the cold-to-warm phase. This asymmetric behavior witnessed in observations is reproduced in simple experiments to some extent, implying that our suggestions capture a part of the air-sea coupled system, which causes the redevelopment of the La Niña event.

The results of this study implicitly suggest that the nonlinear climate response to the ENSO is an important factor to understand the nonlinear ENSO cycle, particularly in its decay phase. The asymmetric response of the atmosphere in the tropical Pacific is a key to understanding the features of the subsequent behavior on the warm and cold events after its mature phase.

In Chapter 4, we conducted a set of experiments by use of a stand-alone CGCM to capture the influence of the El Niño-related SST anomalies in the Indian Ocean on the ENSO transition. During the mature-decay phase of El Niño, the Indian Ocean-BW during the winter enhances the diabatic heating over the tropical Indian Ocean, which is recognized as the enhancement of the ITCZ over the region. The anomalous diabatic heating is linked to enhancement of the low-level easterly in the equatorial western Pacific. As a consequence, the anomalous surface

easterlies in the western Pacific during the mature-decay phase of the El Niño induce an advanced transition to La Niña phase by more generating the negative oceanic Kelvin wave. These results imply that the BW in the Indian Ocean strengthens the transition process of El Niño, to some extent, that could result in an enhancement of the asymmetry of ENSO transition.

In Chapter 5, using the method of one-sided regression/correlation analysis applied to WCRP's CMIP3 multi-model datasets, we have investigated the air-sea coupled process of El Niño and La Niña from the mature to decay phase, in terms of the reproducibility of their transitivity and persistency, respectively. Some of the models reproduce the features of the simulated transition process of El Niño/La Niña, while most models fail to concurrently reproduce the process in both phases. The mechanisms, in relation to a rapid transition of strong El Niño, are mainly related to the intensity of the simulated climatological precipitation over the western central Pacific. The transition process of the models which have weak western central Pacific precipitation is relatively weak compared to those with strong western central Pacific precipitation. In addition, the coupling between the Indian Ocean and the Pacific is an important for simulating the El Niño transitivity. The results of this section confirm the results of Chapters 3 and 4 that the western Pacific easterly anomalies during El Niño could be controlled not only by the air-sea coupled system, but also by the feedback effect from the Indian Ocean.

This relationship is not applicable to the La Niña phase. The reproducibility of La Niña persistency is mainly related to the seasonal evolution of the climatological precipitation in the western central Pacific. In comparison with the eastern Pacific, the annual cycle of the western central Pacific is considerably weaker. As presented in Section 4, the weak annual cycle is one of the causes of La Niña high persistency. Since the sensitivity of the precipitation anomalies to SST anomalies is based on the climatological mean state of rainfall, their seasonal stability is

important to retain the surface wind, and then SST anomalies, in the equatorial central-eastern Pacific.

Differences in the transition process between the warm and cold phase of ENSO events are fundamentally due to the nonlinear atmospheric response to SST, which originates from the distribution of climatological SST and its seasonal changes. The results of the present study indicate that the real simulation of the climatological state, and its seasonality of the western central Pacific, is important to simulate the observed transition process of ENSO. Further study is required to further understand the asymmetry of the ENSO, and the air-sea coupled system between the Indian Ocean and Pacific, that could contribute to further improve the air-sea coupled models for the seasonal and long-term climate forecast.

Acknowledgements

I would like to show my appreciation to all members who have helped the progress of this study. Without the supports from multidiscipline members, the interdisciplinary study could have been deadlocked.

Firstly, I would like to show my sincerest appreciation to advising professor, Associate Prof. Hiroaki Ueda who has supported over research activities in the Graduate School of Life and Environmental Sciences, University of Tsukuba. Supports and advices given by Associate Prof. Ueda improved many parts of this study relating to air-sea interaction of ENSO. Many ideas on analysis in this study were raised at brainstorming with him both in personal and at seminars. Countless comments and suggestions from the viewpoints of meteorology and climatology to this impact assessment study are given from Professors Fujio Kimura, Yousay Hayashi, Hiroshi L. Tanaka, Kenichi Ueno and Hiroyuki Kusaka in the University of Tsukuba, which aid in proceeding development of this study. Additionally, I would like to show my special thanks to my seniors and friends of Univ. of Tsukuba, Drs. Tomoshige Inoue, Sachiho Adachi, Masatake E. Hori, Yasushi Watarai, Tomonori Sato, Mio Matsueda, Noriko Ishizaki, Toshichika Iizumi, Shiori Sugimoto, Koji Terasaki and members of “climate laboratory” for their kind support and comments relating to use the research tools in the present study.

Secondly, I would like to show my great appreciation to Drs. Yoshikatsu Yoshida, Junichi Tsutsui, Norikazu Nakashiki, Daisuke Tsumune, Keiichi Nishizawa, Daisuke Nohara, and global warming project group members in the Central Research Institute of Electric Power Industry (CRIEPI), for their fruitful comments and suggestions.

Thirdly, I also acknowledge Drs Toru Nozawa, Seita Emori, Tatsuya Nagashima, Tomoo

Ogura, Hideo Shiogama, Tokuta Yokohata, Akira Hasegawa, Manabu Abe, Hiroaki Kawase and Toshiharu Nagatomo in the National Institute for Environmental Studies (NIES), for their helpful support during my student time in the Graduate School of Life and Environmental Sciences, University of Tsukuba.

Fourthly, Drs. Akio Kitoh, Tomoaki Ose, Seiji Yukimoto and Osamu Arakawa in the Meteorological Research Institute of Japan Meteorological Agency are acknowledged for providing the source code of MRI-CGCM2.

I also acknowledge the modeling groups, the Program for Climate Model Diagnosis and Intercomparison (PCMDI) and the WCRP's Working Group on Coupled Modeling (WGCM) for their roles in making available the WCRP CMIP3 multi-model dataset. Support of this dataset is provided by the Office of Science, U.S. Department of Energy. This study is partially supported by the Global Environmental Research Fund (S-5-2) of the Ministry of the Environment, Japan. The availability of the WCRP CMIP3 multi-model dataset is realized for the S-5-2 community by the Data Integration & Analysis System (DIAS).

Finally, I would like to show special thanks to my parents. They have kept supporting me mentally and financially. Deepest and particular appreciation should be brought to Ms. Natsuna Matsuishi. The achievement of this study is essentially due to her mental supports and encouragements.

References

AchutaRao, K., and K. Sperber, 2002: Simulation of the El Niño Southern Oscillation: Results from the coupled model intercomparison project. *Climate Dyn.,* **19,** 191–209.

AchutaRao, K., and K. Sperber, 2006: ENSO simulations in coupled ocean–atmosphere models: Are the current models better? *Climate Dyn.,* **27,** 1–16.

Allan, R. J., and Coauthors, 2001: Is there an Indian Ocean dipole independent of the El Niño-Southern Oscillations?, *CLIVAR Exchanges,* **6,** 18–22.

Alexander, M. A., I. Bladé, M. Newman, J. R. Lanzante, N.-C. Lau, and J. D. Scott, 2002: The atmospheric bridge: The influence of ENSO teleconnections on air–sea interaction over the global oceans. *J. Climate,* **15,** 2205–2231.

An, S.-I., and F.-F. Jin, 2000: An eigen analysis of the interdecadal changes in the structure and frequency of ENSO mode. *Geophys. Res. Lett,* **27,** 2573–2576.

An, S.-I., and I.-S. Kang, 2000: A further investigation of the recharge oscillator paradigm for ENSO using a simple coupled model with the zonal mean and eddy separated. *J. Climate,* **13,** 1987–1993.

An, S.-I., and F.-F. Jin, 2004: Nonlinearity and asymmetry of ENSO. *J. Climate,* **17,** 2399–2412.

An, S.-I., Y.-G. Ham, J.-S. Kug, F.-F. Jin, and I.-S. Kang, 2005: El Niño-La Niña asymmetry in the coupled model intercomparison project simulations. *J. Climate*, **18**, 2617–2627.

Annamalai, H., R. Murtugudde, J. Potemra, S. P. Xie, P. Liu, and B. Wang, 2003: Coupled dynamics in the Indian Ocean: Spring initiation of the zonal mode, *Deep-Sea Res.,* **50B,** 2305–2330.

Annamalai, H., S.-P. Xie, J.P. McCreary, and R. Murtugudde, 2005: Impact of Indian Ocean sea surface temperature on developing El Niño. *J. Climate,* **18,** 302-319.

Baquero-Bernal, A., M. Latif, and S. Legutke, 2002: On dipolelike variability of sea surface

temperature in the tropical Indian Ocean. *J. Climate,* **15,** 1358–1368.

Behera, S. K., and T. Yamagata, 2003: Influence of the Indian Ocean Dipole on the Southern Oscillation. *J. Meteor. Soc. Japan,* **81,** 169–177.

Boulanger, J., S. Cravatte, and C. Menkes, 2003: Reflected and locally wind-forced interannual equatorial Kelvin waves in the western Pacific Ocean. *J. Geophys. Res.,* **108 (C10),** doi: 10.1029/2002JC001760.

Burgers, G., and D. B. Stephenson, 1999: The normality of El Niño. *Geophys. Res. Lett.,* **26,** 1027–1030.

Capotondi, A. Wittenberg, and S. Masina, 2006: Spatial and temporal structure of tropical Pacific interannual variability in 20th-century coupled simulations. *Ocean Modell.,* **15,** 274-298.

Carton, J.A., G. Chepurin, and X. Cao, 2000: A simple ocean data assimilation analysis of the global upper ocean 1950–95. Part II: Results. *J. Phys. Oceanogr.,* **30,** 311–326.

Chao, Y., and S. G. H. Philander, 1993: On the structure of the Southern Oscillation. *J. Climate,* **6,** 450–469.

Choi J, An SI, Dewitte B, Hsieh WW, 2009: Interactive feedback between the tropical Pacific decadal oscillation and ENSO in a coupled general circulation model. *J. Climate in Press.*

Dewitte B, Thual S, Yeh SW, An SI, Moon BK, et al., 2009: Low frequency variability of temperature in the vicinity of the equatorial Pacific thermocline in SODA: role of equatorial wave dynamics and ENSO asymmetry. *J. Climate in Press.*

Futami, M., M. Ohba, and H. Ueda, 2009: Role of soil moisture on seasonal evolution in the Asian monsoon, s*ubmitted to Tsukuba Geoenvironmental Sciences.*

Galanti, E., E. Tziperman, M. Harrison, A. Rosati, R. Giering, and Z. Sirkes, 2002: The equatorial thermocline outcropping—A seasonal control on the tropical Pacific ocean–atmosphere instability strength. *J. Climate,* **15,** 2721–2739.

Graham, N. E., and T. P. Barnett, 1987: Sea surface temperature, surface wind divergence, and convection over tropical oceans. *Science*, **238**, 657-659.

Guilyardi E., P. Delecluse, S. Gualdi and A. Navarra, 2003: Mechanisms for ENSO phase change in a coupled GCM. *J. Climate*, **16,** 1141-1158.

Guilyardi, E., 2006: El Niño–mean state–seasonal cycle interactions in a multi-model ensemble. *Climate Dyn.,* **26,** 329–348.

Guilyardi, E., and Coauthors, 2004: Representing El Niño in coupled ocean–atmosphere GCMs: The dominant role of the atmospheric component. *J. Climate,* **17,** 4623–4629.

Guilyardi, E., A. Wittenberg, A. Fedorov, M. Collins, C. Wang, A. Capotondi, G. J. van Oldenborgh, and T. Stockdale, 2009: Understanding El Niño in ocean-atmosphere general circulation models: Progress and challenges. *Bull. Amer. Meteor. Soc.,* **90,** 325-340.

Harrison, D. E. and G. A. Vecchi, 1999: On the termination of El Niño, *Geophys. Res. Lett*., **26**, 1593-1596.

Hasegawa, T., T. Horii, and K. Hanawa, 2006: Two different features of discharge of equatorial upper ocean heat content related to El Niño events. *Geophys. Res. Lett.,* **33,** L02609, doi:10.1029/2005GL024832.

Hastenrath, S., 2002: Dipoles, temperature gradients, and tropical climate anomalies, *Bull. Amer. Meteor. Soc.,* **83,** 735–738.

Hoerling, M. P., A. Kumar, and M. Zhong, 1997: El Niño, La Niña, and the nonlinearity of their teleconnections. *J. Climate,* **10,** 1769-1786.

Hoerling, M. P., A. Kumar, and T.-Y. Xu, 2001: Robustness of the nonlinear atmospheric response to opposite phases of ENSO. *J. Climate,* **14,** 1277-1293.

Hoerling, M. P., and A. Kumar, 2003: The perfect ocean for drought. *Science,* **299,** 691-694.

Horii, T., and K. Hanawa, 2004: A relationship between timing of El Niño onset and subsequent evolution. *Geophy. Res. Lett., **31,*** L06304, doi:10.1029/2003/GL019239.

Ishizaki, N., and H. Ueda, 2006: Seasonal heating processes over the Indochina Peninsula and the Bay of Bengal prior to the monsoon onset in 1998. *J. Meteor. Soc. Japan.* **84,** 375-387.

Jin, F.-F., 1997: An equatorial ocean recharge paradigm for ENSO. Part I: Conceptual model, *J. Atmos. Sci*., **54,** 811-829.

Jin F.-F., and S.-I. An, 1999: Thermocline and zonal advective feedbacks within the equatorial ocean recharge oscillator model for ENSO. *Geophys. Res. Lett,* **26,** 2989-2992.

Jin, F.-F., J.-S. Kug, S.-I. An, and I.-S. Kang, 2003: A near-annual coupled ocean-atmosphere mode in the equatorial Pacific Ocean. *Geophys. Res. Lett.,* **30 (2),** 1080, doi:10.1029/2002GL015983.

Joseph, R., and S. Nigam, 2006: ENSO evolution and teleconnections in IPCC's 20th-century climate simulations: Realistic representation? *J. Climate,* **19,** 4360–4377.

Kang, In-Sik., S.-I. An, F.-F. Jin, 2001: A systematic approximation of the SST anomaly equation for ENSO. *J. Meteor. Soc. Japan,* **79,** 1-10.

Kang, I.-S., and J.-S. Kug, 2002: El Niño and La Niña sea surface temperature anomalies: Asymmetry characteristics associated with their wind stress anomalies. *J. Geophys. Res.,* **107**, 4372, doi:10.1029/2001JD000393.

Kawamura, R., T. Matsuura, and S. Iizuka, 2003: Equatorially symmetric impact of El Niño-Southern Oscillation on the South Asian summer monsoon system. *J. Meteor. Soc. Japan,* **81,** 1329-1352.

Kessler, W. S., 2002: Is ENSO a cycle or a series of events? *Geophys. Res. Lett.*, **29,** 2125, doi:10.1029/2002GL015924.

Kim, D., J.-S. Kug, I. -S. Kang, F.-F. Jin, and A. T. Wittenberg, 2008: Tropical Pacific impacts of convective momentum transport in the SNU coupled GCM. *Climate Dyn.,* **31,** 213–226, doi:10.1007/ s00382-007-0348-4.

Klein, S. A., B. J. Soden, and N. C. Lau, 1999: Remote sea surface temperature variations during ENSO: Evidence for a tropical atmospheric bridge, *J. Climate,* **12,** 917–932.

Kug, J.-S., S.-I. An, F.-F. Jin and I.-S. Kang, 2005: Preconditions for El Niño and La Niña onsets and their relation to the Indian Ocean, *Geophy. Res. Lett.,* **32**, L05706, doi:10.1029/2004GL021674.

Kug, J.-S., and I.-S. Kang, 2006: Interactive feedback between the Indian Ocean and ENSO. *J. Climate,* **19,** 1784-1801.

Kug, J.-S., T. Li, S.-I. An, I.-S. Kang, J-J. Luo, S. Masson, and T. Yamagata, 2006: Role of the ENSO-Indian Ocean Coupling on ENSO variability in a coupled GCM. Geophys. Res. Lett, 33, L09710, doi:10.1029/2005GL024916.

Lau, N.-C., and M. J. Nath, 2003: Atmosphere–ocean variations in the Indo-Pacific sector during ENSO episodes, *J. Climate,* **16,** 3–20.

Lau, N-C., and M. J. Nath, 2003: Atmosphere-ocean variations in the Indo-Pacific sector during ENSO episodes. *J. Climate* **16,** 3-20.

Lau, N.-C., and M. J. Nath, 2004: Coupled GCM simulation of atmosphere-ocean variability associated with zonally asymmetric SST changes in the tropical Indian Ocean, *J. Climate,* **17,** 245-265.

Lengaigne, M and G. Vecchi, 2009: Contrasting the termination of moderate and extreme El Niño events in coupled GCM. *Clim. Dyn.*, DOI: 10.1007/ s00382-009-0562-3

Lin, J. -L., 2007: The double-ITCZ problem in IPCC AR4 coupled GCMs: Ocean-atmosphere feedback analysis. J. Climate, 20, 4497–4525.

Luo, J.J. and T. Yamagata, 2001 : Long-term El Niño-Southern Oscillation (ENSO)-like variation with special emphasis on the South Pacific. *J. Geophys. Res.,* **106,** 22211-22227.

Meinen C.S., M.J. McPhaden, 2000: Observations of warm water volume changes in the equatorial Pacific and their relationship to El Niño and La Niña. *J. Climate,* **13,** 3551-3559.

Minobe S., and F.-F. Jin, 2004: Generation of interannual and interdecadal climate oscillations through nonlinear subharmonic resonance in delayed oscillators, *Geophys. Res. Lett.*, **31**, L16206, 10.1029/2004GL019776.

Murtugudde, R., and A. Busalacchi, 1999: Interannual variability of the dynamics and thermodynamics of the tropical Indian Ocean, *J. Climate*, **12,** 2300-2326.

Murtugudde, R., J. P. McCreary, and A. J. Busalacchi, 2000: Oceanic processes associated with anomalous events in the Indian Ocean with relevance to 1997–98. *J. Geophys. Res.,* **105,** 3295–3306.

Meehl, G. A., C. Covey, T. Delworth, M. Latif, B. McAvaney, J. F. B. Mitchell, R. J. Stouffer, and K. E. Taylor, 2007: The WCRP CMIP3 multimodel dataset: A new era in climate change research. *Bull. Amer. Meteor. Soc.,* **88,** 1383–1394.

Meehl, G. A., P. R. Gent, J. M. Arblaster, B. L. Otto-Bliesner, E. C. Brady, and A. Craig, 2001: Factors that affect the amplitude of El Niño in global coupled climate models. *Climate Dyn.,* **17,** 515–526.

Monahan, A.H., and A. Dai, 2004: The Spatial and Temporal Structure of ENSO Nonlinearity. *J. Climate,* **17,** 3026–3036.

Nagura, M., K. Ando, and K. Mizuno, 2008: Pausing of the ENSO Cycle: A Case Study from 1998 to 2002. *J. Climate*, **21**, 342–363.

Neale, R. B., J. H. Richter, and M. Jochum, 2008: The impact of convection on ENSO: From a delayed oscillator to a series of events. J. Climate, 21, 5904–5924.

Ohba, M., and H. Ueda, 2005: Basin-wide Warming in the Equatorial Indian Ocean Associated with El Niño, *SOLA,* **1,** 89-92.

Ohba, M., and H. Ueda, 2006: A role of Zonal Gradient of SST between the Indian Ocean and the Western Pacific in Localized Convection around the Philippines. *SOLA,* **2,** 176-179.

Ohba, M., and H. Ueda, 2007: An Impact of SST Anomalies in the Indian Ocean in Acceleration of the El Niño to La Niña Transition. *J. Meteor. Soc. Japan,* **85,** 335-348.

Ohba, M., and H. Ueda, 2009a: Seasonally Different Response of the Indian Ocean to the Remote Forcing of El Niño: Linking the Dynamics and Thermodynamics, s*ubmitted to SOLA*.

Ohba, M., and H. Ueda, 2009b: Role of Nonlinear Atmospheric Response to SST on the Asymmetric Transition Process of ENSO. *J. Climate*, **22**, 177–192.

Ohba, M., D. Nohara, J. Tsutsui and Y. Yoshida, 2009: Role of climatological state on the simulation of asymmetric ENSO transition in the WCRP CMIP3 multi-model experiments, *submitted to J. Climate.*

Picaut, J., F. Masia, and Y. du Penhoat, 1997: An advectivereflective conceptual model for the oscillatory nature of the ENSO. *Science*, **277**, 663-666.

Saji, N. H., B. N. Goswami, P. N. Vinayachandran and T. Yamagata, 1999: A dipole mode in the tropical Indian Ocean, *Nature,* **401,** 360-363.

Saji, N.H., S.P. Xie, and T. Yamagata, 2006: Tropical Indian Ocean Variability in the IPCC Twentieth-Century Climate Simulations. *J. Climate*, **19**, 4397–4417.

Schopf, P. S., and M. J. Suarez, 1988: Vacillations in a coupled ocean-atmosphere model. *J. Atmos. Sci.*, **45**, 549-566.

Shibata, K., H. Yoshimura, M. Ohizumi, M. Hosaka, and M. Sugi, 1999: A simulation of troposphere, stratosphere and mesosphere with an MRI/JMA98 GCM. *Pap. in Meteor. and Geophys.*, **50**, 15-53.

Shinoda, T, M. A. Alexander, and H. H. Hendon, 2004: Remote response of the Indian Ocean to interannual SST variations in the tropical Pacific. *J. Climate*, **17,** 362-372.

Simmons, A.J. and J.K Gibsons, 2000: The ERA40 project plan. *ERA40 Project Report Series No. 1,* **14,** 63pp.

Smith, T.M., and R.W. Reynolds, 2004: Improved Extended Reconstruction of SST (1854-1997). *J. Climate*, **17**, 2466-2477.

Terao, T, and T. Kubota, 2005: East-West SST contrast over the tropical oceans and post El Niño western North Pacific summer monsoon, *Geophys. Res. Lett.,* **32,** L1570610.1029/2005GL023010.

Tokinaga, H., and Y. Tanimoto, 2004: Seasonal Transition of SST Anomalies in the Tropical Indian Ocean during El Niño and Indian Ocean Dipole Years, *J. Meteor. Soc. Japan,* **82,** 1007-1018.

Tomita, T., and T. Yasunari, 1993: On the two types of ENSO. *J. Meteor. Soc. Japan,* **71,** 273–284.

Tourre, Y. M., and W. B. White, 1995: ENSO signals in global upper ocean temperature. *J.*

Phys. *Oceanogr*., **25**, 1317–1332.

Ueda, H., and J. Matsumoto, 2000: A possible triggering process of east-west asymmetric anomalies over the Indian Ocean in relation to 1997/98 El Niño, *J. Meteor. Soc. Japan*, **78,** 803-818.

Ueda, H,. and R. Kawamura, 2004: Summertime anomalous warming over the midlatitude western North Pacific and its relationships to the modulation of the Asian monsoon. *Int. J. Climatol*, **24,** 1109 - 1120.

Ueda, H., M. Ohba, and S.-P. Xie, 2009: Important factors for the development of the Asian-Northwest Pacific summer monsoon. *J. Climate,* **22,** 649-669.

van Oldenborgh, G. J., S. Philip, and M. Collins, 2005: El Niño in a changing climate: A multi-model study. *Ocean Sci.,* **1,** 81–95.

Vecchi, G.A. and D. E. Harrison, 2003: On the termination of the 2002-03 El Niño event, *Geophys. Res. Lett*., **30 (18),** Doi:10.1029/2003GL017564.

Vecchi, G.A., and D.E. Harrison 2006: The termination of the 1997-98 El Niño. Part I: mechanisms of oceanic change. *J. Climate.* **19,** 2633-2646.

Vecchi, G.A. 2006: The termination of the 1997-98 El Niño. Part II: mechanisms of atmospheric change. *J. Climate.* **19,** 2647-2664.

Venzke, S., M. Latif, and A. Villwock, 2000: The coupled GCM ECHO-2. Part ❖: Indian Ocean response to ENSO. *J. Climate*, **13**, 1371–1383.

Wang. B, and Q. Zhang 2002: Pacific-East Asian teleconnection, part II: How the Philippine Sea anticyclone established during development of El Niño. *J. Climate*, **15**, 3252-3265.

Wang, B., and S.-I. An, 2005: A method for detecting season-dependent modes of climate variability: S-EOF analysis. *Geophys. Res. Lett.*, **32**, doi:10.1029/2005GL022709.

Wang. B, R. Wu, and X. Fu, 2000: Pacific-East Asia teleconnection: How does ENSO affect East Asian climate? *J. Climate*, **13**, 1517-1536.

Wang. B, R. Wu, R. Lukas, and S. I. An, 2001: A possible mechanism for ENSO turnabout. In "Dynamics of Atmospheric General circulation and Climate", *Ed. IAP/Academia Sinica, China Meteor. Press.* 552-578.

Wang. B, R. Wu, T. Li, 2003: Atmosphere-warm ocean interaction and its impacts on the Asian-Australian monsoon variation. *J. Climate,* **16,** 1195–1211.

Wang C., R. H. Weisberg, and J. I. Virmani, 1999: Western Pacific interannual variability associated with the El Niño-Southern Oscillation. *J. Geophys. Res.,* **104,** 5131-5149.

Wang, C., 2001: A unified oscillator model for the El Niño-Southern Oscillation. *J. Climate*, **14**, 98-115.

Watanabe, M., and F.-F. Jin, 2002: Role of Indian Ocean warming in the development of Philippine Sea anticyclone during ENSO, *Geophys. Res. Lett.*, **29 (10),** 1478, doi: 10.1029 /2001GL014318.

Webster, P. J. A.Moore, J. Loschnigg and R. Leben, 1999: Coupled ocean-atmosphere dynamics in the Indian Ocean during 1997-98, *Nature,* **401,** 356-360.

Weisberg, R. H., and C. Wang, 1997: Slow variability in the equatorial westcentral Pacific in relation to ENSO. *J. Climate*, **10**, 1998-2017.

Wu. R., and B. Kirtman, 2004: Understanding the impacts of the Indian Ocean on ENSO variability in a coupled GCM. *J. Climate,* **17**, 4019–4031.

Wu, R., and B. P. Kirtman, 2005: Near-annual SST variability in the equatorial Pacific in a coupled general circulation model. *J. Climate,* **18,** 4454-4473.

Xie, P., and P. A. Arkin, 1997: Global precipitation: A 17-year monthly analysis based on gauge observation, satellite estimates, and numerical model outputs. *Bull. Amer. Meteor. Soc.,* **78,** 2539–2558.

Xie, S.-P., and H.Annamalai, F. A. Schott, and J. P. McCreary, 2002: Structure and mechanisms of south Indian Ocean climate variability, *J. Climate,* **15,** 864-878.

Yamagata, T., S. Behera, S. A. Rao, Z. Guan, K. Ashok, and N. H. Saji, 2003: Comments on "Dipoles, temperature gradients, and tropical climate anomalies.", *Bull. Amer. Meteor. Soc.,* **84,** 1418–1422.

Yan, B., and R. Wu, 2007: Relative roles of different components of the basic state in the phase locking of El Niño mature phases. *J. Climate*, **20**, 4267–4277.

Yanai, M., S. Esbensen, and J.-H. Chu, 1973: Determination of bulk properties of tropical cloud clusters from large-scale heat and moisture budgets. *J. Atmos. Sci.,* **30,** 611-627.

Yamaguchi, K., and A. Noda, 2006: Global warming patterns over the North Pacific: ENSO versus AO. *J. Meteor. Soc. Japan,* **84,** 221–241.

Yu, J.-Y., C. R. Mechoso, J. C. McWilliams, and A. Arakawa, 2002: Impacts of the Indian Ocean on the ENSO cycle. *Geophys. Res. Lett.*, **29**, 1204, doi: 10.1029 /2001GL014098.

Yu, L., and M. M. Rienecker, 1999: Mechanisms for the Indian Ocean warming during the 1997–1998 El Niño, *Geophys. Res. Lett.,* **26,** 735–738.

Yukimoto, S., and Y. Kitamura, 2003: An investigation of the irregularity of El Niño in a coupled GCM, *J. Meteor. Soc. Japan,* **81**, 599-622.

Yukimoto, S., A. Noda, A. Kitoh, M. Sugi, Y. Kitamura, M. Hosaka, K. Shibata, S. Maeda, and T. Uchiyama, 2001: The new Meteorological Research Institute coupled GCM (MRI-CGCM2) - model climate and variability, *Pap. Meteorol. Geophys.,* **51***,* 47-88.

Yukimoto, S., A. Noda, A. Kitoh, M. Hosaka, H. Yoshimura, T. Uchiyama, K. Shibata, O. Arakawa and S. Kusunoki, 2006: Present-day climate and climate sensitivity in the Meteorological Research Institute coupled GCM version 2.3 (MRI-CGCM2.3). *J. Meteor. Soc. Japan,* **84**, 333-363.

Xie, S.-P., 1995: Interaction between annual and interannual variations in the equatorial Pacific. *J. Phys. Oceanogr.,* **25,** 1930–1941.

Zebiak, S.E. and M.A. Cane, 1987: A model El Niño Southern Oscillation. *Mon. Wea. Rev.,* **115**, 2262-2278.

Zhang, Y., J.M. Wallace, and D.S. Battisti, 1997: ENSO-like Interdecadal Variability: 1900–93. *J. Climate*, **10**, 1004–1020.

Appendices

List of abbreviations

20C3M: 20th Century Climate in Coupled Models

AGCM: Atmospheric general circulation model

BW: basin-wide warming

CGCM: Coupled general circulation model

CMIP3: Coupled Model Intercomparison Project phase 3

DJF: December, January and February

ENSO: El Niño-Southern Oscillation phenomenon

EOF: Empirical orthogonal functions analysis

EPI: ENSO persistency index

ERA-40 : 40-year Reanalysis from the European Centre for Medium-Range Weather Forecasts

FIO-BW: forced Indian Ocean-BW

FIO-DZ: forced Indian Ocean dipole/zonal SST anomalies

FIO-CL: climatological SST are imposed in the Indian Ocean

IODZM: Indian Ocean "Dipole/Zonal Mode"

ITCZ: Intertropical Convergence Zone

JJA: June, July and August

MAM: March, April and May

OBS: observation

OGCM: Oceanic general circulation model

OHC: Ocean heat content

OSN: Forced asymmetric negative phase experiment by use of ocean model

OSP: Forced asymmetric positive phase experiment by use of ocean model

S-EOF: Seasonally reliant EOF

SST: Sea surface temperature

SODA: Simple Ocean Data Assimilation

SON: September, October and Nobember

SN: Forced asymmetric negative phase experiment

SP: Forced asymmetric positive phase experiment

Z20: 20°C isotherm depth